

THESIS

MEASUREMENT OF He-Ne LASER WAVELENGTH FOR CALIBRATION OF METER STANDARD ACCORDING TO THE SI DEFINITION

KANOKPOJ AREEKUL

Graduate School, Kasetsart University

2007



THESIS APPROVAL

GRADUATE SCHOOL, KASETSART UNIVERSITY

Master of Science (Metrology)

DEGREE

Metrology

FIELD

Physics

DEPARTMENT

TITLE: Measurement of He-Ne Laser Wavelength for Calibration of Meter
Standard According to the SI Definition.

NAME: Mr. Kanokpoj Areekul

THIS THESIS HAS BEEN ACCEPTED BY

THESIS ADVISOR

(Associate Professor Bancha Panacharoensawad, Dr.Ing.)

COMMITTEE MEMBER

(Captain Sahapong Kruapech, M.S.E.E.)

COMMITTEE MEMBER

(Assistant Professor Teerasak Veerapaspong, Dr.Eng.)

DEPARTMENT HEAD

(Mr. Ekachai Hoonivathana, M.S.)

APPROVED BY THE GRADUATE SCHOOL ON _____

DEAN

(Associate Professor Vinai Artkongharn, M.A.)

THESIS

**MEASUREMENT OF He-Ne LASER WAVELENGTH FOR
CALIBRATION OF METER STANDARD ACCORDING TO THE
SI DEFINITION**

KANOKPOJ AREEKUL

**A Thesis Submitted in Partial Fulfillment of
the Requirements for the Degree of
Master of Science (Metrology)
Graduate School, Kasetsart University
2007**

Kanokpoj Areekul 2007: Measurement of He-Ne Laser Wavelength for Calibration of Metre Standard According to the SI Definition. Master of Science (Metrology), Major Field: Metrology, Department of Physics.
Thesis Advisor: Associate Professor Bancha Panacharoensawad, Dr.Ing.
95 pages.

Metrology is a new area of study and research in our country. Standard unit of length is one of seven basic standard SI units that calibration requirement demand is 50% of all. Calibration of length and related quantities require traceability to the SI. According to the SI definition of meter in 1983, CIPM recommends (CI-1983) three methods of meter realization. The possible and accurate method is the application of interferometer to measure the wavelength of some standard source such as stabilized HeNe laser. This thesis is proposed to apply scanning confocal Fabry-Perot interferometer for wavelength measurement.

Student's signature

Thesis Advisor's signature

___/___/___

ACKNOWLEDGMENTS

I would like to express my sincere gratitude and deep appreciation to my advisor, Associate Professor Dr. Bancha Panacharoensawad for his initiative idea, encouragement and always available answers. Grateful acknowledgments are likewise extended to my committee members, Dr. Teerasak Veerapasapong and Captain Sahapong Kruapech for their precious suggestion, insight and support.

For much needed technical support and guidance in the laboratory about laser wavelength measurement and usage of the OSA, I would like to special thank Captain Sahapong Kruapech. Special thank to Mr. Panya Kongsawad and Mr. Sakchai Chomkrokroawd for assistance making of many mechanical parts and electronics circuits. For mathematical suggestion I would like to thank Mr. Noparit Jinuntuya and Mr. Sithichai Pinkanchanaroj. Also, I would like to thank student members of MPiR who devoted much of their attempt to carry on many experiments and computer simulation work.

The last but not the least, my special thanks goes to my family, both my side and my wife side, and friends for their inspiration and believing in my dream. Usefulness of this thesis, I dedicate to all of my teachers.

Kanokpoj Areekul

April 2007.

TABLE OF CONTENTS

	Page
TABLE OF CONTENTS	i
LIST OF TABLES	ii
LIST OF FIGURES	iii
LIST OF ABBREVIATIONS	vi
LIST OF SYMBOLS AND VARIABLES	viii
INTRODUCTION	1
OBJECTIVES	4
LITERATURE REVIEWS	5
MATERIALS AND METHODS	53
Material	53
Methods	67
Data Analysis	78
RESULTS AND DISCUSSION	86
Result	86
Discussion	90
CONCLUSION AND RECOMMENDATION	92
LITERATURES CITED	94
APPENDIX	96
Appendix A Spectral Information, Instruments Specification and test certificate	97
Appendix B Experiments procedure	106

LIST OF TABLES

Table		Page
1	Wavelength and brightness comparison for some commercial laser pointer	51
2	Average frequency and standard deviation of the mean of high voltage ramp at the sample frequency and the sample amplitude	78
3	Average frequency and standard uncertainty	78
4	Analysis of amplitude stability	79
5	Linearity of ramp signal at observed amplitude	79
6	Analysis of linearity according to the definition in appendix figure B1	80
7	Evaluate of <i>THD</i> % at difference amplitude	81
8	Evaluation of static sensitivity	81
9	Analysis of the etalon cavity extension co-efficient where the ramp amplitude is change.	83
10	Evaluated the finesse @ 632.8 nm	83
11	Wavelength measurement result of laser LHRP-0151	84
12	Uncertainty budget of wavelength measurement from table 11	85
13	Wavelength measurement result of laser LHRP-0051	85
14	Uncertainty budget of wavelength measurement from table 13	85
Appendix table		
A1	A list of recommended radiations, 1983	102
A2	A list of recommended radiations of Spectral Lamps	103
A3	Possible spectrum of He-Ne laser	104

LIST OF FIGURES

Figure		Page
1	Transmission and reflection of dielectric slab	24
2	Reversibility by the Stokes Relations	26
3	Diagram showing two adjacent parallel transmitted rays for a Fabry-Perot étalon	28
4	Plot of the transmission light	30
5	Plot of the reflected light	30
6	Illustrate the FWHM (ϵ) and FSR	31
7	Fabry-Perot interferometer	34
8	Plot of transmission interference pattern of Fabry-Perot interferometer which 0.4 and 0.8 reflectance	34
9	Plot of reflection interference pattern of Fabry-Perot interferometer which reflectance of 0.4 and 0.8	35
10	Plot of two wavelength λ_1 (589.600 000 nm) and λ_2 (589.399 850 nm) that satisfy the Rayleigh criterion of a Fabry-Perot etalon which finesse 199	36
11	Scanning Fabry-Perot with controller and oscilloscope display	39
12	Spherical Fabry-Perot	39
13	Computer simulation show successive interference beam transmitted from a FPI	42
14	Instruments setup for relative wavelength measurement	45
15	Computer simulation of FPI which cavity length 10.000 mm, R 0.99 (finesse 312.6)	46
16	The helium-neon laser lasing process	47
17	Basic Structure of Laser Diode	49
18	Optical Spectrum Analyzer System	53
19	Optical Spectrum Analyzer model 240	54
20	Specification of OSA model 240 from its brochure	55
21	Specification of OSA model 240 from its manual	55

LIST OF FIGURES (continued)

Figure		Page
22	The OSA controller model 251	57
23	The Sensor: Silicon PIN Photo Diode	57
24	Silicon PIN Photo Diode relative response	58
25	Spectra-Physics Model 117 Stabilized HeNe Laser System	60
26	543 nm He-Ne laser model LHRP-0051	62
27	TDS 220, Real-Time Digital Storage Oscilloscope	63
28	Agilent 33401A 6½ Digits Digital Multi-meter	64
29	Real-Time FFT Analyzer Tektronix 2642A	65
30	Arbitrary Function Generator Tektronix AFG1501	66
31	Definition of (non)-linearity of ramp signal	68
32	Fourier transform of linear ramp signal	69
33	Rear panel of the controller model 251	70
34	Calculation of slope of input and output triangular wave	70
35	SP117 laser head is aligned direct into the OSA to evaluate the Etalon cavity expansion co-efficient	73
36	Oscilloscope screen show 6 successive interference peak of 632.8 nm Laser	73
37	FSR measurement	74
38	FWHM measurement	75
39	Instruments alignment to measure or compare wavelength of laser diode	76
40	Comparison of 632.8 nm Stabilized HeNe laser (center peak) and 630 nm nominal wavelength of laser pointer	77
41	Shape of harmonic peaks may have ‘side band’ added	80
42	Frequency response of the amplifier of the 251 controller	81
43	Unexposed I-V characteristics	82

LIST OF FIGURES (continued)

Appendix Figure	Page
A1 1 Test certificate of the OSA model 240	98
A2 Specification of SP117 632.8 nm stabilized HeNe Laser	99
A3 Scanned page 1 of the specification of UDT photo-voltaic series	100
A4 Scanned page 2 of the Specification of UDT photo-voltaic series that show specification of PIN 125DPL	101
B1 Measurement definition of ramp linearity	109
B2 Zero Offset Ramp and Ramp with DC Offset	110
B3 Ramp wave form of period 0.5 s, rise time 0.49 s, duty cycle 98%	112
B4 FFT of the same ramp, show 30 peaks harmonics form 300 components	112
B5 Measurement of Diode Characteristic with HM6042	118

LIST OF ABBREVIATIONS

atm	=	atmosphere (relative unit of pressure, not SI)
^A I	=	Symbol of Element “Iodine Isotope A”
BIPM	=	Bureau International des Poids et Mesures
CCDM	=	Consulting Committee for the Definition of the Metre
CCL	=	Consultative Committee for Length
CCM	=	Comité Consultatif pour la Masse et les Grandeurs Apparentées
CCTF	=	Consultative Committee for Time and Frequency
CEI	=	Commission Electrotechnique Internationale
CGPM	=	Conférence Générale des Poids et Mesures
CIE	=	Commission Internationale de l’Eclairage
CIML	=	International Committee for Legal Metrology
CIPM	=	International Committee of Weight and Measures
CO ₂	=	Carbondioxide molecule
Cs	=	Symbol of Element “Cesium”
°C	=	degree Celcius
DTI	=	Department of Trade & Industry (UK.)
esa	=	European Space Agency
Eq.	=	Equation
FIR	=	Far Infrared
FPI	=	Fabry-Perot Interferometer
FSR	=	Free Spectral Range
FWHM	=	Full Width at Half Maximum
fm ₁₉₈₃	=	femtometer (according to 1983 meter definition)
GHz	=	GigaHertz
HeNe, He-Ne	=	Helium Neon
IAU	=	International Astronomical Union
ISO	=	International Organization for Standardization
ISO	=	The Infrared Space Observatory
LASER, laser	=	Light Amplification by Stimulated Emission Radiation

LIST OF ABBREVIATIONS (continued)

LWS	=	Long Wavelength Spectrometer)
mm	=	millimeter
m/s	=	Meter per second
m/s ²	=	Meter per square second
m ₁₉₆₀ ⁻¹	=	per meter (according to 1960 meter definition)
MHz	=	MegaHertz
MRA	=	Mutual Recognition Arrangement
MW	=	Megawatt
mW	=	Milliwatt
nm	=	nanometer
NPL	=	Nation Physics Laboraoty (UK.)
N. A.	=	Not Available
N/A ²	=	Newton per square Ampare
N/V	=	Newton per Volt
OPD	=	Optical Path Difference
OSA	=	Optical Spectrum Analyzer
PTB	=	Physikalisch-Technische Bundesanstalt (Ger.)
RegMet	=	Metrology For Improved Measurement In International Regulation And Trade
SI	=	Systbme International
Torr.	=	Torr. (1 Torr. = 1 mmHg, relative unit of pressure, not SI)
VLB	=	Very Long Baseline Measurements
V·s/A·m	=	Volt-second per Ampare-meter
μm	=	micrometer
⁸⁶ Kr	=	Krypton atom isotope 86
¹⁹⁸ Hg	=	Mercury atom isotope 198
¹¹⁴ Cd	=	Cadmium isotope 114
¹²⁷ I	=	Iodine atom isotope 127
¹²⁹ I	=	Iodine atom isotope 129

LIST OF SYMBOLS AND VARIABLES

A	= Surface Losses Coefficients
$a(r, z)$	= Gaussian Beam Distance
\mathbf{b}	= Gravitation Fields
c, c_{mat}	= Speed of Light Propagating in Material
c_o, c_{vac}	= Speed of Light in Free Space or in Vacuum
d	= Distance of Mirrors, along the optical axis of the cavity
E	= Photons of energy,
E_t	= Magnitude of Electric Field Component of transmitted rays
E	= Magnitude of Electric Field Component, of electromagnetic wave
E_{rp}	= Magnitude of Electric Field Component of reflected ray “ p ”
E_r^*	= Conjugate of Magnitude of Electric Field Component
F	= The Co-efficient of Finesse or Contrast
g	= Acceleration due to Earth Gravitation
H	= Plank’s constant
I_r	= Intensity of Reflected Rays
I	= Intensity of Rays
I_t	= Intensity of transmitted Rays
k	= Coverage Factor
$k(ku_c)$	= Coverage factor for combine uncertainty
k, k_0	= Circular Wave Number ($2\pi/\lambda$) in Medium n, n_o
m	= Mass of Particle
m, n	= Rectangular Mode Numbers (in metrology only $m = n = 0$ is of interest)
n, n_o	= Refractive Index
$n(\lambda)$	= Dispersion of The Refractive Index,
q	= Number of Nodes, in a standing wave between the mirrors
$q + 1$	= The order of interference as usual.
r	= Distance on Radial Direction
r	= Internal Amplitude Reflection Coefficients
r'	= External Amplitude Reflection Coefficients

LIST OF SYMBOLS AND VARIABLES (continued)

r_1, r_2	= Radii of Curvature, of the spherical mirrors
R	= Reflectance (= r^2)
t	= Internal Amplitude Transmission Coefficients
t'	= External Amplitude Transmission Coefficients
t	= Time
T	= Transmittance (= tt')
T	= Period of Electromagnetic Wave
THD	= Total Harmonic Distorsion
$THD\%$	= Percentage Total Harmonic Distorsion
$u_c/y, u_{rel}$	= Relative Combine Uncertainty of variable y
u_c	= Combined Uncertainty
U	= Uncetainty (total)
w_0	= Beam Waist
x	= Distance on z Axis
z	= Height, Distance on z Axis
ϵ_o	= Electric Field Constant or Permittivity of the Vacuum
$\Delta\lambda_{FSR}$	= Free Spectral Range (in term of wavelength)
Δf_{FSR}	= Free Spectral Range (in term of frequency)
$\Delta\lambda_{res}$	= Resolution (in term of wavelength)
λ	= Wavelength
ϕ	= Gravitation Potential
ν	= Frequency of Electromagnetic Wave
Δr	= Traveling Path in Gravitation Potential Field
ν_q	= Resonance Frequency of a Mode Matched Wave,
ν_o	= Frequency Distance Between Neighboring Longitudinal Resonant Modes, counted by the integer q , $\nu_o = \frac{c_o}{2d}$
μ_0	= Permeability of the Vacuum
δ	= Phase Difference Between Adjacent Reflected Rays

LIST OF SYMBOLS AND VARIABLES (continued)

φ, φ_0	= Phase Difference
$\theta, \theta', \theta_0$	= Angle
δ	= Optical Path Difference between two adjacent rays
ω	= Angular Frequency
σ	= Spatial Periods per Unit of Length ($k/2\pi$)
\mathfrak{F}	= Finesse
ϕ	= Phase Change Upon Reflection

MEASUREMENT OF He-Ne LASER WAVELENGTH FOR CALIBRATION OF METER STANDARD ACCORDING TO THE SI DEFINITION

INTRODUCTION

The problem of interest for this thesis is how accurate measurement of length we can do. To find this solution, I start to study metrological development in our country and converse with many people who work in metrology area. I found many difference in metrological development aspect comparing to other development countries. Most or nearly all of metrological organizations or laboratories are calibration service providers. They prefer technological transfer to research work. My conclusion, that probable wrong, is that most people think the research is importance but it difficult to do and funded. Now, I think they are right.

Metrology is a new area of study and research in our country. Though, The kingdom of Thailand has signed the Meter Convention since 1912, but neither activity nor contribution is given at all except some requested services in the recent year. In other view, it may say that we do not realize the importance of metrology as much as our neighbor country. To day, worldwide knowledge on Metrology is the key for successful development of science, technology and trade.

T. J. Quint, Director of BIPM notes the importance of metrology in the “Open letter concerning the growing importance of metrology and the benefits of participation in the Metre Convention, notably the CIPM MRA”. The impetus of facilitating world trade and the associated need to eliminate technical barriers to trade is leading to a greater awareness worldwide of the role that measurement plays in underpinning activities in all areas of science and technology. It is now recognized that metrology provides a fundamental basis not only for the physical sciences and engineering, but also for chemistry, the biological sciences and related areas such as the environment, medicine, agriculture and food. Various high-level studies demonstrate the impact of measurement to society; most recently, the report Evolving

Needs for Metrology in Trade, Industry and Society and the Role of the BIPM highlights current drivers and strategies to address the worldwide need for reliable measurement. (Quint, 2003).

Fiona Redgrave, Senior Project Manager in the International Office and manager of the DTI International Metrology Programme at NPL, she notes the importance of metrology and quality of life on the abstract of “Metrology for Improved Measurements in International Regulation and Trade” The operation of the economy on a global scale and the quality of life for the individual citizen depends on reliable measurements and tests, which are trusted and accepted internationally. Although broadly harmonized, differences in measurement practice amongst regulators and associated bodies still exist even within the EU. This is because the approach by the regulatory community in Europe is still influenced by historical practice and awareness of measurement issues varies significantly. Equally, development of national measurement capability does not always take optimum account of the regulatory perspective. A partnership of nine European National Metrology Institutes, the European Commission’s Joint Research Centre and the European Organization for Conformity Assessment, with partial support from the European Commission, are engaged in the RegMet project with the regulatory community to overcome this historical legacy. This paper describes the aims, findings and progress of the RegMet project, including the concept of the development of a measurement template for regulators. (Redgrave et al., 2003).

In everyday life, we always concern with “measurement” in some way some how. Example, a housekeeper goes to buy a pound of meat from a super market. She needs to weigh that piece of meat with a certified balance. Drivers full up their cars at a gas station. They need to know exactly how many liters that filled in their tank. In some occupation such as the engineers, the mechanics, the scientist they spend most of time on very critical measurement. If we look through a broad view, one of an importance part of manufacturing, industry and modern agriculture is “measurement”. In fact, most of the science and technology development that base ups our civilization

concern with measurement. Most of our known scientific truth is base on our knowledge of measurement.

Manfred Kochsiek, Vice-President of PTB and First Vice-President of CIML, give some comment about how importance of a uniform metrology system on “Trends in legal metrology towards a global measurement system”, ISO Bulletin, May 2003: The key nations of the past such as the Greeks, Romans, Incas, Chinese and others had all recognized the importance of a uniform metrology system and had consequently implemented it in their empires. The decisive step towards a worldwide uniform system of units was however accomplished in 1875 with the signing of the Meter Convention in Paris by seventeen countries. Its aim was to secure international agreement on and improve the Metric System; this agreement was finally reached in 1960 with the introduction of the International System of Units, the SI. Unfortunately, although most countries have since joined the Meter Convention, the SI is still not yet fully implemented some 125 years after it was instigated. (Kochsiek, 2003)

There for, one of the key knowledge to the uniform measurement is the capability of realizing of the unit standard. This point of interest leads me to the objectives of this research. Though, the objectives are back to very basic research and look not attractive but since 1912 we, our country, have no research activity to express our capability on realization of any SI primary unit. This thesis is report a study of accurate wavelength measurement with Fabry-Perot Interferometer. This subject is not new and rather difficult to get something new under many limitation, but I think the knowledge of accurate wavelength measurement is the importance basic of Photonic Metrology.

Charles M. P. A. Fabry (1867-1945) and Alfred J.-B. Perot (1863-1925) described the Fabry-Perot Interferometer, a novel of invention, in 1899. FPI is a multiple beam interference application with a simple configuration but very high wavelength resolution. It enables high-resolution spectral observation. More than the half century passes, this instrument play an importance roll in realization of the optical frequency standard.

OBJECTIVES

1. Study the Optical Spectrum Analyzer (OSA) using con-focal Fabry-Perot interferometer and applications for wavelength measurement.
2. To measure wavelength of some LASER and Spectral source compare with the frequency stabilized HeNe LASER using the OSA.
3. To study traceability possibility of the wavelength calibration procedure.

Scope of This Research

1. The calibration procedure use in this research is preliminary and only to adapt with the available instruments because of some limitation of the instruments.
2. The numerical result for wavelength comparison depends on the known wavelength of the frequency stabilized HeNe LASER.

LITERATURE REVIEW

1. The CIPM's Definition and Realization of Metre

Bayer-Helms F., give an explicit explanation on the definition of metre and it's realization base on the CIPM solutions brought up during the symposium on "Metrology in Physics" held at the Physikalisch-Technische Bundesanstalt at Braunschweig, Germany in 1987 (Madelung, et al. 1991.).

1.1 The Meter SI Definition 1983

The metre is the length of the path travelled by light in vacuum during a time interval of $1/299\,792\,458$ of a second.

This formulation was adopted by the 17th "General Conference of Weight and Measures" (CGPM) on October 20th, 1983, as definition of the basic unit of length within the "International System of Units" (SI). It concerns an important physical constant, the speed of light.

Already in 1948 the definition of another basic unit of the SI, the ampere, involved of the magnetic field constant μ_0 , the permeability of the vacuum. The value is define as

$$\mu_0 = 4\pi \cdot 10^{-7} \text{ N/A}^2 \text{ (or V}\cdot\text{s/A}\cdot\text{m)}.$$

Then the magnetic field can be measured by a current balance. (cf. section 4.2.4.)

1.2 Consequences of The 1983 Definition

In the SI the value of the speed of light is:

$$c_0 = 299\,792\,458 \text{ m/s}$$

under reference conditions (cf. section 4.1.5). Thus, since 1983 any measurement of the speed of light is neither necessary nor possible. In calculations no uncertainty contribution coming from the value of c_o must be taken into account since 1983.

The definition of the metre is based on the definition of the second. Any realization of the metre (cf. section 4.2) is traceable to any realization of the second. On the other hand, any change of the definition of the second in the future will not influence the definition of the metre, it would certainly affect the realization. The metre is now metrologically dependent on the second. It is the basic of SI unit.

According to the Maxwellian relation

$$\mu_o \varepsilon_o = c_o^{-2}$$

besides c_o and μ_o the electric field constant or the permittivity of the vacuum ε_o is fixed as well, but in another manner. The value of ε_o is not given explicitly but can be calculated exactly. In the case of c_o the value has been given by the metre definition with 9 figures (see above). At the need of more decimals, convention is to fill up all following decimal places with zeros. Concerning, μ_o the number π is known super precisely ($10^5 \dots 10^9$ figures). On this basis anyone can calculate the electric field constant as far as he wants to do, e.g.:

$$\varepsilon_o = 0.885\,418\,781\,762 \cdot 10^{-11} \text{ A}\cdot\text{s/V}\cdot\text{m (or N/V)}.$$

1.3 The Word “light” and The Dispersion of c_o

It was not clearly stated in the documents of the metre definition what the word light means. An international standardization of the word light is given trilingually in the vocabulary of the CEI and the CIE as “perceived light” (perceived by the human eye) or as “visible light”

The speed of light c propagating in material like gases, e.g. in air, shows dispersion. The speed of light propagating in free space, c_o , is generally assumed to be dispersion free. There seems to be no need to specify any spectral point or any spectral region as a reference condition. Cosmologic theories sometimes deal with the question of dispersion of c_o . Some estimates any possible dispersion base on astronomical observations on the emission from pulsars e.g. they are far under all uncertainty levels of metrology today, e.g.

$$\Delta c_o/c_o \approx 10^{-16}$$

for dispersion effects in the visible region. If any measurable dispersion will be detected in the future, a suitable reference condition has to be introduced.

1.4 Variation of c_o with Time?

In the theory of relativity there exists the famous postulation of Einstein that c_o is a limiting quantity and has the same value in all systems of observation.

In verifying possible variation of c_o with time by measurements the problem is compound with the question of irregularities of the clock realizing the momentary definitions of time interval. Variation of universal constants with time has been discussed and measurements of c_o till 1983 have been compiled and evaluated in detail elsewhere.

1.5 Reference Conditions

The speed of light, the phase velocity of visible electromagnetic waves, depends on some physical parameters. It is unavoidable to declare a reference condition for each parameter. Three parameters of different origin and of different magnitudes of influence are medium of propagation of the light, structure of the wave, and local variation of the gravitation in the space of propagation.

Rough estimates for the relative magnitude of influence in practical cases, which means in real experiments in the atmosphere on the surface of the earth, may be taken for remembrance as a geometric such as 10^{-4} , 10^{-6} , 10^{-12} .

The influence of medium of propagation is usually described by the refractive index, e.g.

$$n = \frac{c_{vac}}{c_{mat}}$$

in homogenous medium. In gases n is near 1, especially in air under normal atmospheric conditions

$$n - 1 \approx 2.7 \cdot 10^{-4},$$

that means the influence is in the order of 10^{-4} . According to the sentence of the definition itself (section 4.1.1) reference condition is the vacuum, where the space of propagation is free from material particles.

In any case of a real experiment the propagation of light must be limited laterally giving rise to diffraction effects. Exactly characterized, the light waves are not plane waves, rather they will get a more complicate structure. The phase velocity varies from point to point in the space of propagation, even in a stationary wave. The Gaussian beam is a mathematically well-described example, approximately realized by a laser beam. The phase velocity is locally higher around the waist until the maximum in the axis point of the waist:

$$\frac{\Delta c_o}{c_o} \approx 2 \left(\frac{\lambda}{2\pi w_o} \right)^2 \quad (1)$$

(cf. Eq. (3)). Taken as a rough estimate for $\lambda = 600$ nm and radius of the waist $w_o = 1$ mm

$$\frac{\Delta c_o}{c_o} \approx 10^{-8}.$$

According to the realization recommendation CI-1983 of the CIPM (section 4.2.1) the reference condition concerning the structure of the wave is the plane laterally unlimited wave.

Long distance measurements in astronomy by traveling time observation on light going to a star and scattered back to the observer depend on gravitational potential. The distance from the earth to the planet Mars e.g. seems to become larger, if the sun with its great mass approaches the way of the light under observation. The effect occurs in the course of some weeks, and is compound with a bending of light rays too. It depends on gravitational potential variation with time on the way of propagation. The potential is determined by the distribution of masses in the space, that means, it is varied by the approach of the sun. The recommendation CI-1983 (section 4.2.1) postulates, “that corrections are applied to take account of actual conditions such as ... gravitation ..”, without description of the reference condition. It has been proposed as to be most reasonable to declare as reference condition of the space without any gravitation field or, as an identical statement, the space with a constant gravitation potential.

According to Einstein’s theory gravitation fields are acceleration fields

$$\mathbf{b} = -\nabla\varphi,$$

where φ is the gravitational potential. At the surface of the earth

$$|\mathbf{b}| = g \approx 9.8 \text{ m/s}^2.$$

The potential variation with the height z above the geoids surface is approximately

$$\Delta\varphi = g z.$$

Photons of energy

$$E = h\nu$$

are provided with the mass

$$m = \frac{E}{c_o^2}.$$

Travelling the path Δr with potential difference $\Delta\phi$ they will get an acceleration b and an energy difference

$$\Delta E = m(b\Delta r) = \frac{E\Delta\phi}{c_o^2}.$$

The relative variations $\Delta m/m$, $\Delta E/E$, $\Delta v/v$, and $\Delta\lambda/\lambda$ equal all $\Delta\phi/c_o^2$, except for the sign only. Restricting the space of an experiment under consideration to the height of $z < 10$ km the effect of gravitation is limited by:

$$\frac{gz}{c_o^2} \lesssim 1.1 \cdot 10^{-12}$$

This is the explanation of the third estimate given above. Those estimates are neither corrections for a certain experiment nor uncertainties for a certain experiment.

All the three reference conditions mentioned are ideal conditions that mean, they are in principle not completely realizable but they can be approximated experimentally to a high and satisfactory degree. The deviation of reality from reference must be taken into account of the correction, often based on estimates. This is the reason that all realizations of the definition will have unavoidably an uncertainty. It is the art of metrology to manage an experiment in such a manner that low and reliable corrections occur.

2. Realization

The definitions of the international basic units became more and more abstract. Till now there are already three definitions for the metre adopted in 1889, 1960, and 1983. The first definition was based directly on a prototype (see below). It is realized by itself, so to speak, by one selected specimen of a special type of material measure.

2.1 General Recommendations

Recommendation I (CI-1983) for the realization have been prepared by the CCDDM which adopted and issued by the CIPM together with the adoption of the new definition that the metre be realized by one of the following methods. The main part is repeated below; another part-the list of recommended radiations, 1983 - is abbreviated in appendix table A1 and A2.

2.1.1 by means of the length l of the path traveled in vacuum by a plane electro-magnetic wave in a time t ; this length is obtained from the measured time t , using the relation $l = c_o t$ and the value of the speed of light in vacuum $c_o = 299\,792\,458$ m/s;

2.1.2 by means of the wavelength in vacuum λ of a plane electromagnetic wave of frequency ν ; this wavelength is obtained from the measured frequency ν , using the relation $\lambda = c_o/\nu$ and the value of the speed of light in vacuum

$$c_o = 299\,792\,458 \text{ m/s};$$

2.1.3 by means of one of the radiations from the list whose stated wavelength in vacuum, or whose stated frequency, can be used with the uncertainty shown, provided that the given specifications and accepted good practice are followed and that in all cases any necessary corrections be applied to take account of actual conditions such as diffraction, gravitation, or imperfection in the vacuum.

2.2. Direct Realization. Realization of a Nonmaterial Distance

Measurements of the traveling time of light may be specified as “direct” realization. The time interval measured in s is transferred into the distance given in m by calculation with the defined value of the speed of light c_o . Traveling time measurement is practically restricted to a long distance of a third kind of length that means, to a distance in space without any material bridge between the ends. The

relative uncertainty of time interval measurement rests valid for the calculated distance too. Some contribution comes from correction uncertainty.

The distances in astronomy to stars, planets, to the moon, or satellites, and very long baseline measurements (VLB) in geodesy form the domain of “direct” realization. In the last cases the precision of time scale dissemination is fully applied, because the signals or the positions of a satellite are recorded by at least two stages of observation with time as a significant parameter. The position of a satellite is here sometimes an intermediate result, in order to determine the distance of the observation points at the earth’s surface.

In the case of shorter distance, precision is limited in recognizing the ends of the interval and the time interval itself. In the example of 1 m, distance traveling time is only about $3 \cdot 10^{-9} \text{ s} = 3 \text{ ns}$. The realization uncertainty $2 \cdot 10^{-14} \text{ s}$ by the Cs atomic clock of the definition of the second should give a limit of about 10^{-5} for the relative uncertainty in the case of the “direct” realization of just 1 m in length.

2.3 Realization of Wavelengths and Frequencies

The development of laser technology created frequency generators of very high frequency and of extremely high reproducibility attaining not only the far infrared (FIR) but even the visible region. Those generators are also called “**optical frequency standards**”. In order to come from a measured frequency to wavelength a basic relation $\lambda \nu = c_0$ is applied.

The mathematical description of an electromagnetic radiation, $\sin(\omega t - kx)$ e.g., several coefficients of time and of space coordinates are introduced, like circular frequency ω , frequency $\nu = \omega/2\pi$, period (in time) or cycle $T = 1/\nu$, and circular wave number k , wave number (spatial periods per unit of length) $\sigma = k/2\pi$, wavelength (period in length) $\lambda = 1/\sigma = 2\pi/k$. The ratios of suitable pairs of coefficients have the meaning of phase velocity of the wave:

$$c_o = \omega/k = 1/(\sigma T) = \lambda/T = \lambda \nu. \quad (2)$$

The term λ/T evidently means: period in space divided by period in time equals velocity. These relations follow simply from the meaning of the coefficients introduced. They are not a physical law, that means, they cannot and must not be confirmed by independent measurements of e.g., λ , ν , and c_o .

Any wave will have the same phase situation at an arbitrary but fixed time in spatial points forming a face. The name of the quantity λ shall indicate the interpretation as distance between faces representing equal phase situation (or phase (mod 2π)). Seriously taken, this distance is constant in the field of the wave only, if there would be the ideal appearance of a plane wave with equidistant and plane faces of constant phase.

In order to describe any structure of the wave the sine-function may get a spatially varying factor. Then not only is the amplitude varied but also the phase. The faces of constant phase will be bent and no more equidistant. In the case of a Gaussian beam their distance $a(r, z)$ is described by the formula:

$$\frac{a(r, z) - \lambda}{\lambda} = \frac{2(w_o/(2z_o))^2}{1 + z^2/z_o^2} \left(1 - \frac{r^2/w_o^2}{1 + z^2/z_o^2} \right) \quad (3)$$

in the same order of approximation as the Gaussian beam is a solution of the wave

equation; r and z cylindrical coordinates, beam axis $r = 0$, $z_o = \frac{\pi w_o^2}{\lambda}$ or $w_o/(2z_o) =$

$\lambda/(2\pi w_o) < 1$ another structural parameter (w_o = radius of the waist). In the centre point of the waist, $r = 0$ and $z = 0$, Eq. (1) follows.

Nevertheless the quantity $\lambda = c_o/\nu$ is treated as a constant and is to interpret, in order to be more precise, as “wavelength in the ideal case of a plane wave of frequency ν in the vacuum”. The deviation from a strong spatial periodicity in solutions of the wave equation is possible by compensation within the three dimensional Laplace operator of our space. So wave structure is permitted, and is the

basic reason for the diffraction correction in length measurements.

2.3.1 Frequency measurement and wavelength calculation

As long as c_o was not fixed, measurements of wavelength and frequency at the same radiation gave a determination of c_o . Since c_o has been fixed any generation of a standard radiation reproduces a standard value of frequency and at the same time a standard value of wavelength with the same relative reproducibility and the same relative uncertainty of realization. Once a frequency standard apparatus has been technologically developed its frequency has to be measured in principle against the Cs atomic clock. There are three contributions to the realization uncertainty:

- a) realization uncertainty of the definition of the second,
- b) measurement uncertainty of the frequency ratio, and
- c) reproducibility of the frequency standard under consideration.

For the time being, b) and c) are in competition (10^{-10} to 10^{-12} relative), and a) is to neglect with $2 \cdot 10^{-14}$ against b) and c).

The first metrological connection between the definitions of length and time units adopted in 1960 and 1967 was performed in 1972. Frequency and wavelength of a hyperfine structure component in the molecule of methane have been measured by frequency comparison with a chain of measurements brought together to the Cs atomic clock and by interferometric wavelength comparison to the ^{86}Kr standard lamp. The results culminated in an actual new value of the speed of light with an uncertainty of about 100 times smaller as before. It was limited by the realization uncertainty of the metre definition from 1960 with the ^{86}Kr standard lamp to $4 \cdot 10^{-9}$ relative, cause to bring about the new definition.

During the following time some more developments and measurements have been performed, see also below. The CCDM has gathered and evaluated the results and has compiled them in 1982 to a recommendation (later

called U-1983) for application. Those values are given in appendix table A1 and A2. The original recommendation quotes as far as necessary experimental conditions for the excitation of the standard radiations like about the cold finger temperature of the iodine absorption cell in He-Ne laser systems stabilized by saturated absorption in iodine vapor. The compilation shall be modernized from time to time. It contains for the time being five pairs of recommended values for stabilized laser radiations with their typical figures of “estimated overall relative uncertainty”, i.e. the threefold standard deviation.

An important supplement by experimental progress has to be mentioned. In the case of the methane stabilized frequency the hyperfine structure has been further resolved, the frequency can now be related to the centre component of a triplet (about 20 kHz apart), and the frequency chain is working now phase-coherently for several hours. This entitles really to speak about an “optical clock”. The progress has been reported by two groups, Chebotaev et al., and C. O. Weiss et al.. The independent results agree to 88 376 181 599.7 kHz within quoted relative uncertainties of about $1 \cdot 10^{-11}$ (compare appendix table A1 and A2).

Furthermore the recommendation CI-1983 takes over the realization of the former definition, however not as defining wave number, $1\,650\,763.73\,\text{m}^{-1}_{1960}$ but as a measured wavelength, $605\,780\,210\,\text{fm}_{1983}$. From these figures one can ascertain by calculation a relative continuity within $1 \cdot 10^{-9}$, corresponding to the earlier determined reproducibility of the ^{86}Kr standard lamp of $1 \cdot 10^{-9}$ too. The recommendation CI-1983 contains also 12 wavelength standards adopted earlier in 1962 (appendix table A1 and A2), including their rather high uncertainties and their excitation conditions.

The intention of this official recommendation is as follows: Anyone needs only to have a source of standard wavelength radiation excited under the specified experimental conditions, in order to be justified to apply the recommended values with their quoted uncertainties. He needs not to repeat a complicate and

expensive measurement of the frequency of his wavelength standard source. In the case of standard wavelength laser radiation a lot of comparison measurements preceded the recommendation. They comprise beat frequency recordings between differently developed stabilized lasers observing also several pairs of hyperfine structure components. In the case of a newly built up laser stabilization it became custom to get confirmation by comparison to other well established standard apparatus.

The development of several laser systems stabilized by saturated absorption of the iodine molecules gave cause to numerous investigations of hyperfine structures in $^{127}\text{I}_2$, $^{129}\text{I}_2$, and $^{127}\text{I}^{129}\text{I}$ molecular spectra, to the detection and classification of new transitions.

2.4 Realization of Material Lengths. Traceability of Industrial Measurements

The principle of length measurement by interferometry is very important as link between the two different kinds of length, a wavelength and a material length. It allows to compare these two kinds of length. The appropriate diffraction correction has fully to be taken into account, if necessary. The material length must be performed as the distance between two mirrors or between two positions of one mirror. The distance may be an interferometrically virtual one, like the difference of light paths in two interferometer arms. The shift of one mirror can be observed, e.g. as the shift between two positions of a photoelectric microscope aiming at two different marks on a scale, one after the other. Or the distance may be a real one, forming a step height in one arm of the interferometer with different light paths in different parts of the field of view. A block gage wrung to an auxiliary plate of the same material is an example of practical and widespread application.

Block gages make possible the immediate connection between wavelength and material length. They were technologically developed by C.E. Johansson in Sweden about 1900 followed by interferential metrology with special block gage interferometers, especially e.g. by Kösters. A reliable and ingenious apparatus is the

so-called “vacuum wavelength comparator” for block gages till to 1 m in length. It contains evacuated chambers in order to act at the same time as a refractometer. The Kösters interferometer types are characterized by his interference double prism that replacing the beam-dividing mirror of a Michelson interferometer. Because of that the interferometer arms are parallel and adjoining advantageous for homogeneous temperature.

Interferometry is a suitable and adequate basis for all practical purposes. Visual estimates of fringe fraction in the order of 0.02 ... 0.1 give already an uncertainty of $(0.02 \dots 0.1) \lambda/2 \approx 6 \dots 30 \text{ nm}$. The application of optoelectric aids allows even much higher precision or automatization as well.

A material standard once measured by interferometry is a standard for further comparisons of other material length or other standards. It is most obvious in this field, that every length measurement is a comparison between at least two objects. One object is always needed applied as a standard; the other ones are objects under test. In practice a broad branching exists with stepwise decreasing precision, decreasing effort, and increasing uncertainty. This is the wide field of length measurement in industry, craftsmanship, and trade. The traceability to the international unit of the SI system guarantees the uniformity and interchangeability of production within the stated uncertainty round the world.

3. Dissemination and Maintenance

3.1 Interferential Wavelength Comparisons

The basic relation $\lambda\nu = c_o$ (cf. section 4.2.3) comprises a formal parity of frequency and wavelength, in as much as an interferential wavelength comparison represents the same result as a frequency ratio measurement, $\lambda_1/\lambda_2 = \nu_1/\nu_2$. But in principle and in practice there is to make a distinction. Frequency ratio measurements, i.e. counting of oscillations in the same or in equal time intervals; become the more precise the longer the observation time has been chosen. Another limitation will

finally interfere coming from the finite reproducibility that means from the restricted constancy or from irregularities in the oscillation period. On the other side interferential wavelength comparison means in principle is counting of the vibrations of at least two radiations along the same path. For instance, this is performed by counting the fringes with an electro-optic detector during the shift of a mirror in the common path of the observed radiations (counting interferometer). In this method the counting of integers is not the problem for highest precision, but the determination of fraction, corresponding to the difference of both phases at the ends of the spatial interval against the counting of the occurrence of the same phase during the march past of the fringes. Sometimes integer counting is an auxiliary procedure only to get a preliminary value of the virtual distance of one mirror in two locally well defined positions.

The number of oscillations - integer and fraction - must be reduced to the number of wavelengths (cf. sections 4.2.3 and 4.1.5). In general this diffraction correction is not easy to determine. It is proportional to the square of λ and inversely proportional to the cross section of the beam. Therefore, a long interference path and a big cross section of the beam reduce the relative correction depending in detail on intensity distribution and wave front curvature within the cross section of the beam.

The only beam structure with theoretically well known and closed diffraction correction formulas is the Gaussian beam. In the case of a multiple-beam interferometer the last part of the resonance condition formula of a spherical cavity:

$$v_q = v_o \left(q + 1 + \frac{m + n + 1}{\pi} \arccos \sqrt{\left(1 - \frac{d}{r_1}\right) \left(1 - \frac{d}{r_2}\right)} \right) \quad (4)$$

just corresponds to the diffraction correction.

v_q resonance frequency of a mode matched wave,

v_o frequency distance between neighboring longitudinal resonant modes counted

by the integer q , $v_o = \frac{c_o}{2d}$

- m, n rectangular mode numbers (in metrology only $m = n = 0$ is of interest),
 d distance of mirrors along the optical axis of the cavity,
 r_1, r_2 radii of curvature of the spherical mirrors,
 q number of nodes in a standing wave between the mirrors, and
 $q + 1$ the order of interference as usual.

Any radiation with wavelength $\lambda = c_o/v_q$ being out of resonance with the cavity may be described by a non-integer q . It follows from Eq. 4 as diffraction correction:

$$d - (q + 1) \frac{\lambda}{2} = (m + n + 1) \frac{\lambda}{2\pi} \arccos \sqrt{\left(1 - \frac{d}{r_1}\right) \left(1 - \frac{d}{r_2}\right)}. \quad (5)$$

To resolve this equation for d it is practice and precise enough to insert a preliminary value for d in the right hand side.

The spherical cavity is most applied not as a length measurement device but as a frequency or mode analyzer of laser radiations. The theory of the diffraction correction is more complicate for the spherical cavity, if a solid aperture is introduced, most between the mirrors, as well as for the multiple-beam interferometer with plane mirrors, the elder and original Fabry-Perot.

On the other hand interferometry has an important advantage for wavelength measurement, it works in a broad band, e.g. with optics made of quartz from ultraviolet to infrared at 3.3 urn wavelength. Against that pure frequency methods have an extremely small band at disposal. Several laser frequency or wavelength standards taken into the list of recommended values (appendix table A1 and A2) have been determined with contributions of interferometry till now.

3.2 Wavelength Standards in Air

Interferential length measurements are most performed with light propagation in air. Exceptions are seldom or for the sake of precise ratio determinations of wavelengths in vacuum by special interferometer apparatus. Otherwise the actual refraction index of the air must be known in order to apply the correction at the value of wavelength standard in vacuum. The refractive index depends on the composition of the air and on the density. It is easier or more reliable to measure pressure and temperature instead of density and to measure differences of these parameters against standardized values. Therefore, it came to the practice to relate interferential length measurements to values of wavelength in a standard air.

Doing so the dispersion of the refractive index, $n(\lambda)$, is most important for the consistency of length measurement results with several standard wavelengths. In the course of decades, Edlén and united had been evaluated air refractive index determinations to a dispersion formula. In 1955 the “International Astronomical Union” (IAU) recommended this formula for general adoption:

$$(n - 1)_{\text{stand.air}} \cdot 10^7 = 643.28 + \frac{294981}{146 - \sigma^2} + \frac{2554.0}{41 - \sigma^2}, \quad (6)$$

with $\sigma = 1/\lambda_{\text{vac}}$, standard air having a pressure of “1 atm” (760 Torr = 101 325 Pa), a temperature of 15°C (!), and 0.03% volume CO₂ (corresponding to 0.23 Torr = 31 Pa partial pressure). Edlén observed new results and revised his formula in 1966.

A further conversion from this elder “spectroscopic” standard air to a “metrological” standard air, nearer to the conditions of practical length measurement, 20°C instead of 15°C and “10 mm Hg” (1333 Pa) instead of no water vapour, was generally performed. The main part of the conversion comes from a density factor. In another field of metrology, to take into account the buoyancy in air at mass comparisons with balances, density of air plays an important role. The responsible consulting committee (CCM, “Comité Consultatif pour la Masse et les Grandeurs Apparentées”) has compiled research and formulae and has recommended them for

application. The content of CO₂ in the atmosphere increases slowly but steady by combustion. Both aspects have been considered by Muijlwijk propagating “new standard conditions” for dry air, 20°C, 1000 hPa, and 0.04% CO₂, and giving revised and partly simplified formulae for application.

Wavelengths in standard air are intermediate length standards for the practice and may be calculated from wavelength standards in vacuum (cf. appendix table A1 and A2) and the refractive index according to:

$$\lambda_{\text{air}} = \lambda_{\text{vac}} / n_{\text{air}} \quad (7)$$

4. The Present Practical Realization of Metre

In 2003, BIPM publish an international report on “Practical realization of the definition of the metre, including recommended radiations of other practical frequency standards (2001)”. (Quinn, 2003) Some part that relate is follow.

4.1 Recommendation 1 (CI-2002). Revision of the practical realization of the definition of the metre by the Comité International des Poids et Mesures.

The CIPM recalling:

- that in 1983 the 17th Conférence Générale des Poids et Mesures (CGPM) adopted a new definition of the metre;
- that in the same year the CGPM invited the CIPM – to draw up instructions for the practical realization of the metre,
 - to choose radiations which can be recommended as standards of wavelength for the interferometric measurement of length and draw up instructions for their use,
 - to pursue studies undertaken to improve these standards and in due course to extend or revise these instructions;

- that in response to this invitation the CIPM adopted Recommendation 1 (CI-1983) (*mise en pratique* of the definition of the metre) to the effect:

- that the metre should be realized by one of the following methods:
(cf. section 4.2.1)

- that in all cases any necessary corrections be applied to take account of actual conditions such as diffraction, gravitation or imperfection in the vacuum;

- that in the context of general relativity, the metre is considered a unit of proper length. Its definition, therefore, applies only within a spatial extent sufficiently small so that the effects of the nonuniformity of the gravitational field can be ignored. In this case, the effects to be taken into account are those of special relativity only.

The local methods for the realization of the metre recommended in (b) and (c) provide the proper metre but not necessarily that given in (a). Method (a) should therefore be restricted to lengths l which are sufficiently short for the effects predicted by general relativity to be negligible with respect to the uncertainties of realization. For advice on the interpretation of measurements in which this is not the case, see the report of the Consultative Committee for Time and Frequency (CCTF) working group on the application of general relativity to metrology [1].

- that the CIPM had already recommended a list of radiations for this purpose;

recalling also that in 1992 and in 1997 the CIPM revised the practical realization of the definition of the metre;

4.2 Recommended radiations of stabilized lasers (quoted only concerned wavelength)

Absorbing molecule $^{127}\text{I}_2$, a_{16} , or f , component, $R(127)11-5$ transition.

The values

$$f = 473\,612\,353\,604 \text{ kHz}$$

$$\lambda = 632\,991\,212.58 \text{ fm}$$

with a relative standard uncertainty of 2.1×10^{-11} apply to the radiation of a He-Ne laser with an internal iodine cell, stabilized using the third harmonic detection technique, subject to the conditions:

- cell-wall temperature $(25 \pm 5)^\circ\text{C}$;

- cold-finger temperature $(15.0 \pm 0.2) ^\circ\text{C}$;
- frequency modulation width, peak-to-peak, $(6.0 \pm 0.3) \text{ MHz}$;
- one-way intracavity beam power (i.e. the output power divided by the transmittance of the output mirror) $(10 \pm 5) \text{ mW}$ for an absolute value of the power shift coefficient $\leq 1.0 \text{ kHzmW}^{-1}$.

These conditions are by themselves insufficient to ensure that the stated standard uncertainty will be achieved. It is also necessary for the optical and electronic control systems to be operating with the appropriate technical performance. The iodine cell may also be operated under relaxed conditions, leading to the larger uncertainty specified.

The source data are all given in respect to the BIPM4 laser standard frequency. The relative standard uncertainty includes the uncertainty in the absolute frequency measurement and the uncertainty obtained by comparing the different frequency standards with the BIPM4 standard. The CCL proposed that the recommended radiation for the R(127) 11-5 transition, using 633 nm He–Ne lasers, no longer correspond to the a13, or i, component, but is replaced by the a16, or f, component, which was decided by the CIPM 2002.

The CCL adopted a correction of the previous recommended frequency by +7 kHz, giving the frequency of the f component to be 473 612 353 604 kHz. The CCL also revised the coefficient of the tolerated one-way intra-cavity beam power influencing the average uncertainty of beat-frequency measurements between two stabilized lasers. This results in a combined uncertainty of $u_c = 10 \text{ kHz}$, corresponding to a relative uncertainty of $u_c/y = 2.1 \times 10^{-11}$. The grouped laser comparisons from national laboratories undertaken by the BIPM (1993–2000) confirm that the choice of a relative standard uncertainty of 2.1×10^{-11} is valid. This series of comparison is a key comparison BIPM.L-K10 and is reported on the BIPM web-site <http://www.bipm.org/kcdb>.

5. Multiple Beam Interference

The key understanding of Fabry-Perot Interferometer is the multiple beam interference. While others types of interferometer apply double beam interference, the FPI gives very sharp fringes depend on transmittance of mirrors coating.

5.1 Airy's Formula

Wyant, (2000) and Weisstein, (1996b) First, for the case of no absorption, considered the dielectric slab, which is infinite in extent. The geometry is then that of a Fabry-Perot étalon. Let a wave with electric field amplitude E impinge obliquely on a slab of thickness d with index of refraction n immersed in a medium with index of refraction $n_0 < n$ (Figure 1).

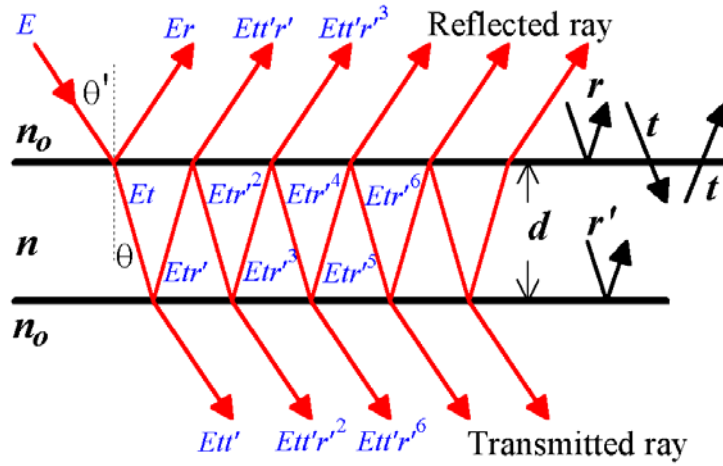


Figure 1 Transmission and reflection of dielectric slab

Let r and t be the internal amplitude reflection and transmission coefficients. And also r' and t' are the external amplitude reflection and transmission coefficients. Then the electric field amplitudes of the reflected rays are

$$E_{r1} = Er$$

$$E_{r2} = E_{tt'r'}e^{-i\delta}$$

$$E_{r3} = E_{tt'r'^3}e^{-2i\delta}$$

...

$$E_{rp} = E t t' r'^{(2p-3)} e^{-(p-1)i\delta}.$$

Where the phase difference between adjacent reflected rays is δ .

Reflected light

$$\begin{aligned} E_r &= E(r + t t' r' e^{-i\delta} + t t' r'^3 e^{-2i\delta} + \dots + t t' r'^{(2p-3)} e^{-(p-1)i\delta} + \dots \infty) \\ &= E\{r + t t' r' e^{-i\delta} (1 + r'^2 e^{-2i\delta} + \dots + (r'^2 e^{-2i\delta})^{(p-2)} + \dots \infty)\} \\ &= E\left\{r + t t' r' e^{-i\delta} \left(\frac{1}{1 - r'^2 e^{-2i\delta}}\right)\right\} \end{aligned} \quad (8)$$

Transmitted light

$$\begin{aligned} E_{t1} &= E t t' \\ E_{t2} &= E t t' r'^2 e^{-2i\delta} \\ E_{t3} &= E t t' r'^4 e^{-2i\delta} \\ &\dots \\ E_{tp} &= E t t' r'^{2(p-1)} e^{-(p-1)i\delta} \\ E_t &= E t t' + E t t' r'^2 e^{-2i\delta} + E t t' r'^4 e^{-2i\delta} + \dots + E t t' r'^{2(p-1)} e^{-(p-1)i\delta} + \dots \infty \\ &= E t t' (1 + r'^2 e^{-2i\delta} + r'^4 e^{-2i\delta} + \dots + (r'^2 e^{-2i\delta})^{(p-1)} + \dots \infty) \\ &= E \left(\frac{t t'}{1 - r'^2 e^{-2i\delta}} \right) \end{aligned} \quad (9)$$

5.2 Stokes Relations

Weisstein, 1996¹. Follow the Stokes Relations if there are no losses a wave's propagation must be reversible.

Stokes Relations:

$$X = E_{rr} + E_{tt'} \quad (10)$$

$$Y = Etr' + Ert. \quad (11)$$

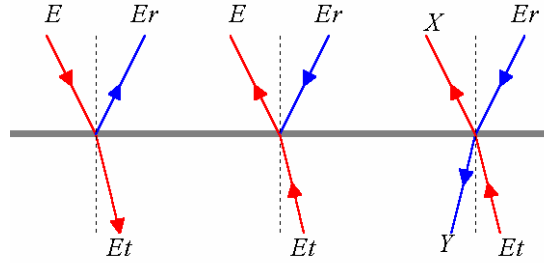


Figure 2 Reversibility by the Stokes Relations

To make the relations agree with real reflection and transmission, given $X = E$ and $Y = 0$. Equations derived from Stokes Relations are

$$tt' + r^2 = 1$$

$$tr' + rt = 0$$

$$tt' = 1 - r^2 \quad (12)$$

$$r = -r'. \quad (13)$$

5.3 Reflectance and Co-efficient of Finesse

Wyant, 2000. The reflectance is $R = r^2$ and Transmittance is $T = tt'$ where $T + R = 1$. Let F be the co-efficient of finesse

$$F = \frac{4R}{(1-R)^2}. \quad (14)$$

5.4 Reflected Light

Substitute (12), (13) and (14) into (8),

$$E_r = E \left\{ r + (1 - r^2)r e^{-i\delta} \left(\frac{1}{1 - r^2 e^{-i\delta}} \right) \right\}$$

$$E_r = Er \left(\frac{1 - r^2 e^{-i\delta} - e^{-i\delta} + r^2 e^{-i\delta}}{1 - r^2 e^{-i\delta}} \right)$$

$$I_r = E_r \cdot E_r^* = E^2 r^2 \frac{(1 + e^{-i\delta})(1 + e^{i\delta})}{(1 - r^2 e^{-i\delta})(1 - r^2 e^{i\delta})}$$

$$I_r = IR \frac{2 - 2 \cos \delta}{(1 + R)^2 + 2R \cos \delta}$$

$$I_r = I \frac{4R \sin(\frac{\delta}{2})^2}{(1 + R)^2 + 4R \sin(\frac{\delta}{2})^2} = I \frac{\frac{4R}{(1+R)^2} \sin(\frac{\delta}{2})^2}{1 + \frac{4R}{(1+R)^2} \sin(\frac{\delta}{2})^2}.$$

Then the Airy function of reflected light is

$$\frac{I_r}{I} = \frac{F \sin(\frac{\delta}{2})^2}{1 + F \sin(\frac{\delta}{2})^2}. \quad (15)$$

5.5 Transmitted Light

Substitute (12), (13) and (14) into (9),

$$E_t = E \left(\frac{1 - r^2}{1 - r^2 e^{-i\delta}} \right)$$

$$I_t = E_t \cdot E_t^* = E^2 \frac{(1 - r^2)^2}{(1 - r^2 e^{-i\delta})(1 - r^2 e^{i\delta})}$$

$$I_t = I \frac{(1 - R)^2}{(1 + R)^2 + 4R \sin(\frac{\delta}{2})^2} = I \frac{1}{1 + \frac{4R}{(1 - R)^2} \sin(\frac{\delta}{2})^2}.$$

Then the Airy function of transmitted light is

$$\frac{I_t}{I} = \frac{1}{1 + F \sin(\frac{\delta}{2})^2}. \quad (16)$$

5.6 Phase Due to OPD

Weisstein, (1996b). Phase difference between adjacent transmitted rays is Referring to Figure 3 is the phase advancement for one pass through the slab, and is the phase advancement in air which the transmitted ray undergoes in “catching up” to perpendicular of the transmitted ray at the point where it exits the slab. k_0 is the wave number in medium n_0 . A minus sign has been explicitly added to since it is the difference of the phases between adjacent rays which is significant.

Consulting Figure 3 gives $z = d \tan \theta$

$$d' = \frac{d}{\cos \theta}$$

$$h = 2z \sin \theta_0 = 2d \tan \theta \sin \theta_0 \quad (17)$$

Snell's law $n_0 \sin \theta_0 = n \sin \theta$

and
$$\frac{k_0}{n_0} = \frac{k}{n} \quad (18)$$

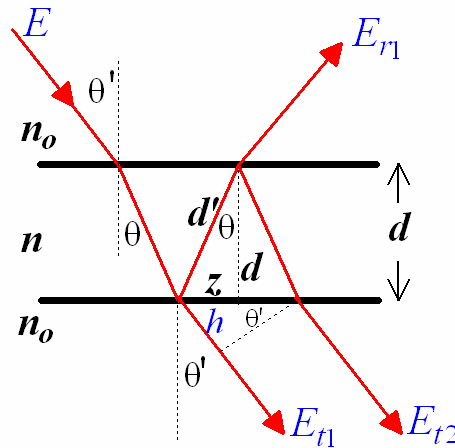


Figure 3 Diagram showing two adjacent parallel-transmitted rays for a Fabry-Perot étalon. This shows that the reflected and transmitted light is complementary.

Let's phase difference due to optical path d' is $\varphi = d'k$ and due to optical path h is $\varphi_o = d'k_o$. Then optical path difference (δ) between two adjacent parallel-transmitted rays is,

$$\begin{aligned}\delta &= 3\varphi - (\varphi + \varphi_o) = 2\varphi - \varphi_o \\ &= 2\frac{n}{n_o}d'k_o - hk_o = \frac{k_o}{n_o}(2d'n - hn_o). \quad (19)\end{aligned}$$

Replace (17), (18) into (19), $\delta = \frac{2\pi}{n_o\lambda_o}\left(\frac{2dn}{\cos\theta} - 2dn_o \tan\theta \sin\theta_o\right)$

$$\begin{aligned}&= \frac{4\pi d}{n_o\lambda_o}\left(\frac{n}{\cos\theta} - n_o \tan\theta \cdot \frac{n}{n_o}\sin\theta\right) \\ &= \frac{4\pi nd}{n_o\lambda_o \cos\theta}(1 - \sin^2\theta) = \frac{4\pi nd \cos\theta}{n_o\lambda_o}. \quad (20)\end{aligned}$$

Case the refractive index of the out side medium $n_o \approx 1$

$$\delta = \frac{4\pi nd}{\lambda_o} \cos\theta. \quad (21)$$

Case the refractive index of the out side medium and of the dielectric slab $n_o \approx n \approx 1$

$$\delta = \frac{4\pi d}{\lambda_o} \cos\theta. \quad (22)$$

Equation (21) always applies to the optical path difference of a plain mirrors air cavity Fabry-Pérot étalon. The mirrors separation or cavity length is d and the incidence angle is θ .

5.7 Discussion on the Airy Function

Wyant, 2000. If the transmitted ray undergoes constructive interference the path difference must equal to $m\lambda$. Consider equation (16), maximum of I_t/I is occur when $\sin(\delta/2) = 0$. Then,

$$(\delta/2) = m\pi = \frac{1}{2} \left(\frac{4\pi d}{\lambda_o} \cos\theta \right); \quad m = 0, 1, 2, \dots$$

$$2 n d \cos(\theta) = m\lambda \quad (23)$$

In case of scanning mirror Fabry-Perot etalon, assumed the incident ray perpendicular to mirror surface. Number of mode in the cavity is m . Every time the scanned distance d equal to multiple of λ the transmitted light is maximum. This is resonance condition of the cavity. The computer plot is shown in figure 04 and 05.

$$m = 2d/\lambda \quad (24)$$

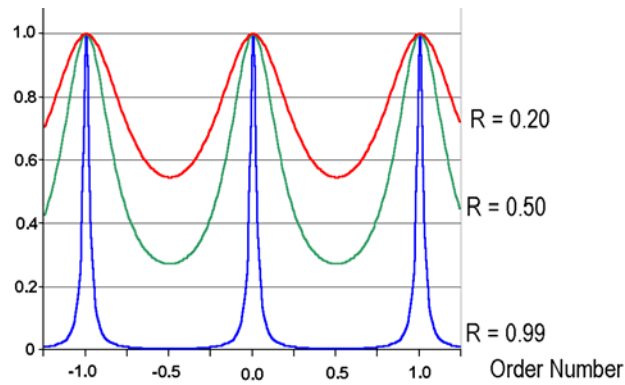


Figure 4 Plot of the transmission light

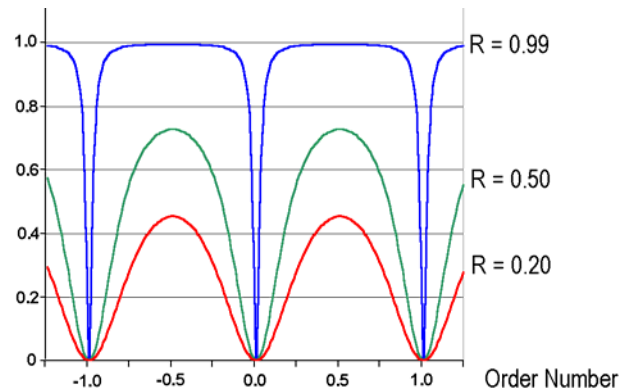


Figure 5 Plot of the reflected light

5.7.1 Low Reflectivity Approximations

If R is small, F is also small, and the equations for the reflected and transmitted light can be approximated as

$$\frac{I_r}{I} \approx F \sin^2\left(\frac{\delta}{2}\right) = \frac{F}{2}(1 - \cos \delta)$$

$$\frac{I_t}{I} \approx 1 - F \sin^2\left(\frac{\delta}{2}\right) = 1 - \frac{F}{2}(1 - \cos \delta).$$

These equations are the same as characteristic equation of two-beam interference. This means that the Fabry-Perot Interferometer, which made from low quality mirror, can give interference result as those two-beam interferometers.

5.7.3 Fringe Sharpness

Sharpness of fringes conveniently measured by their half intensity width which for transmitted light is the width between points on either side of maximum where intensity has fallen to half its maximum value. This calls Full Width at Half Maximum (FWHM; ϵ). The ratio between separation of the adjacent fringes and FWHM is finesse (\mathcal{F}).

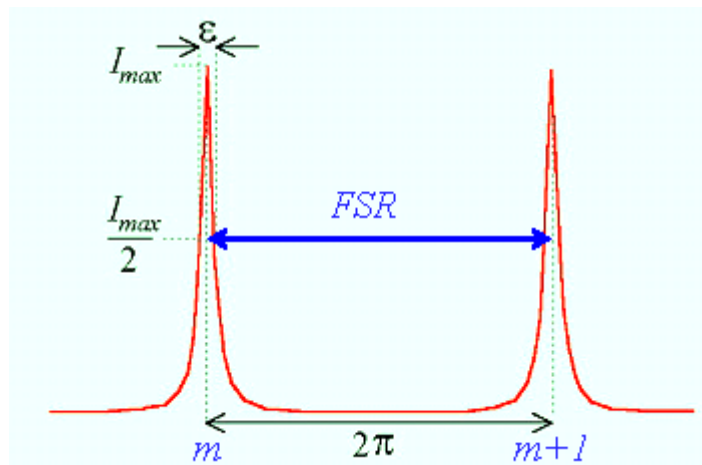


Figure 6 Illustrate the FWHM (ϵ) and FSR

$$\mathfrak{F} = \frac{2\pi}{\varepsilon}$$

For intensity at half max $\delta = 2m\pi \pm \frac{\varepsilon}{2}$

Thus $\frac{1}{2} = \frac{1}{1 + F \sin\left(\frac{\varepsilon}{4}\right)^2}$

If F is very large ε is small so $\sin\left(\frac{\varepsilon}{4}\right)^2 \approx \frac{\varepsilon}{4}$

Finesse $\mathfrak{F} = \frac{2\pi}{\varepsilon} = \frac{2\pi}{4/\sqrt{F}} = \frac{\pi}{2/\sqrt{F}} = \frac{\pi\sqrt{R}}{1-R} \quad (25)$

Equation (25) shows that Finesse is depended on reflectivity of the mirrors. Since reflectivity is physical property of mirror coating that varies as the wavelength change. Though, finesse also depended on wavelength.

5.7.4 Absorption of mirror coating

There are many reasons that cause the transmitted intensity differ from equation (16). If the two surfaces of the plate are identical, but there are losses, the value of I_t/I be determined as follows.

$$\delta = \frac{2\pi}{\lambda_0} 2nd \cos(\theta) + 2\phi \quad (26)$$

ϕ is the phase change upon reflection for each surface.

We can still write

$$\frac{I_t}{I} = \frac{T^2}{(1-R)^2 + 4R \sin(\delta/2)^2} = \frac{T^2}{(1-R)^2} \frac{1}{1 + F \sin(\delta/2)^2}$$

However, now we have losses of an amount A so we must write

$$R + T + A = 1 \quad \text{or} \quad T = (1 - R) - A$$

It follows that

$$\frac{I_t}{I} = \left(1 - \frac{A}{1-R}\right)^2 \frac{1}{1 + F \sin(\delta/2)^2}$$

then

$$T_{\max} = \left(1 - \frac{A}{1-R}\right)^2 = \left(\frac{1}{1 + A/T}\right)^2.$$

The effect of absorption is to reduce transmitted intensity and shift fringes. For the maximum transmitted intensity the important quantity is T . Even though A may be very small, if T is also small (R large), A/T may become large and the maximum transmitted intensity may be very small. As an example let $R = 99.7\%$ and $A = 0.2\%$, so T is approximately 0.1% . A/T is now 11% . However, let $R = 99.7\%$ and $A = 0.29\%$. Now T is 0.01% and A/T becomes 0.11% . What is happening physically is that while for each reflection there is very little loss, the reflectivity is so high that there are many effective reflections and the total loss becomes large.

While the phase shifts due to ϕ is normally not a problem at normal incidence there may be a problem at non-normal incidence because ϕ is a function of polarization. At normal incidence ϕ is equivalent to an increase of $\phi\lambda_0/2\pi$ in optical thickness of the plate.

The reflection case is more complicated because first reflection experiences no absorption. As a result the interference pattern does not go to zero.

5.8 Fabry-Perot

The multiple beam interference fringes from two highly reflecting surfaces illuminated near normal incidence are used in the classical Fabry-Perot interferometer. A Fabry-Perot interferometer is useful for spectroscopy.

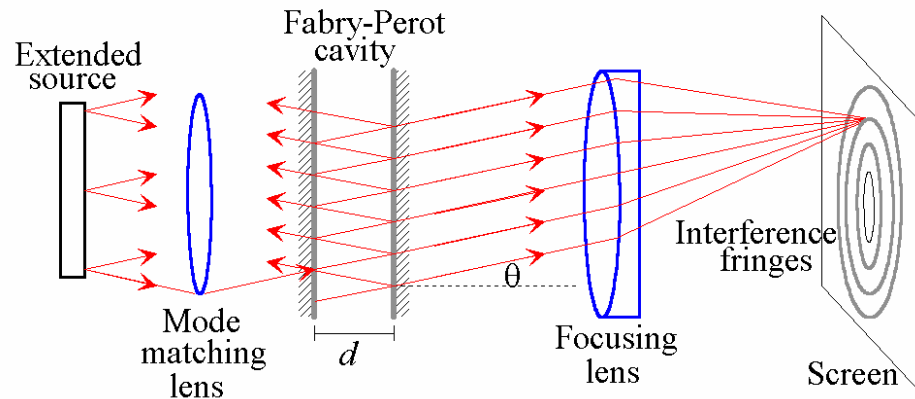


Figure 7 Fabry-Perot interferometer

Narrow bright circular fringes are obtained. For a bright fringe of order m

From (23)

$$m = \frac{\delta}{2\pi} = \frac{2nd \cos(\theta)}{\lambda_o} + \frac{\phi}{\pi}$$

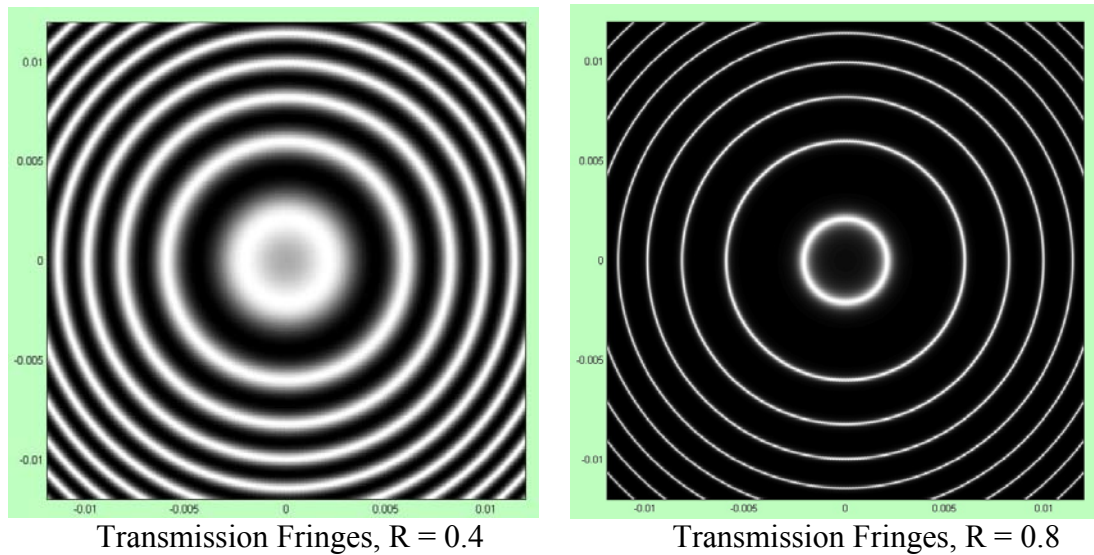


Figure 8 Plot of transmission interference pattern of Fabry-Perot interferometer which reflectance of 0.4 and 0.8. The figure is MatLab simulation (by Athikomkulchai et al. 2004).

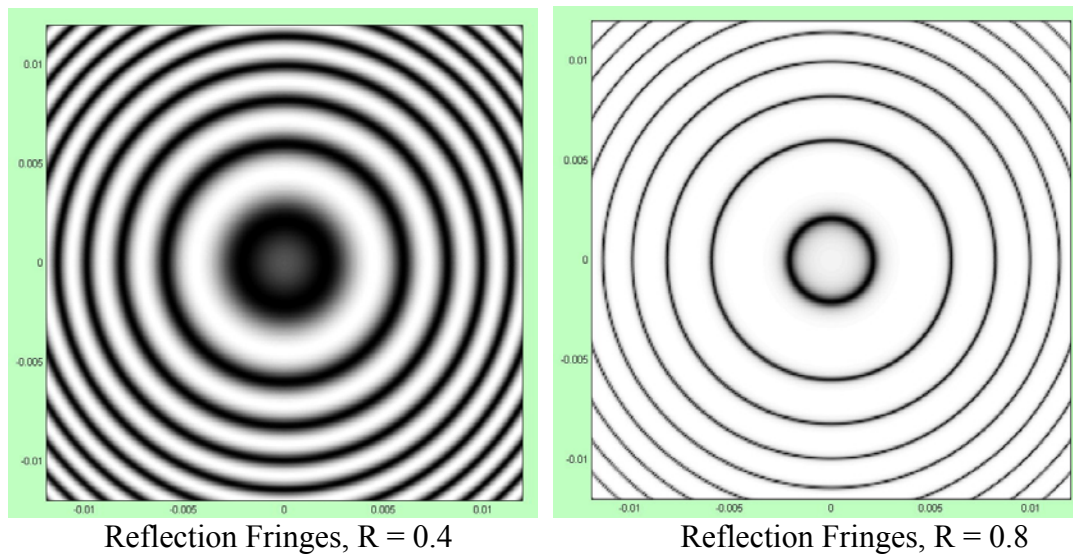


Figure 9 Plot of reflection interference pattern of Fabry-Perot interferometer which reflectance of 0.4 and 0.8. The figure is MatLab simulation (by Athikomkulchai et al. 2004).

5.8 Resolving Power

If more than one wavelength is present we see a superposition of the transmission pattern for each wavelength. Let there be two wavelengths present, λ_1 and $\lambda_2 = \lambda_1 + \Delta\lambda$. Our criterion for resolution is that the lines are just resolvable if the half maximum intensity of the peak of order m for one wavelength coincides with the half maximum intensity of the peak of order m for the second wavelength.

The left side of figure 10 shows the individual intensity contours of two Fabry-Perot fringes that are just resolved. The right side shows the two intensity contours added to give the observed effect.

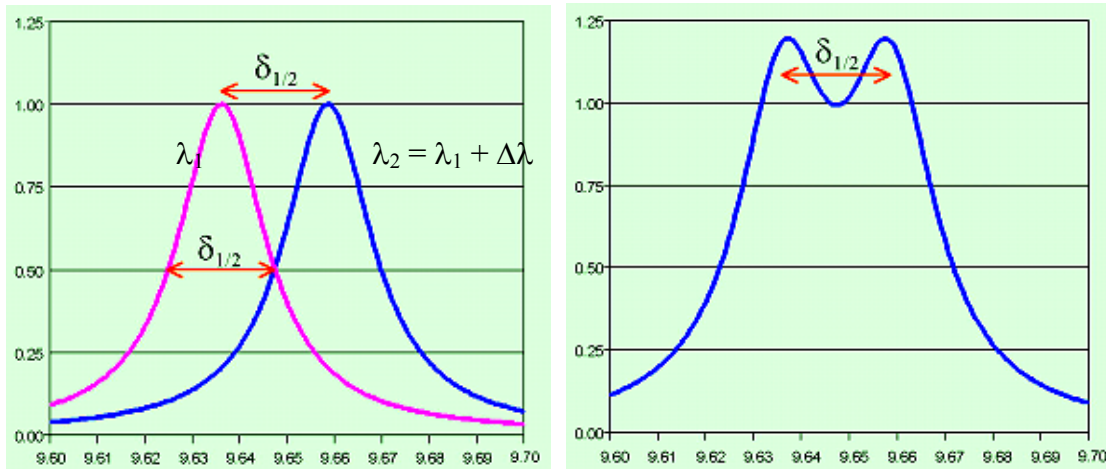


Figure 10 Plot of two wavelength λ_1 (589.600 000 nm) and λ_2 (589.399 850 nm) that satisfy the Rayleigh criterion of a Fabry-Perot etalon which finesse 199. The figure at right is superposition of the two wavelengths (the plot do not normalized).

It should be noted that some books such as Born & Wolf have a different criterion. They choose a separation such that the sum of the two intensities equals 0.811 that of the maximum. This agrees with the Rayleigh criterion that if we had a function the intensity maximum of one line would coincide with the minimum of the second line. Using this criterion we would get a resolution equal to 0.97 the resolution we get using our criterion.

The phase difference between the two interfering beams is

$$\delta = \frac{4\pi}{\lambda_o} nd \cos(\theta) + 2\phi$$

where 2ϕ is much smaller than $\frac{4\pi}{\lambda_o} nd \cos(\theta)$, then

$$\Delta\delta_{1/2} = \frac{2\pi}{\mathcal{F}}$$

$$\Delta\delta = \frac{1}{\lambda_o} \delta\Delta\lambda$$

$$\left| \frac{\lambda_o}{\Delta\lambda} \right| = \frac{\delta}{\Delta\delta} = \frac{2\pi m}{2\pi/\mathcal{F}} = m\mathcal{F}$$

resolving power $\frac{\lambda_o}{\Delta\lambda} = m\mathcal{F}$

near normal incidence $m \approx \frac{2nd}{\lambda_o}$

resolving power $\approx \frac{2nd}{\lambda_o} \mathcal{F}$ (27)

Thus the resolution is proportional to the mirror separation. As an example let the finesse be 200.00 ($R = 0.984415$), $nd = 10.000$ mm, $\lambda = 600.00$ nm, then the resolving power is 6.7×10^6 and $\Delta\lambda_{\text{res}}$ is 0.001 nm. The question is why not keep increasing the resolution by increasing the separation of the Fabry-Perot plates indefinitely? The problem is that we would have an overlapping of orders. The wavelength difference which overlapping takes place is called the free spectral range.

5.9 Free Spectral Range

Overlapping takes place when order m of wavelength $\lambda_2 = \lambda_1 + \Delta\lambda$ falls on top of order $m+1$ of wavelength λ_1

$$(m+1)\lambda_1 = m\lambda_2 = m(\lambda_1 + \Delta\lambda)$$

Thus

$$\Delta\lambda = \frac{\lambda}{m}$$

From (23) $\Delta\lambda_{\text{FSR}} = \frac{\lambda}{m} = \frac{\lambda^2}{2nd \cos[\theta]}$

Near normal incidence $\cos[\theta] \approx 1$

$$\Delta\lambda_{\text{FSR}} = \frac{\lambda^2}{2nd}$$

So increasing the resolving power by increasing the cavity thickness gives a reduction in the FSR.

$$\Delta\lambda_{\text{FSR}} = \frac{\lambda}{m}; \quad \Delta\lambda_{\text{res}} = \frac{\lambda}{m(\text{finesse})}$$

$$\frac{\Delta\lambda_{\text{FSR}}}{\Delta\lambda_{\text{res}}} = \text{finesse} = \frac{\pi\sqrt{F}}{2} = \frac{\pi\sqrt{R}}{1-R}$$

Most of commercial available Fabry-Perot is given a Free Spectral Range in term of frequency. From equation (21), by definition above, $\delta = 2\pi$ then $\lambda \rightarrow \Delta\lambda_{\text{FSR}}$

$$\delta = 2\pi = \frac{4\pi n d}{\lambda_{\text{FSR}}} \cos\theta.$$

$$\text{Thus, } \Delta\lambda_{\text{FSR}} = c / \Delta f_{\text{FSR}}; \quad \Delta f_{\text{FSR}} = \frac{c}{2nd \cos\theta}$$

Near normal incidence $\cos\theta \approx 1$

$$\Delta f_{\text{FSR}} = \frac{c}{2nd} \quad (28)$$

FSR usually has an order about GHz or MHz.

5.10 Scanning Fabry-Perot

The scanning Fabry-Perot is useful when only a few discrete wavelengths are present as is often the case with a laser. The scanning can be achieved by mounting one of the Fabry-Perot mirrors on a PZT. Since for a given fringe

$$2d = m\lambda; \quad 2\Delta d = m\Delta\lambda = \frac{2d}{\lambda}\Delta\lambda$$

$$\text{Thus} \quad \frac{\Delta d}{d} = \frac{\Delta\lambda}{\lambda} \quad (29)$$

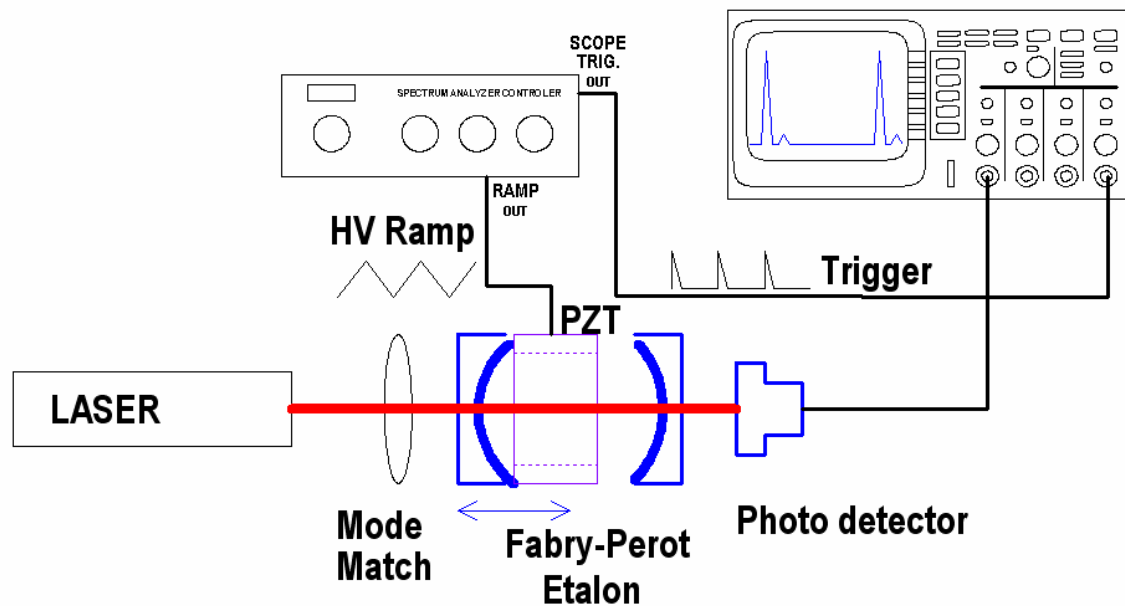


Figure 11 Scanning Fabry-Perot with controller and oscilloscope display

As d is varied different wavelengths will be transmitted through the Fabry-Perot and the oscilloscope display will show the wavelengths present.

5.11 Spherical Fabry-Perot

The figure below shows one form of a spherical Fabry-Perot. In the drawing the lower half of each spherical mirror is totally reflecting and the upper half is semi-transparent. The center of curvature of each mirror is located on the opposite mirror.

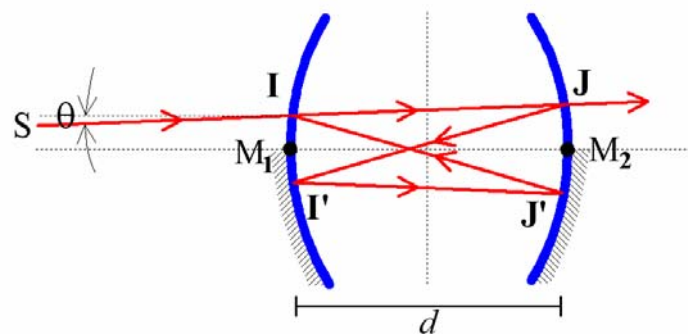


Figure 12 Spherical Fabry-Perot

In the paraxial region the path difference between the initial ray IJ and ray $IJJ'I'J$ is equal to $4d$, where d is the distance between M_1 and M_2 .

Instead of obtaining a series of parallel emerging rays originating from a single incident ray, as is the case with a plane parallel plate Fabry-Perot, we have a series of overlapping rays traveling along JT . The phase difference between consecutive rays is given by

$$\phi = \frac{2\pi}{\lambda}(4nd) \quad (30)$$

which is independent of the inclination of the rays and their azimuth within the limits of the Gaussian approximation.

The intensity expression is the same as for a regular parallel plate Fabry-Perot, except we have a flat tint all over the field. If rays are inclined to the axis third-order aberrations produce variations of the path difference and we find the flat tint surrounded by circular fringes. We can reduce aberrations by placing two identical circular diaphragms centered on M_1 and M_2 .

This interferometer is well suited to the large path differences corresponding to a high spectral resolution. Also, the Free Spectral Range from equation (28) can be rewritten as,

$$\Delta f_{\text{FSR}} = \frac{c}{4nd}. \quad (31)$$

6. Wavelength Measurement with OSA

There are at least two methods for wavelength measurement with OSA. The first, may be called the absolute method, this method the exact cavity length or number of mode must be known. The second is relative method, this method the unknown wavelength is compared to the reference wavelength.

6.1 Direct Method

Suppose initial length of a cavity of a scanning confocal Fabry-Perot interferometer is d_0 . One mirror of the FPI attached to a piezo actuator which extension coefficient α_V nm/V. High voltage ramp which amplitude V_A volt and rise time t_r is applied to the piezo actuator. A reference light source such as a frequency stabilized single mode HeNe , 632.8 nm, is aligned normally through optical axis of the FPI. From equation (23) and (40) yield; $4nd = m\lambda$ or

$$d = \frac{m\lambda}{4n} \quad (32)$$

The first transmit beam is occurred when the cavity length is the multiple of $\lambda/4$, as shown in figure 13. At that instant, the cavity length is d_0 and resonance mode is m_0 . At the ramp voltage increased, the next pulse beam is occurred at cavity length d_1 and resonance mode m_1 , and so on.

$$d_0 = \frac{\lambda}{4n} m_0 \quad (33)$$

$$d_1 = \frac{\lambda}{4n} m_1 \quad (34)$$

$$d_2 = \frac{\lambda}{4n} m_2 \quad (35)$$

...

$$d_i = \frac{\lambda}{4n} m_i \quad (36)$$

The cavity length extension Δd_i is

$$\Delta d_i = d_i - d_0 = \alpha_V \text{ (nm/V)} \cdot S \text{ (V/s)} \cdot \Delta t_i \text{ (s)}.$$

Where S is slew rate of ramp (V_A/t_r) and Δt_i time interval between the first transmitted beam peak and the i^{th} peak read out from oscilloscope. The initial

length of the cavity, d_o , is inconvenient to determine so that the initial mode number m_0 . Then difference equations are formed as;

$$\Delta t_i = \frac{\lambda}{4n \cdot \alpha_V \cdot S} \Delta m_i \quad (37)$$

Where $\Delta m_i = m_i - m_0$, this is a relative mode number that running from 0, 1, 2, .. i , to j . ' j ' is the last mode number in this rise time period of this ramp. The separation of i^{th} transmitted peak, $\Delta t_i = t_i - t_0$, is corresponded to the relative mode number. If there are j peaks occurred in one period of rise time as shown in figure 13, then

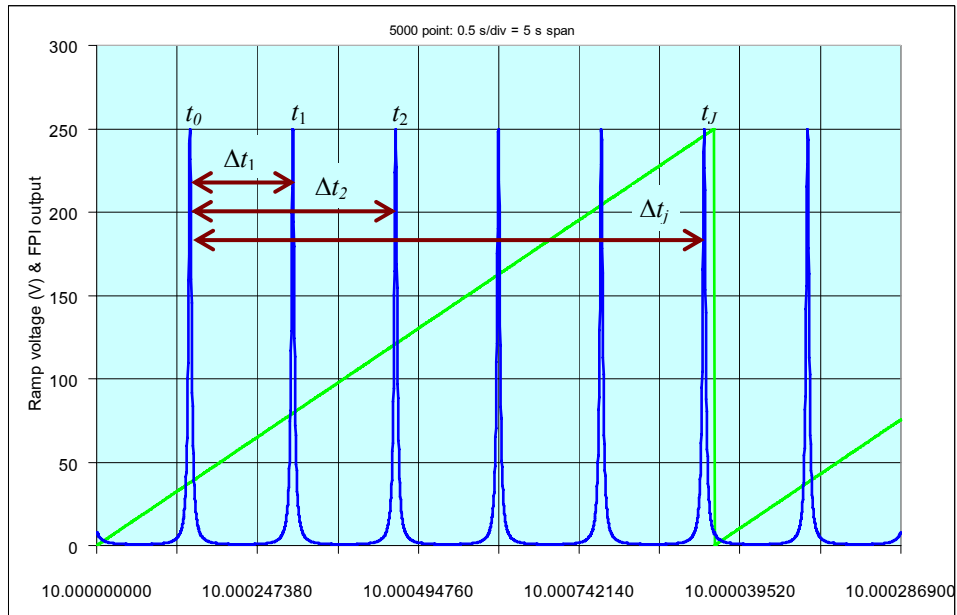


Figure 13 Computer simulation show successive interference beam transmitted from a FPI cavity of 10.000 000 000 mm, while applied ideal ramp voltage amplitude 250.000 000 V and 4.000 000 s rise time

for $i = 0$;

$$0 = \frac{\lambda}{4n \cdot \alpha_V \cdot S} \cdot 0 \quad (38)$$

$$\begin{aligned}
&\text{for } i = 1; & \Delta t_1 &= \frac{\lambda}{4n \cdot \alpha_v \cdot S} \cdot 1 \\
& & \dots & \\
&\text{for } i = j; & \Delta t_j &= \frac{\lambda}{4n \cdot \alpha_v \cdot S} \Delta m_j
\end{aligned} \tag{39}$$

Equations (36) to (37) are linear modeling, which each pair of i and Δt_i are linearly independent on each measurement. Linear least-squares method is applied to find the solution. If column matrix $\mathbf{Y} = [\Delta t_i] = [0 \ \Delta t_1 \ \Delta t_2 \ \dots \ \Delta t_j]^T$ and column matrix $\mathbf{X} = [\Delta m_i] = [0 \ 1 \ 2 \ \dots \ j]^T$ and $a = \lambda / 4n \cdot \alpha_v \cdot S$ is assigned. The matrix form is;

$$\mathbf{Y} = a \mathbf{X}.$$

Then, $\mathbf{X}^T \mathbf{Y} = a(\mathbf{X}^T \mathbf{X})$

$$a = [\mathbf{X}^T \mathbf{X}]^{-1} \mathbf{X}^T \mathbf{Y} \tag{40}$$

In most case of linear least squares ‘ a ’ always 1×2 matrix and \mathbf{X} is $n \times 2$ matrix, n are numbers of measurement result. In case of difference equation, graph always intercept at the origin, so that, ‘ a ’ is scalar. Equation (38) can explicitly express to

$$\begin{aligned}
\mathbf{X}^T \mathbf{X} &= [0 \ 1 \ 2 \ \dots \ j] \begin{bmatrix} 0 \\ 1 \\ 2 \\ \vdots \\ j \end{bmatrix} \\
&= (0 + 1^2 + 2^2 + \dots + j^2) = \sum_{i=0}^j i^2 \\
\mathbf{X}^T \mathbf{Y} &= [0 \ 1 \ 2 \ \dots \ j] \begin{bmatrix} 0 \\ \Delta t_1 \\ \Delta t_2 \\ \vdots \\ \Delta t_j \end{bmatrix}
\end{aligned}$$

$$= (0 + \Delta t_1 + 2\Delta t_2 + \dots + j \cdot \Delta t_j) = \sum_{i=0}^j i \cdot \Delta t_i .$$

Then

$$a = \frac{\sum_{i=0}^j i \cdot \Delta t_i}{\sum_{i=0}^j i^2} \quad (41)$$

From (39) the wavelength λ is evaluated

$$\lambda = 4n \cdot \alpha_v \cdot S \cdot \frac{\sum_{i=0}^j i \cdot \Delta t_i}{\sum_{i=0}^j i^2} \quad (42)$$

To evaluate the uncertainty, 'a' is considered as a slope of graph of Δm_i (x-axis) vs. Δt_i (y-axis). Δm_i are integers, so, considered counting error is zero. If Δt_i is the measure data point and $\Delta t_i'$ is the point on graph line then error is

$$\text{Error} = \Delta t_i - \Delta t_i'$$

where

$$\Delta t_i' = \Delta m_i \cdot a = \Delta m_i \cdot \frac{\sum_{i=0}^j i \cdot \Delta t_i}{\sum_{i=0}^j i^2} .$$

Then standard deviation of Δt_i is

$$\text{S.D.}(\Delta t_i) = \sqrt{\frac{\sum_{i=0}^j \{(\Delta t_i - \Delta t_i') - (\Delta t_i - \Delta t_i')\}^2}{j-1}} \quad (43)$$

6.2 Comparison Method

Wavelength comparison or relative method is quick measurement from oscilloscope read out, so that the accuracy is limited. The instrument setup is shown in figure 14.

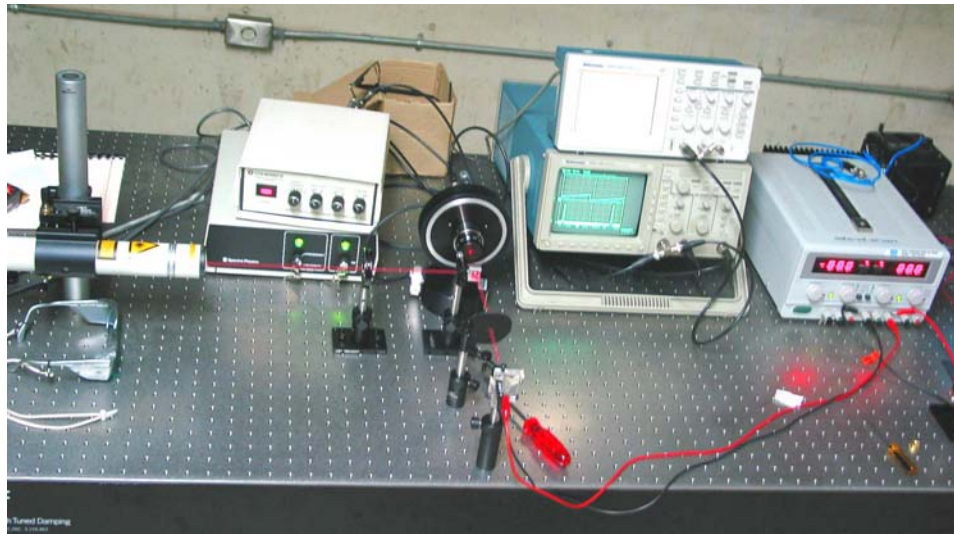


Figure 14 Instruments setup for relative wavelength measurement

At left hand side is stabilized HeNe laser, as a reference source, and at the bottom is commercially diode laser (Laser Pointer), as a unknown wavelength source. A laser beam from the two source are aligned in to the OSA by using a beam splitter.

Figure 15 is computer simulation of FPI which cavity length 10.000 mm, reflectance 0.99 (finesse 312.6). The simulation window shows adjacent output peak of laser wavelength 632.8 nm at relative mode number $m = 0$ and 1. The cavity length separation between the two peak is the Free Spectral Range. In case of confocal FPI the separation is $\lambda/4$.

If an unknown wavelength beam is aligned co-incident to the OSA and its wavelength is closed to the reference wavelength. The unknown wavelength is able to

estimate from separation distance from peak of the reference wavelength. In order to avoid confusing wavelength difference must less than $\lambda/8$.

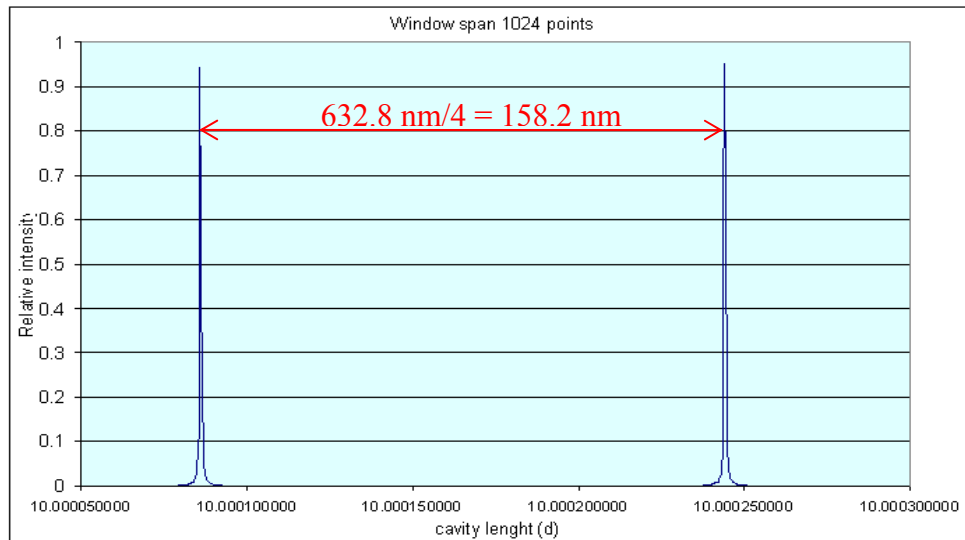


Figure 15 Computer simulation of FPI which cavity length 10.000 mm, reflectance 0.99 (finesse 312.6). Separation between two adjacent peak is FSR equivalent to $\lambda/4$.

Horizontal axis of oscilloscope screen is time scale depend on time/div setting. Equation (29) is applied to evaluate value of the unknown wavelength.

7. Spectral source

7.1 Spectrum of HeNe Laser

On Hyperphysics web site, a brief description of helium-neon lasing is given. Nave (2005) The most common and inexpensive gas laser, the helium-neon laser is usually constructed to operate in the red at 632.8 nm. It can also be constructed to produce laser action in the green at 543.5 nm and in the infrared at 1523 nm.

One of the excited levels of helium at 20.61 eV is very close to a level in neon at 20.66 eV, so close in fact that upon collision of a helium and a neon atom, the

energy can be transferred from the helium to the neon atom. Helium-neon lasers are common in the introductory physics laboratories, but they can still be dangerous! An unfocused 1-mW HeNe laser has a brightness equal to sunshine on a clear day (0.1 watt/cm^2) and is just as dangerous to stare at directly.

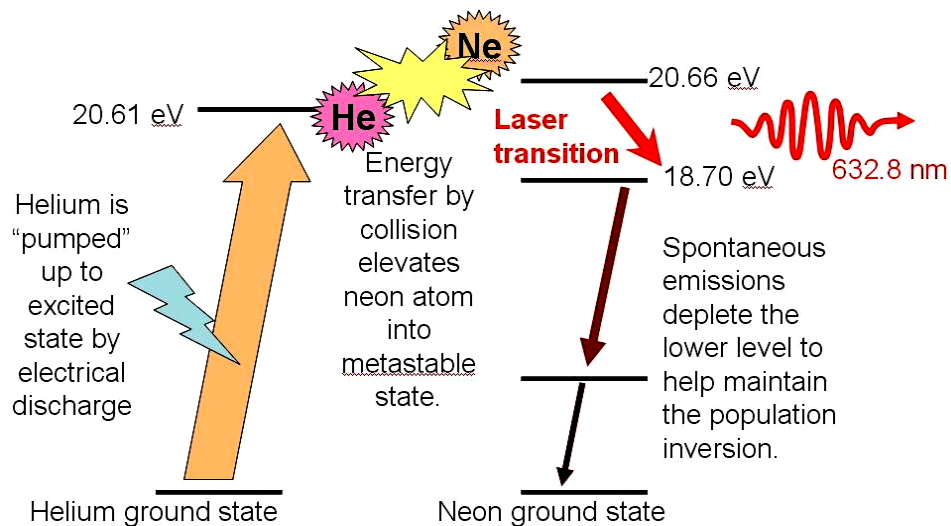


Figure 16 The helium-neon laser lasing process

The helium gas in the laser tube provides the pumping medium to attain the necessary population inversion for laser action. Helium-Neon Laser

On Sam's laser web site, they discuss and give may information about helium-neon laser spectrum. Goldwasser, (2005) The HeNe laser depends on energy level transitions in the neon gas. In the case of neon, there are dozens if not hundreds of possible wavelength lines of light in this spectrum. Some of the stronger ones are near the 632.8 nm line of the common red HeNe laser - but this is not the strongest:

The strongest red line is 640.2 nm. There is one almost as strong at 633.4 nm. That's right, 633.4 nm and not 632.8 nm. The 632.8 nm one is quite weak in an ordinary neon spectrum, due to the high energy levels in the neon atom used to produce this line. See: Bright Line Spectra of Helium and Neon. (The relative brightnesses of these don't appear to be accurate though at present.) The comment

about the output wavelength not being one of the stronger lines is valid for most lasers as if it were, that energy level would be depleted by spontaneous emission, which isn't what is wanted! There are also many infra-red lines and some in the orange, yellow, and green regions of the spectrum as well.

There are many possible transitions in neon from the excited state to a lower energy state that can result in laser action. The most important (from our perspective) are listed in Appendix table 3.

7.2 Laser Diode: Laser Pointer

The first semiconductor laser diode was demonstrated by Dr. Robert N. Hall, the team headed, on Sunday, September 16, 1962, at the General Electric Research Development Center in Schenectady, New York. (Dupuis, 2003) That GaAs laser diode lasing spectrum in infrared range. The achievement of the first 300°K continuous wave diode laser was reported in Investigation of the influence of the AlGaAs-GaAs heterostructure parameters on the laser threshold current and the realization of the continuous emission at the room temperature by Dmitri Garbuzov in 1964. No document was found that who's claim the first invention of laser diode pointer but after 1990 development of inexpensive red laser diode, key chain laser pointer is commercially available.

Goldwasser, (2006b) describe explicit detail about laser diode on Sam's Laser FAQ website. In the old days, a stick was using to point out something on a screen or blackboard. The earliest optical pointers used tiny incandescent bulbs, a lens, and mask or transparency to project a dot or an arrow. Such devices were about as big as a full size (D-cell) flashlight. It required a separate power pack attached by wires or probably plugged into the wall.

The first laser pointers used helium-neon lasers with their high voltage power supplies packaged as compactly as possible but still required a separate power pack or bulky case which included heavy batteries.

The real laser pointer revolution was come as a result of the development of inexpensive visible laser diodes. Laser diodes are only slightly larger than a grain of sand, run on low voltage low current, and can be mass produced - originally driven by the CD player/CDROM revolution, barcode scanners, and other applications where a compact low cost laser source is needed. Now manufactured by the millions, these laser diodes cost well under \$1.

A laser diode is a semiconductor device, formed by doping a very thin layer on the surface of a crystal wafer. The crystal is doped to produce an n-type region and a p-type region, one above the other, resulting in a p-n junction, or diode.

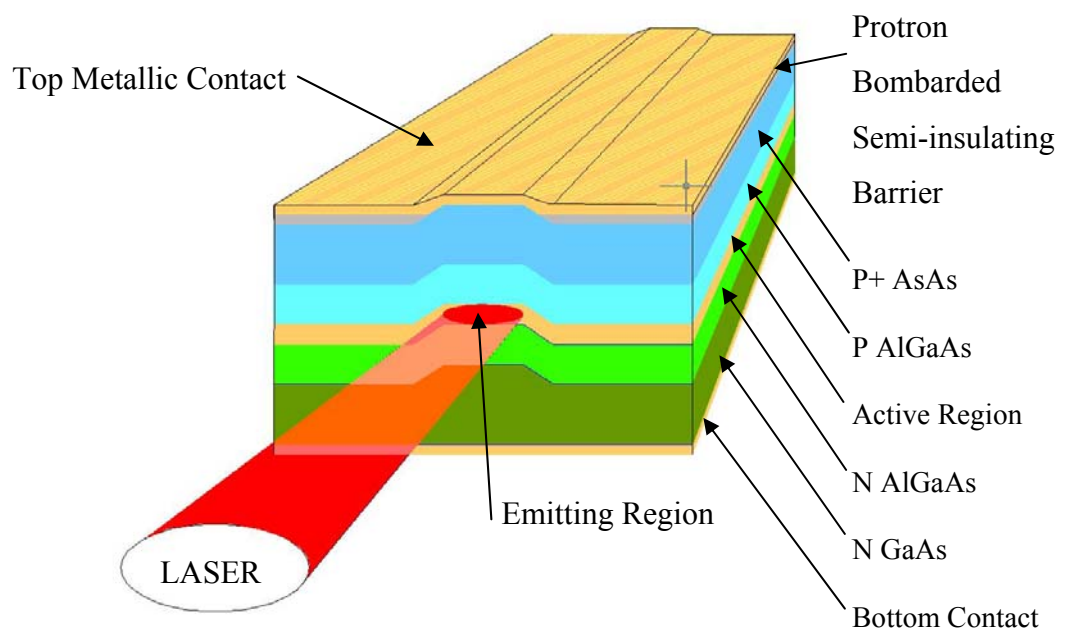


Figure 17 Basic structure of Laser Diode

When this structure is forward biased, holes from the p-region are injected into the n-region, where electrons are the majority carrier. Similarly, electrons from the n-region are injected into the p-region, where holes are the majority carrier. When an electron and a hole are present in the same region, they may recombine by spontaneous emission, that is, the electron may re-occupy the energy state of the hole,

emitting a photon with energy equal to the difference between the electron and hole states involved.

These injected electrons and holes represent the injection current of the diode, and spontaneous emission gives the laser diode below lasing threshold. Spontaneous emission is necessary to initiate laser oscillation, but it is a source of inefficiency once the laser is oscillating.

Under suitable conditions, the electron and the hole may coexist in the same area for quite some time (on the order of microseconds) before they recombine. Then a nearby photon with energy equal to the recombination energy can cause recombination by stimulated emission. This generates another photon of the same frequency, travelling in the same direction, with the same polarization and phase as the first photon. This means that stimulated emission causes gain in an optical wave (of the correct wavelength) in the injection region, and the gain increases as the number of electrons and holes injected across the junction increases. The spontaneous and stimulated emission processes are vastly more efficient in direct band-gap semiconductors than in indirect band-gap semiconductors, thus silicon is not a common material for laser diodes.

As in other lasers, the gain region is surrounded with an optical cavity to form a laser. In the simplest form of laser diode, an optical waveguide is made on that crystal surface, such that the light is confined to a relatively narrow line. The two ends of the crystal are cleaved to form perfectly smooth, parallel edges, forming a Fabry-Perot resonator. Photons emitted into a mode of the waveguide will travel along the waveguide and be reflected several times from each end face before they are emitted. As a light wave passes through the cavity, it is amplified by stimulated emission, but light is also lost due to absorption and by incomplete reflection from the end facets. Finally, if there is more amplification than loss, the diode begins to "lase".

Some important properties of laser diodes are determined by the geometry of the optical cavity. Generally, in the vertical direction, the light is contained in a

very thin layer, and the structure supports only a single optical mode in the direction perpendicular to the layers. In the lateral direction, if the waveguide is wide compared to the wavelength of light, then the waveguide can support multiple lateral optical modes, and the laser is known as "multi-mode". These laterally multi-mode lasers are adequate in cases where one needs a very large amount of power, but not a small diffraction-limited beam; for example in printing, activating chemicals, or pumping other types of lasers.

Table 1 Wavelength and brightness comparison for some commercial laser pointer

Wavelength	Relative	Factor	Color	Type
555 nm	1.000	33	Green	Reference peak
543.5 nm	0.974	30	"	Green HeNe laser
532 nm	0.885	28	"	Green DPSS laser
632.8 nm	0.237	8	Orange-red	Red HeNe laser
635 nm	0.217	7	"	Red diode laser
640 nm	0.175	5	"	"
650 nm	0.107	3	Red	"
660 nm	0.061	2	"	"
670 nm	0.032	1	"	"

Note: The term "Relative" refers to the visibility compared to the 555 nm peak of human vision; the "factor" compares the brightness to that of an older 670 nm pointer. Note that visual perception of brightness is not linear. Thus, a 1 mW 532 nm green laser pointer isn't actually going to appear 28 times brighter than a 1 mW 670 nm red model. What it means is that a 1 mW green pointer will appear similar in brightness to a 28 mW 670 nm red one (if such a thing existed).

Source: Goldwasser (2006b)

Some companies that sell laser pointers, rate them in terms of 'equivalent brightness' compared to a 670 nm device. The Mark-I eyeball is about 7 times more sensitive to light at 635 nm compared to 670 nm. So that, Green laser pointers at 532 nm will multiply this by another factor of 4 or 5. For example, several of these companies offer laser pointers with a '30 mW equivalent' output. This just means they are comparing a 635 nm device optimistically to one of 670 nm. The actual output power is still less than 5 mW. Here is a handy quick comparison chart for common and not so common laser pointer wavelengths:

MATERIALS AND METHODS

MATERIALS

1. The Optical Spectrum Analyzer System

To day, there are many type of Optical Spectrum Analyzer available for matching any fields of optical work. This spectrum analyzer is used to examine the fine details of the line spectra of CW lasers. Such detail is usually due to the laser operating in more than one longitudinal or transverse mode of the laser cavity. Thought, the confocal Scanning Fabry-Perot Interferometer is selected. The OSA system include the OSA head model 240, the controller model 251, the optical detector and some of others optical instruments.



Figure 18 Optical Spectrum Analyzer (OSA) System

1.1 Optical Spectrum Analyzer model 240

Coherent, (n.d.) The analyzer is scanning double concave-mirror Fabry-Perot cavities. A ramp-scan voltage is applied to a piezoelectric section of the mirror spacer to vary the separation of the two mirrors by a small amount, and hence change the cavity resonant spectral frequency. The two mirrors are mounted in the confocal

configuration to make the system easy to use and provide for an unambiguous set of transmitted spectral maxima and minima, detected visually or by a photo-detector connected to an oscilloscope. The user-provided oscilloscope is synchronized to the cavity scan rate to display the spectrum of laser line structure variation with frequency across the screen.

The Free Spectral Range (FSR) of a spectrum analyzer is the maximum optical spectral span created by the variation of the separation of the two mirrors as the piezoelectric spacer is repeatedly ramped. It is dependent on the mirror mean separation d , as $FSR = c/4d$ in frequency units. The mirror pairs and tube-assemblies are chosen to provide a choice of FSR values 7.5 GHz. These correspond to wavelength ranges of 0.01 nm at 635 nm. Clearly these are ultrahigh resolution instruments.

If the chosen FSR is too small for the line structure to be examined, then there will be a confusion of overlapping spectra on the screen. If the chosen FSR is too large, then the effective resolution will be decreased. Since the effective resolving power is the ratio (FSR/F) where F is the instrument Finesse (>200 for this system). Thus, the resolving power is about 10 MHz.

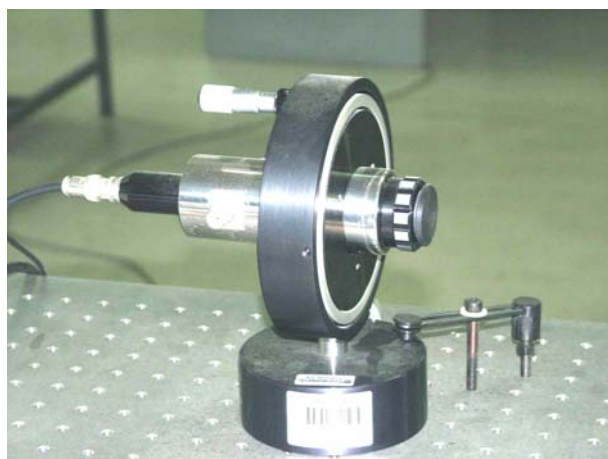



Figure 19 Optical Spectrum Analyzer model 240

The spectrum analyzer systems consist of a mirror set, spacer-tube and lens assembly, detector and adjustable mount. A laser beam can be transmitted straight into the spectrum analyzer, or optional beam splitters are available to deflect only ~10% of a beam into the analyzer. These beam splitters (16 mm aperture) attach to the front of the spectrum analyzer and allow 90% of the beam to continue uninterrupted.

Specifications				
Free Spectral Range:	7.5 GHz	1.5 GHz	30 GHz	300 MHz
Cavity Type:	1 cm confocal	5 cm confocal	1/4 cm confocal	25 cm confocal
Finesse:	>200	>200	>100	>200
Instrumental Bandwidth:	37.5 MHz	7.5 MHz	300 MHz	1.5 MHz
Aperture:	4.3 mm	7.5 mm	2.0 mm	10.0 mm

Piezoelectric Motion: ~4 nm/volt
Volts per FSR at 600 nm (nominal): 37.5 volts
Maximum Voltage: 450 VDC
Crystal Capacitance: 0.04 μ F
Maximum Sweep Rate: 1-2 msec
Scan Non-linearity: 2% at 100 VDC


ISO 9002 Certified



COHERENT®
AUBURN DIVISION

A Member of Coherent Photonics Group

USA



2303 Lindbergh Street
Auburn, CA 95602
Toll Free: 1-800-343-4912
Tel: (530) 889-5365
Fax: (530) 889-5366
<http://catalog.CoherentInc.com>

Figure 20 Specification of OSA model 240 from its brochure

MODEL 240 OPERATOR MANUAL	A-800009 (A)	PAGE 11 of 28
3. PERFORMANCE AND OPERATING SPECIFICATIONS		
TABLE I		
NOMINAL SPECIFICATIONS FOR THE		MODEL 240
SPECTRUM ANALYZER		
Free Spectral Range	_____	1500 Mhz (or 7500 Mhz)
Instrumental Bandwidth	_____	75 Mhz (or 37.5 Mhz)
Spectral Resolving Power	_____	8 x 10
Finesse	_____	200
Spectral Region Covered	_____	4500A-5500A; 6000A-7000A; or 1.05-1.15u.
Peak Instrumental Transmission	_____	20% to 30% (?)

Figure 21 Specification of OSA model 240 from its manual

This spectrum analyzer is supplied with a 4.3 mm aperture lens to match the laser beam to the input aperture of the 1 cm confocal cavity. The combination of this confocal design gives the (nominal) instrumental band width of 37.5 MHz and 7.5 GHz free spectral range.

The most importance parameter, which effect to wavelength measurement, is the cavity length. In case of the confocal the cavity length is equal to radius of the confocal mirrors. (cf. section 4.5.11)

From equation (31) free spectral range (Δf_{FSR}) of the confocal Fabry-Perot is 7.5 GHz and refractive index of air (n) is 1.00027 (from section 4.1.5), then the cavity length d is

$$\begin{aligned} d &= \frac{c_o}{4n(\Delta\lambda_{FSR})} \\ &= \frac{299\,729\,458\,(\text{ms}^{-1})}{4 \cdot 1.00027 \cdot 7.5 \times 10^9\,(\text{s}^{-1})} \\ &= 0.00999038\,\text{m}. \end{aligned}$$

This calculation shows that the actual cavity length is a little bit difference, 9.6 μm , from the nominal size from specification. The expansion of cavity controlled by a piezo actuator which nominal coefficient about 4 nm/V. The OSA controller supply maximum ramp amplitude about 250 Volt, then maximum displacement of the cavity is 1 μm nominally.

1.2 OSA Controller model 251

Coherent, (n.d. b) The Spectrum Analyzer Controller connects between the laser spectrum analyzer and a oscilloscope which bandwidth more than 20 MHz. The controller provides the required ramp voltage, 0-250 VDC, for spectral scan. It also allows full control of the scan time form 10 ms to 5 s and variable amplitude to control spectral range. In addition, the controller provides the required conditioning and signal amplification for the detector, and synchronization of the oscilloscope trace to the detector signal.



Figure 22 The OSA controller model 251

A convenient zoom function is integrated into the controller that allows 1, 2, 5, 10, 20 and 50X increase of the spectral display resolution. The controller is 115/230 VAC selectable and is supplied with detachable AC mains cord, manual and cables.

1.3 Sensor: Silicon PIN Photo Diode

There are many kind of optical detector available in market today, but silicon PIN Photo Diode is the low cost high sensitivity and very practical detector. The letter I is designated for “Intrinsic” like the latter P and N are for “Positive” and “Negative” type semiconductor. This means that the photo diode has an intrinsic layer between P and N layer. Most PIN photodiodes are made from silicon and as shown on Figure 23, have specific response curves.



Figure 23 The Sensor: Silicon PIN Photo Diode

(Johnson, 2005) The device is most sensitive to the near infrared wavelengths at about 900 nanometers. Notice that the device's response falls off sharply beyond 1000 nanometers, but has a more gradual slope toward the shorter wavelengths, including the entire visible portion of the spectrum. In addition, the device's response drops to about its peak at the visible red wavelength (640 nm).

The PIN photo diode has two photonic responses process. Photo voltaic response is like solar cell. The PIN photodiode will produce a voltage (about 0.5 V) in response to light and will also generate a current proportional to the intensity of the light striking it. However, this unbiased current source mode is seldom used since it is less efficient and is slow in responding to short light flashes. The most common configuration is the "reversed biased" or "photo-conductive" scheme.

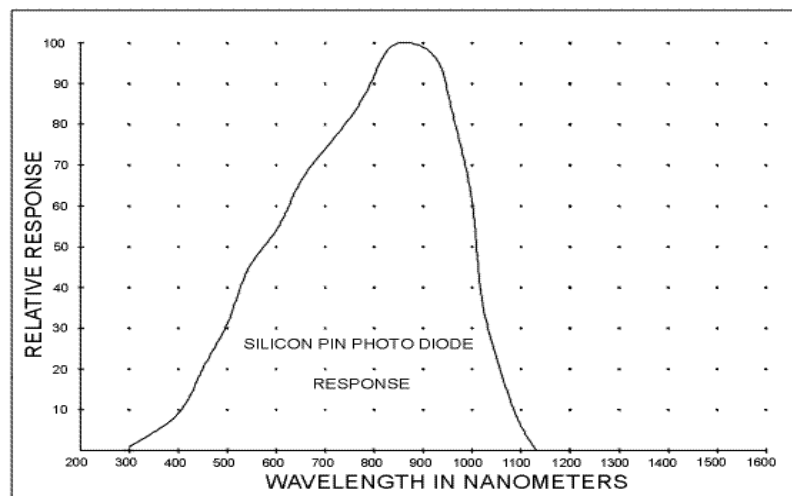


Figure 24 Silicon PIN Photo Diode relative response

Source: Johnson (2005)

The reversed biased mode, PIN photo diode is biased by an external direct current power supply enable ranging from a few volts to as high as 50 volts. The biased device behaves as a leaky diode whose leakage current is dependent on the intensity of the light striking the device's active area. It is important to note that the intensity of a light source is defined in terms of power, not energy. When detecting

infrared light at its 900 nanometer peak response point, a typical PIN diode will leak about one milliamp of current for every two milliwatts of light power striking it (50% efficiency).

For most devices this relationship is linear over a 120 dB (1 million to one) span, ranging from tens of milliwatts to nanowatts. Of course wavelengths other than the ideal 900 nanometer peak will not be converted with the same 50% efficiency. If a visible red light source were used the light to current efficiency would drop to only 25%.

Current output and light power input relationship is the most important characteristic of the PIN photodiode. The relationship helps to define the characteristic transfer for optical power measurement. The light power to electrical current relationship also implies that the conversion is independent of the duration of any light pulse. As long as the detector is fast enough, it will produce the same amount of current whether the light pulse lasts one second or one nanosecond.

There is no data sheet for the silicon PIN photo diode that comes together with the OSA model 240. However, the device has code number “UDT-125DPL”, the Internet search give a short result. This device manufactured by UDT Sensor Inc. (www.udt.com) From specification (see appendix B1) “PIN-125DPL” is a planar diffuse silicon photo diode designed for photo-voltaic application. This is some comment and application guide from the manufacturer.

“The UDT’s Photovoltaic Detector series is utilized for applications requiring high sensitivity and moderate response speeds, with an additional sensitivity in the visible-blue region for the blue enhanced series. The spectral response ranges from 350 nm to 1100 nm.

These detectors have high shunt resistance (1 G Ω , minimum) and low noise (NEP = 2.1×10^{-15} WHz $^{1/2}$), and exhibit long term stability. Unbiased operation of these detectors offers stability under wide temperature variations in DC or low speed

applications. For high light levels (greater than 10 mW/cm^2), the PV Series detectors is considered better linearity.

These detectors are not designed to be reverse biased! Very slight improvement in response time may be obtained with a slight bias. Applying a reverse bias of more than a few volts ($>3\text{V}$) will permanently damage the detectors.”

From this comment, the operation in photoconductive mode is prohibited. The way to increase sensitivity of the OSA model 240 is to change for more sensitive detector.

2 Light Source

2.1 HeNe Laser 632.8 nm L.P.

Goldwasser, (2006b) The SP-117A is a stabilized He-Ne laser which produces a single longitudinal mode output with a nominal frequency of $473.612\,54 \text{ THz}$. The output laser is a linearly polarized single mode and may be either stabilized in frequency or stabilized in amplitude. The system is consists of a cylindrical laser head and power supply/controller.



Figure 25 Spectra-Physics Model 117 Stabilized HeNe Laser System

A typical SP-117 is shown in figure 25. The SP-117A is in an similar package with the Frequency/Intensity mode keylock switch and Locked LED added.

The He-Ne laser head is powered from a He-Ne laser power supply, approximately 1,700 V at 4.5 mA, via the Spectra-Physics screw-lock HV connector. A photodiode signals and heater power are supply via separate cable with a DB9 connector. However, to turn on requires that the interlock plug be present on the back of the controller. The micro switch inside the HV connector be depressed by a plastic pin in the HV plug, and that pins 2 and 7 on the signal connector be jumpered.

After an initial warm-up period where the heater is run continuously, the controller enables the feedback loop which monitors the two outputs of the beam sampler and maintains cavity length using the heater so that one of the orthogonal polarized longitudinal modes is on a slope of the gain curve (frequency stabilized) or where one mode is closer to the center of the gain curve (amplitude stabilized).

The user controls on the SP-117A consist of a switch for power and a switch to select between frequency and amplitude stabilization. There are indicators for AC power and Stabilized. After a warm-up period of about 15 to 20 minutes for the laser head to reach operating temperature, the Stabilized indicator will come on and may flash for a few seconds, and after that should remain solidly on. This really indicates only that the stabilization feedback loop is active, but don't mean that the laser is actually stabilized and meets specs. It's may require another minute or so.

In fact, the way they are designed, everything is identical in both modes until the Stabilized indicator comes on, then it switches to the Intensity signal for locking. If power is cycled, the delay to Stabilized is much shorter, so no actual counter delay is involved, just some circuit watching for the mode changes to slow down below some threshold. Indeed, if the photodiodes are disconnected, Stabilized will come on in under a minute even though the modes are varying wildly.

2.2 HeNe Laser 632 nm LHRP-0151

LHRP 0501 is a He-Ne laser head manufacturing by Research Electro-Optics Inc. Its lasing wavelength is 633 nm nominal and maximum output 5.0 mW. The specification declared the structure TEM00 > 99% and linearly polarization ratio more than 500:1. Others details are shown in appendix B2.

2.3 HeNe Laser 543 nm LHGP-0051

LHRP-0051 is a He-Ne laser head also manufacturing by Research Electro-Optics Inc. Its lasing wavelength is 543 nm nominal and maximum output 0.5 mW. This low power is due to the very low gain transition of helium lasing $3s2 - >2p10$ transition. The specification declared the structure TEM00 > 99% and linearly polarization ratio more than 500:1. Others details are shown in appendix B3.



Figure 26 543 nm He-Ne laser model LHRP-0051

3. Signal Measuring and Analysis Instruments

3.1 Digital Storage Oscilloscope (DSO) model TDS 220

Most of oscilloscope user prefers an analog scope because it is convenient and easy to use. Analog scope has a capable of real-time measurement that required for many scientific experiments. However analog scope has many limitations on

waveform measurement and processing. Some analog scopes have capability of digital measurement it is called a digitizing oscilloscope, but most of them rather expensive

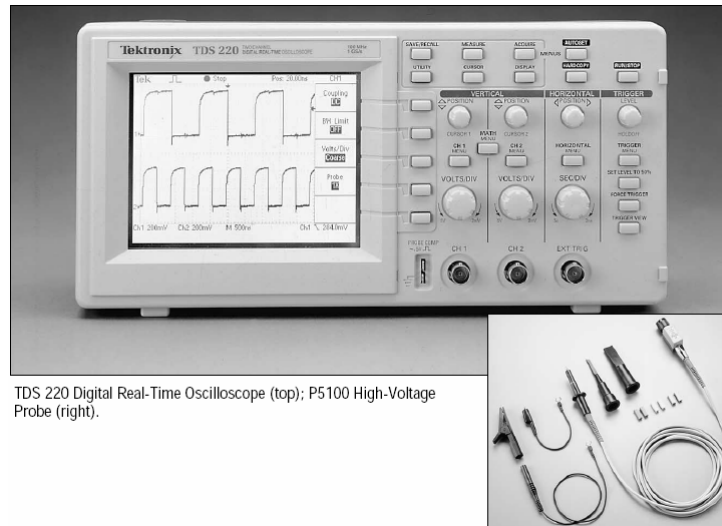


Figure 27 TDS 220, a real-time Digital Storage Oscilloscope used in experiments

Textronix TDS 220 is a Digital Storage Oscilloscope that available in our laboratory and matched requirement for the OSA system. TDS 220 has two channels with a full function digital storage and wave form measurement. The TDS 220 oscilloscope has bandwidth 100 MHz and able to limit bandwidth to 20 MHz with maximum sample rate of 1 GS/s. Its sample rate is very high so, the manufacturer claimed that TDS 220 is a digital real time oscilloscope. Others details are shown in appendix B4.

The TDS 220 DSO used in the experiment is calibrated by Trinergy Co., Ltd. Who is the authorized dealer form Textronix Corp. The calibration laboratory is ISO certificated and traceable to national and international standard.

3.2 6½ Digits Digital Multi-meter (DMM) model 33401A

Agilent 33401A is a general propose multi-meter. This instrument provides basic DCV uncertainty about 0.0015% (24 hour) and basic ACV uncertainty

about 0.06% (1 year). It is given rather wide band width 3 Hz to 300 kHz while reading rate is automatically selected which be maximized to 1000 reading/sec.



Figure 28 Agilent 33401A 6½ Digits Digital Multi-meter

Commonly accessed attributes, such as functions, ranges, and resolution are selected with a single button press. Advanced features are available using menu functions that able to optimize the 33401A for any applications. Others details are shown in appendix B5.

3.3 Real-Time FFT Analyzer Tektronix 2642A

Textronix name the real-time FFT Analyzer as “Personal FFT Analyzer 2600 series. Now, this series is discontinued production. Though, this series is obsolete but the 2642A in our laboratory still working well.

FFT Analyzer is a type of spectrum analyzer, most of them are not a real-time operation instrument. FFT Analyzer use Digital Signal Processing (DSP) technique to transform time sequence signal to frequency domain. With some special technique of Textronix, the multiple CPU are synchronized process on the same data bin and give out result nearly real-time. Though, the processing speed not fast as a swept spectrum analyzer but for low frequency their speed are not much difference.

Most FFT analyzer designed for frequency range from few milli-Hertz to 100 kHz, but bandwidth of the 2642A is 200 kHz.



Figure 29 Real-Time FFT Analyzer Tektronix 2642A

The FFT Analyzer 2642A is a full computer control instrument, so it always connect directly to personal computer. The preferred PC model is 486 CPU operate on DOS mode. The 2642A programming manual is given full guide for control code and application programming, but for general analysis work the “IP” and “Math” program are appropriated. Others details are shown in appendix B6.

3.4 Arbitrary Function Generator model AFG1501

Arbitrary Function Generator is a kind of digital synthesis signal generator which can generate many type of signal such as sine, square, triangular or custom design signal. Like the model 2642A, the AFG5101 are discontinued production and obsolete.

AFG5101 is a programmable Arbitrary Function Generator. It has 2 volatile 8 kbyte waveform memory with fast execution buffer. With a short rise time of 150 ns its bandwidth is span from 12 mHz to 12 MHz at average (nominal?) relative

uncertainty about 0.2%. Amplitude voltage is programmable from 10 mV to 9.99 V with 2% relative uncertainty. Others details are shown in appendix B7.



Figure 30 Arbitrary Function Generator Tektronix AFG1501

METHODS

To study method of accurate wavelength measurement with a scanning Fabry-Perot Interferometer, many experiments are setup to study physical properties and measurement characteristics. Though, Fabry-Perot Interferometer is a hundred year invention of very powerful instrument but very few of Thai physicists are interested on it. The OSA model 240 is a very fine instrument but there are some limitations. This experimental plan is proposed to study cause of error and evaluate factors of uncertainties if possible.

The experiments are set into 3 groups. The first group is a set of experiments for study electrical and signal characteristic of the controller and optical detector in order to find the sources of uncertainties. The second is a set of experiments for study optical characteristics and response of the OSA. And the third group is a set of experiments for measurement wavelength of some light source available in the laboratory. Detail and experiments procedure are given in appendix B.

1. Experiment set 1 Electrical Characteristics

The OSA controller model 251 is provided three electronic functions which applied to the OSA head and the oscilloscope. First, it generate high voltage ramp signal that supply to a piezo-electric actuator in order to control elongation of the cavity length of Fabry-Perot. Second, it provides an amplification of the optical detector signal. The third, it provide synchronous signal to trig the oscilloscope.

1.1 High Voltage Ramp Characteristics

The stability and linearity of the high voltage ramp is an importance factor for stable elongation of Fabry-Perot cavity. So that the first experiments set is proposed to study characteristics of the high voltage ramp signal. Parameters of the high voltage ramp such as frequency range, frequency stability, rise-time & duty-cycle associated with frequency, amplitude range, amplitude linearity, amplitude

stability, and DC offset voltage range and stability are observed and measured with the calibrated DSO.

Methods used for signal analysis is DC load analysis. In this case the input impedance of oscilloscope, $1\text{ M}\Omega$ parallel to 25 pF , is considered suitable. The instruments used in these experiments are TDS 220, Real-time FFT analyzer 2642A and Digital Multi-meter 33401A. The experiments procedure is shown in appendix B8. Each parameter is measured for 10-12 samples over an equal period of time to observe the stability.

Experiment 1.1 is Frequency characteristics of the OSA controller. This experiment is proposed to observe frequency span frequency and raise time stability. Stability of rise time is taken direct effect to spectral stability while it measured. The procedure is observing and recording frequency and period at sample frequency 0.25 Hz, 0.5 Hz, 1.0 Hz, 2.5 Hz, 5 Hz, 10 Hz, 25 Hz, and 50 Hz at amplitude 250 V, 200 V, 150 V, 100 V, and 50 V in 1 hour. Then determine average frequency and standard deviation at each sample frequency.

Experiment 1.2 is Amplitude characteristics of the OSA controller. This experiment is to observe amplitude range and stability. Stability of amplitude is taken direct effect to spectral stability while it measured. Use data from experiment 1.1 to determine average amplitude and standard deviation at each sample amplitude.

Experiment 1.3 Linearity of ramp signal. Elongation of piezo actuator is controlled the space between a pair of mirrors of Fabry-Perot cavity.

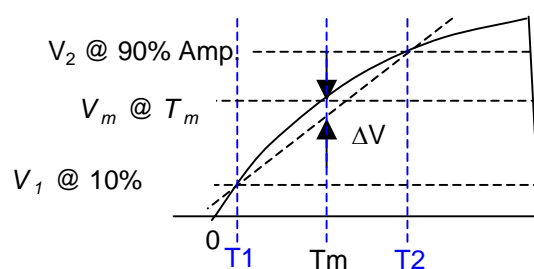


Figure 31 Definition of (non)-linearity of ramp signal

So, the ultra linear motion of the mirror is very necessary for the uniform spacing between successive interference fringes. This experiment is to determine how linearity of the high voltage ramp. Procedure is to compare half amplitude voltage to 0.5 VDD.

Experiment 1.4 Harmonic distortion of ramp signal. Total Harmonic Distortion (*THD*) is parameter that indicates how correct shape of the signal. In the case of linear ramp signal *THD* is possible to indicate a very small non-linearity. There are many definition of *THD* depend on instruments applied. In this experiment, the Real-Time FFT Analyzer is applied. The procedure to evaluate *THD* is to compare root of the sum square of Fourier component over specify significant amplitude considered over range of harmonics.

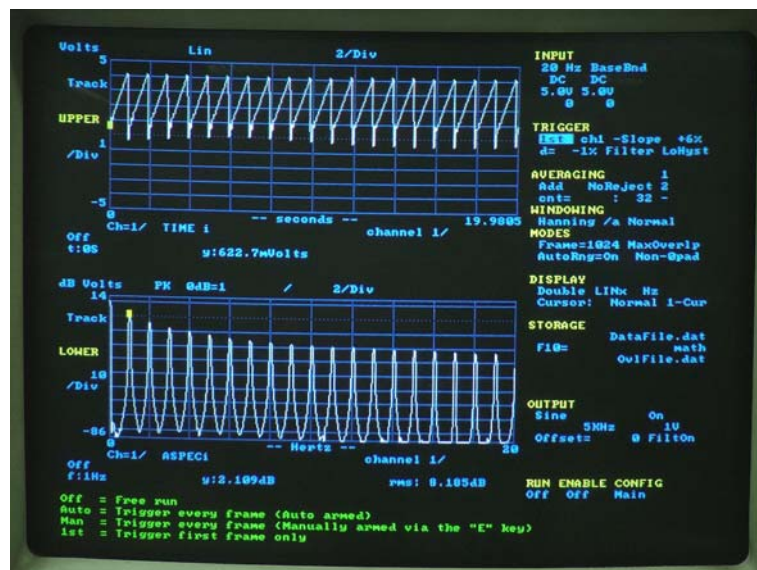


Figure 32 Fourier transform of linear ramp signal. Upper screen is Y-t display of 622.7 mV, 1.000 Hz linear ramp. Lower screen is Fourier transform of the ramp shows sequence of odd harmonics.

Each set of data is evaluated for factors of uncertainties that effect to stability of the cavity elongation. The others source of the uncertainties such as harmonic distortion and noise are also observed.

1.2 Signal amplifier characteristics

The second function of the controller model 251 is signal amplification. Signal from PIN photo-diode detector is connected to the controller via the detector input channel shown in figure 33. The detector output channel is connected to the oscilloscope input.

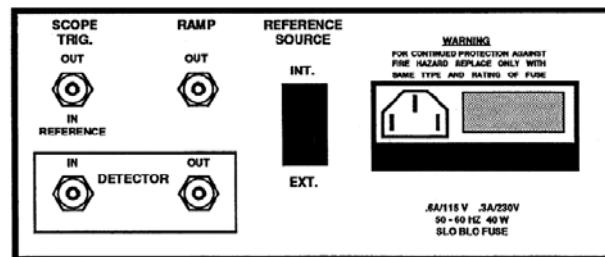


Figure 33 Rear panel of the controller model 251

The amplification parameters proposed to study are input range and sensitivity, frequency response and impulse response. The objectives of these experiments set are to observe signal gain and distortion.

The static response method is applied to observe and measure the input range and sensitivity. The other method is applied low frequency ramp or triangular wave, such as 1.00 Hz or lower, which amplitude 5 mV to the amplifier.

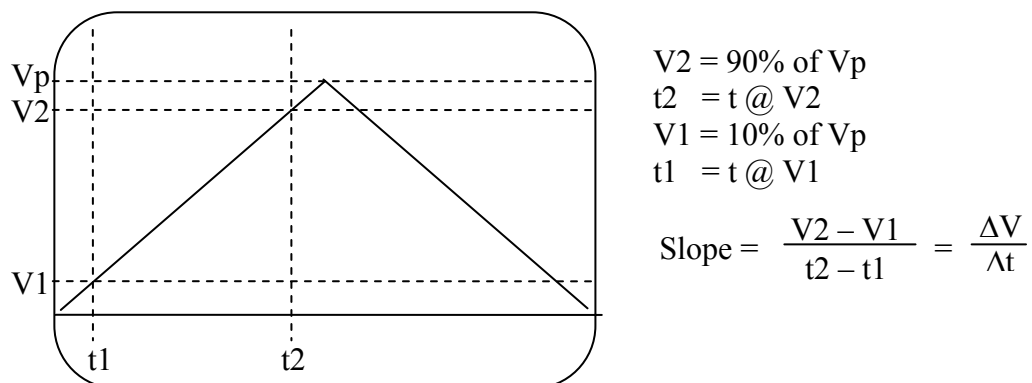


Figure 34 Calculation of slope of input and output triangular wave

The instruments such as oscilloscope, arbitrary function generator and digital multi-meter are applied to these experiments. To evaluate sensitivity the ratio of input slope and output slope is calculated. Slope of can calculated as shown in figure 34.

Frequency response of the amplifier is observed and measured with swept sine method. This method, a synthesis sine wave from arbitrary function generator is applied to the amplifier. The sine wave frequency is changed from 1 Hz to 100 kHz. Then output signal is analyzed by the real-time FFT analyzer which can measure both amplitude and harmonics response.

Experiment 2.1 Sensitivity and input range of the controller model 251 amplifier. This experiment is proposed to observe and evaluate static sensitivity of the amplifier. Two simple methods are applied. The first method is DC sensitivity, Stabilized DC voltage from 0, 1 mV to 10 mV is fed to the amplifier input and output voltage is measured. Then DC gain is evaluated. The second method, 0.2 Hz square wave which amplitude 1 mV to 10 mV is fed to the amplifier and the out put amplitude is measured. Then DC sensitivity is evaluated, also raise time, fall time, time delay and settling time may observed.

Experiment 2.2 Frequency response to 3 dB cutoff of the amplifier. Any amplifiers always have specific frequency response. The preferred signal amplifiers must have a constant gain on broad frequency range. Cutoff frequency is the frequency which the output signal is half power of the input signal or the voltage gain is $1/\sqrt{2}$. Swept sine method is applied to this experiment. Frequency is varied from 1 Hz to 1 MHz in 1:2:5 steps except between 50 kHz to 100 kHz 2 kHz per step is preferred.

1.3 Optical detector characteristics

Many type of optical detector can applied to the OSA model 240. The detector that comes together with this OSA is PIN photo diode model PIN-125DPL.

This detector designed for photo-voltaic operation with moderate sensitivity and response. Electro-optical such as optical intensity exposed on detector's effective area v.s. output voltage or current.

Experiment 3.1 Unexposed I-V characteristics. I-V characteristic of diode is a basic electrical property that shows relation of the diode current and voltage. The characteristic in an unexposed condition must be the same as ordinary diodes but junction voltage may be about 2 V or more. To observe this characteristic the curve tracer (Hameg HM 6042) is applied for direct measurement and observation.

Experiment 3.2 Exposed I-V characteristics. The curve of Exposed characteristic always looks the same as the unexposed one but relatively higher position on I-V diagram. This is due to saturated photo electron-hole pair regenerate by the injected photon. The I-V characteristic at different exposed intensity gives relation about intensity and diode voltage or current.

2. Experiment set 2 The OSA characteristics

The OSA model 240 test certificate from the manufacturer (appendix B9) is given test value of finesse 367.2 at 632.8 nm and 7.5 GHz free spectral range. This part of study is objected to investigate and evaluate some specific parameters of this OSA model 240.

2.1 Etalon cavity expansion & co-efficient

Many documents and texts, Fabry-Perot pair of mirrors is called 'etalon'. This word is from the French word étalon, means 'measuring gauge' or 'reference'. It is very necessary to know the exact effective cavity separation (d) and expansion when high voltage is applied. The nominal value of the cavity length is 10 mm, but not exactly. When high DC voltage is applied to the piezo actuator the cavity length is extended. The extension length is proportional to the voltage. So that, the successive interference output beam is depended on repeatability and stability of linear extension caused by the applied linear ramp voltage

Experiment 4.1 The Etalon cavity expansion & co-efficient.



Figure 35 SP117 laser head is aligned direct into the OSA to evaluate the Etalon cavity expansion co-efficient

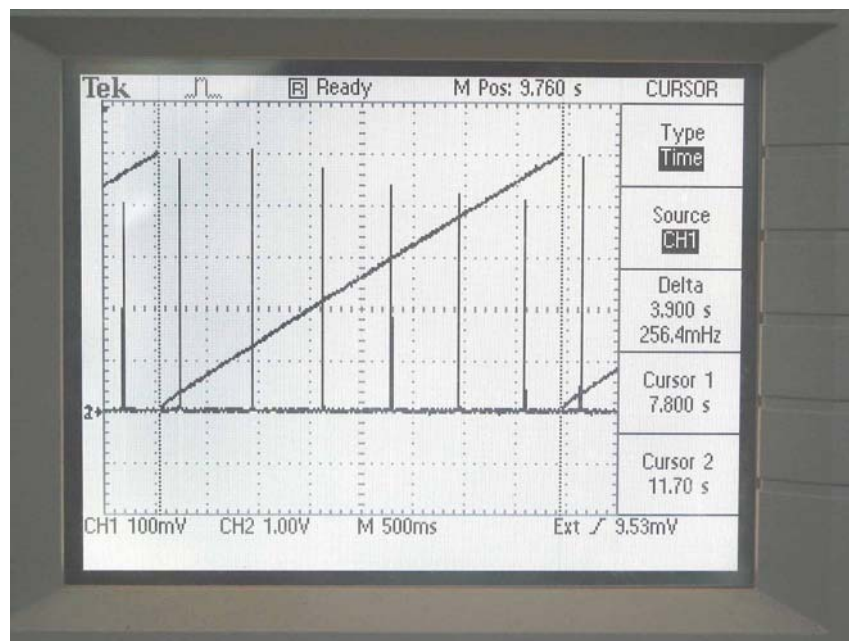


Figure 36 Oscilloscope screen show 6 successive interference peak of 632.8 nm Laser output form the OSA model 240 when apply with 250 V and 4 Hz linear ramp

Stabilized HeNe Laser SP117 is used as the reference light source. After aligned the laser beam to give the maximum signal output seen on the TDS 220, adjust scanned frequency (the high voltage ramp frequency) to the lowest stable frequency about 250 mHz. Adjust ramp amplitude voltage to 250 V. Six successive interference peak will show on oscilloscope screen, as in figure 36.

In figure 37 the separation between each output peak is $\lambda/4$. If the linear ramp amplitude is decrease, such as 200 V, 150 V, and 100 V, the number of successive interference peak is also decrease proportionally. Then the extension coefficient is able to calculate.

2.2 Evaluated the finesse

Experiment 4.2 Evaluated the finesse @ 632.8 nm. Definition of finesse is described in section 4.5.7 and the evaluation is described in section 4.5.9. Finesse is a number that indicate how sharpness of interference fringes the OSA can produce. Finesse is the ratio of FSR and FWHM. As shown in equation (28) the exact FSR in term of frequency can evaluate if the exact cavity length and cavity refractive index is known. In practical, the value of finesse can evaluate directly by high quality digitized scope.

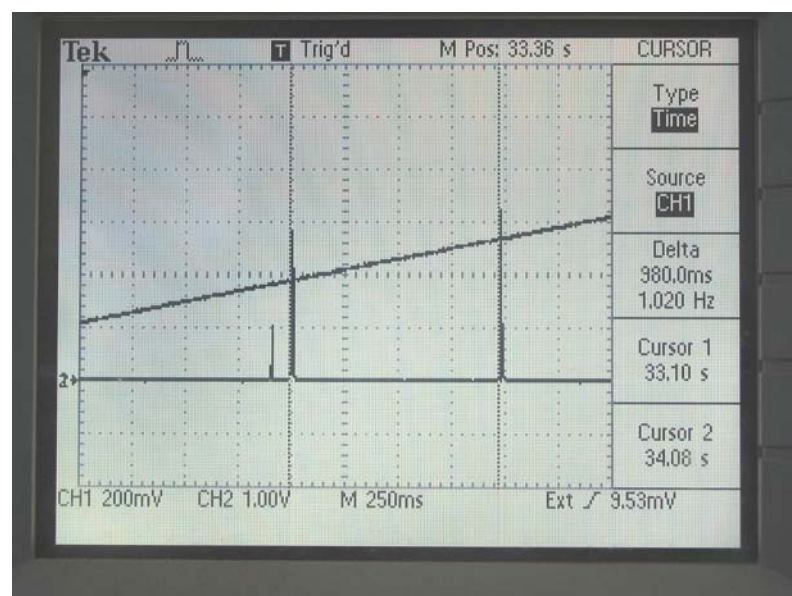


Figure 37 FSR measurement

This experiment use frequency stabilized HeNe laser (Spectra Physics SP-117) as a reference wavelength. After align the laser beam into the OSA, Adjust sweep Amplitude of high voltage ramp until two peak is shown, the measure the FSR. Adjust trigger position and time/div to zoom into one peak, then measure FWHM. Change amplitude and sweep time (ramp frequency) then measure in other condition.

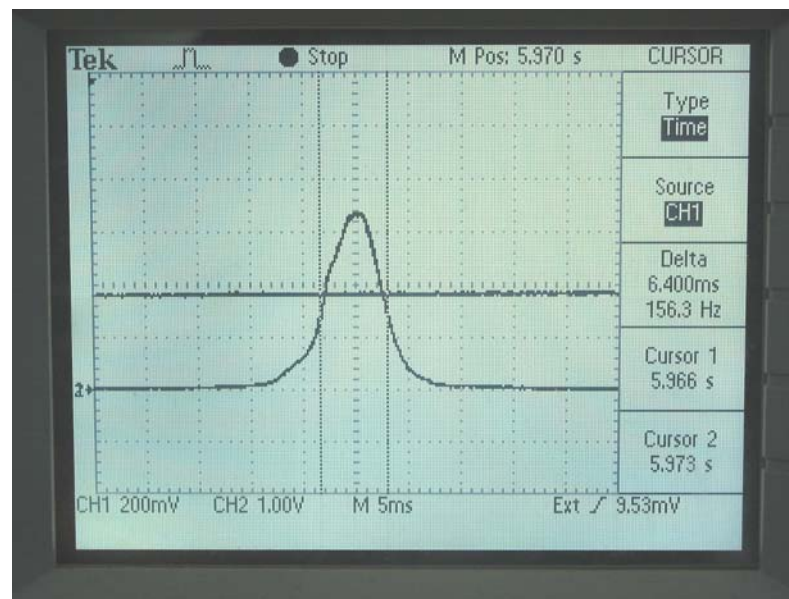


Figure 38 FWHM measurement.

This experiment use frequency stabilized HeNe laser (Spectra Physics SP-117) as a reference wavelength. After align the laser beam into the OSA, Adjust sweep Amplitude of high voltage ramp until two peak is shown, the measure the FSR. Adjust trigger position and time/div to zoom into one peak, then measure FWHM. Change amplitude and sweep time (frequency of ramp) then measure FSR and FWHM in other condition.

3. Experiment set 3 Wavelength measurement

Experiment 5.1 Measure wavelength of HeNe laser model LHRP-0151. This model of laser head is 632 nm wavelength nominal, its power is 1.5 mW and designed for general use and it dose not a frequency stabilized. The direct measurement

method is applied. The laser head model LHRP-0151 beam is aligned direct in to the OSA. The instruments setup is the same as illustrated in figure 35. The laser head SP117 is replaced with LHRP-0151.

Set the ramp amplitude at 250 V, rise time at 5 s, DC offset at 0 V, sweep range at 1x. Adjust the OSA until maximum transmitted peak is shown on scope screen. Then measure separation of each transmitted peak with cursor.

Experiment 5.2 Measure Wavelength of Laser LHRP-0051. This model of laser head is double frequency output wavelength 543 nm nominal. Its power is 0.5 mW and designed for general use. The direct measurement method is applied. The instruments setup and alignment is the same as experiment 5.1.

Experiment 5.3 Measure Wavelength of 630 nm Laser diode. Figure 39 show alignment to compare the unknown laser wavelength to reference wavelength. This experiment use 632.8 nm frequency stabilized HeNe laser as a reference wavelength and the unknown laser source is a commercial laser pointer. Laser pointer is a cheap laser diode that, usually, reduces manufacturing cost by using simple current regulator and no heat sink provided or uses its metal case as heat sink.

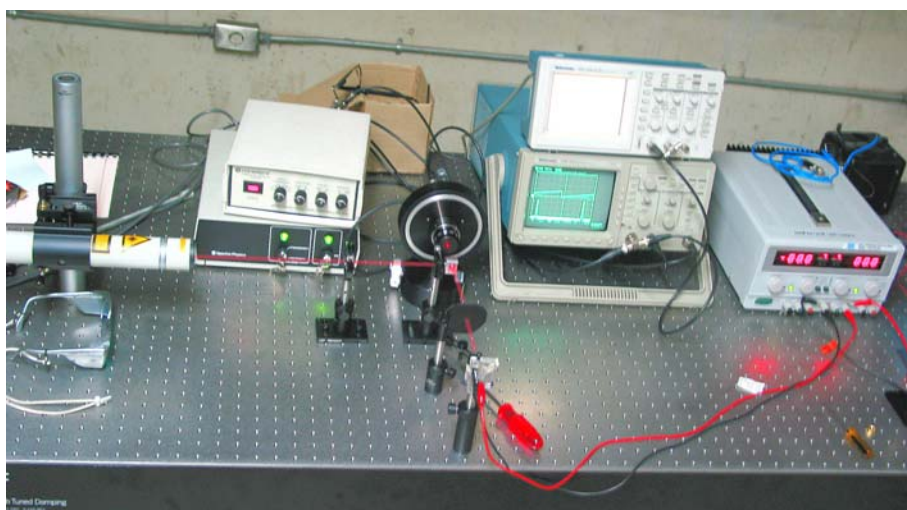


Figure 39 Instruments alignment to measure or compare wavelength of laser diode

Reference beam is sampled in to the OSA with a beam splitter while the unknown beam is aligned direct in to the OSA. After hours for alignment two beam in line together and make successive peak on the scope screen as shown in figure 40. Wavelength of laser pointer is evaluated by measure separation between peaks (ms). If a cavity extension coefficient is known then applies equation (29).

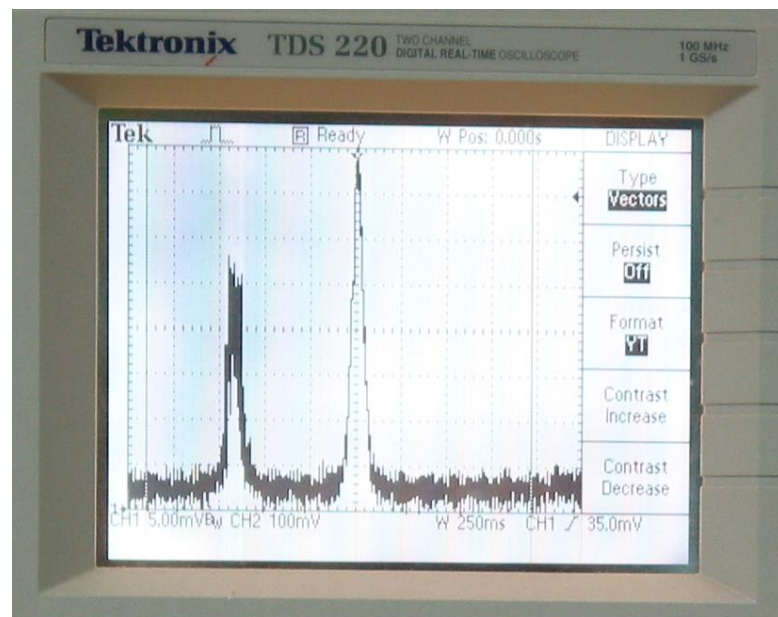


Figure 40 Comparison of 632.8 nm Stabilized HeNe laser (center peak) and 630 nm nominal wavelength of laser pointer

DATA ANALYSIS

1. Experiment set 1 Electrical Characteristics

1.1 Experiment 1.1 is Frequency characteristics of the OSA controller

Frequency stability of high voltage ramp observed at 0.25 Hz, 0.5 Hz, 1 Hz, 2.5 Hz, 5 Hz, 10 Hz, 25 Hz, 50 Hz, and amplitude 250 V, 200 V, 150 V, and 100 V. The experiment procedure detail is shown in appendix B1. Table 2 and table 3 show analysis of frequency stability.

Table 2 Average frequency and standard deviation of the mean of high voltage ramp at the sample frequency and the sample amplitude

	Amplitude 250 V		Amplitude 200 V		Amplitude 150 V		Amplitude 100 V	
Freq.	Average	Std. of M	Average	Std of M	Average	Std of M	Average	Std of M
0.25 Hz	0.2728	0.0015	0.2571	0.0001	0.2562	0.0002	0.2570	0.0001
0.5 Hz	0.5037	0.0003	0.5025	0.0003	0.5021	0.0003	0.5013	0.0001
1 Hz	1.003	0.0002	1.014	0.001	1.012	0.001	1.031	0.0006
2.5 Hz	2.519	0.002	2.533	0.001	2.509	0.001	2.517	0.000
5 Hz	5.071	0.002	5.078	0.004	5.044	0.001	5.019	0.003
10 Hz	10.06	0.01	10.11	0.01	10.64	0.01	10.08	0.01
25 Hz	25.22	0.02	25.38	0.03	25.55	0.01	25.32	0.01
50 Hz	51.54	0.03	51.60	0.03	51.63	0.01	51.41	0.01

If we claimed the standard deviation of the mean as standard uncertainty, the standard uncertainty of each average frequency can evaluated by include standard uncertainty of horizontal sweep time of TDS 220. Calculation is shown in table 3

Table 3 Average frequency and standard uncertainty

DSO sweep time (s)	Rel. uncert.	Average freq.	Std. uncert. (Hz)	Rel. uncert. %
5	5.00E-04	0.2608	0.0015	0.57%
2.5	2.50E-04	0.5024	0.0006	0.12%
1	1.00E-04	1.015	0.002	0.16%
0.5	5.00E-05	2.519	0.003	0.10%
0.25	2.50E-05	5.053	0.006	0.11%
0.1	1.00E-05	10.22	0.02	0.19%
0.05	5.00E-06	25.37	0.04	0.15%
0.025	2.50E-06	51.54	0.04	0.08%

1.2 Experiment 1.2 is Amplitude characteristics of the OSA controller.

Table 4 shows average amplitude value at each nominal amplitude setup. The standard deviations of the mean, which claimed as unbiased standard uncertainty, are about 0.1 percent.

Table 4 Analysis for amplitude stability

Nominal Amplitude	250 V	200 V	150 V	100 V
Average Amplitude (V)	250.34	200.21	149.40	100.14
Standard Deviation (V)	0.93	0.60	1.14	0.79
S.D. of the Mean (V)	0.19	0.13	0.24	0.17
Deg of freedom	23	23	23	23
Rel. Unbiased Uncertainty	0.077%	0.063%	0.159%	0.165%

1.3 Experiment 1.3 is Linearity of the ramp signal.

Measurement result is shown in table 5 and analysis of linearity according to the definition in figure 20 in shown in table 6

Table 5 Linearity of ramp signal at observed amplitude

Controller setup: Amplitude 250 V, Sweep expansion x1, DC Offset 0V					
	Amplitude (V)	V1 (V)	Vm (V)	V2	ΔV (V)
Average	250.5	25.1	125.9	225.5	0.66
Standard Deviation	1.3	0.1	0.8	0.9	0.42
S.D. of the mean	0.3	0.0	0.2	0.2	0.09
Degree of freedom	20	20	20	20	20
Controller setup: Amplitude 200 V, Sweep expansion x1, DC Offset 0V					
	Amplitude (V)	V1 (V)	Vm (V)	V2	ΔV (V)
Average	200.4	20.0	100.7	180.4	0.47
Standard Deviation	1.3	0.1	0.5	0.8	0.31
S.D. of the mean	0.3	0.0	0.1	0.2	0.07
Degree of freedom	20	20	20	20	20
Controller setup: Amplitude 150 V, Sweep expansion x1, DC Offset 0V					
	Amplitude (V)	V1 (V)	Vm (V)	V2	ΔV (V)
Average	150.3	15.0	75.6	135.3	0.41
Standard Deviation	0.8	0.0	0.3	0.4	0.19
S.D. of the mean	0.2	0.0	0.1	0.1	0.04
Degree of freedom	20	20	20	20	20
Controller setup: Amplitude 100 V, Sweep expansion x1, DC Offset 0V					
	Amplitude (V)	V1 (V)	Vm (V)	V2	ΔV (V)
Average	100.0	10.0	50.2	90.0	0.20
Standard Deviation	0.6	0.0	0.3	0.3	0.12
S.D. of the mean	0.1	0.0	0.1	0.1	0.03
Degree of freedom	20	20	20	20	20

Table 6 Analysis of linearity according to the definition in appendix figure B1

Everged Amplitude (V)	V_m (V)	ΔV (V)	$V_m/\Delta V$ %
250.5	125.9	0.66	0.523%
200.4	100.7	0.47	0.466%
150.3	75.6	0.41	0.541%
100.0	50.2	0.20	0.400%

Percentage of the ratio of mean voltage (V_m) and differential voltage (ΔV) is considered as percentage of nonlinearity ($V_m/\Delta V$ %). From table 5 and 6 the percentage of nonlinearity is 0.482% with standard deviation 0.064% and unbiased uncertainty of 0.032%. This value is too small!

1.4 Experiment 1.4 Harmonic distortion of ramp signal.

The test for harmonic distortion of linear ramp is applied with Tektronix 2642A Personal Real-time Fast Fourier Analyzer. The high voltage ramp is fed to 2642A via a 50:1 attenuator. The Total Harmonic Distortion ($THD\%$) is evaluate from 19 Fourier components by procedure shown in appendix B1.

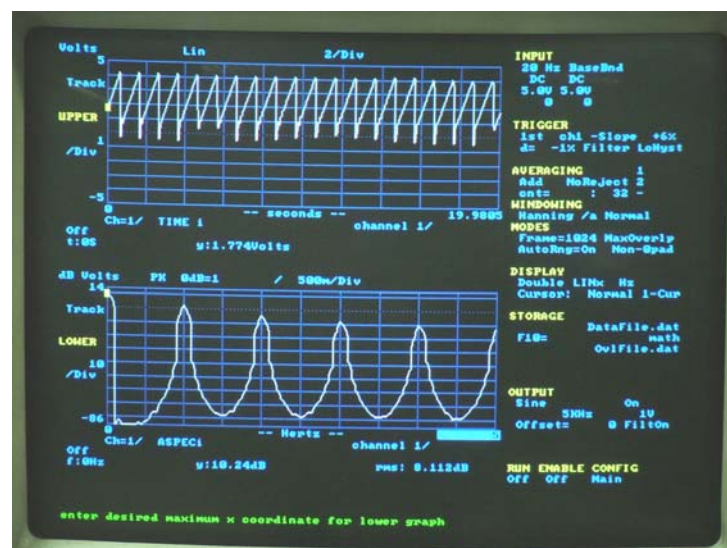
**Figure 41** Shape of harmonic peaks that show ‘side band’ added

Table 7 Evaluate of $THD\%$ at difference amplitude

Frequency Hz	Amlitude V	50:1 Att. V	TDH_X	TDH_{Ref}	TDH_X / TDH_{Ref}	$TDH\%$
1.000	256.6	2.566	2.479	2.509	98.83%	1.17%
1.000	200.0	1.999	3.191	3.230	98.79%	1.21%
1.000	100	1.011	6.314	6.378	98.99%	1.01%

The $THD\%$ is about 1.2%, this not agrees with experiment 1.3. Note that shape of harmonic peak did not look like it should be, as see in figure 36.

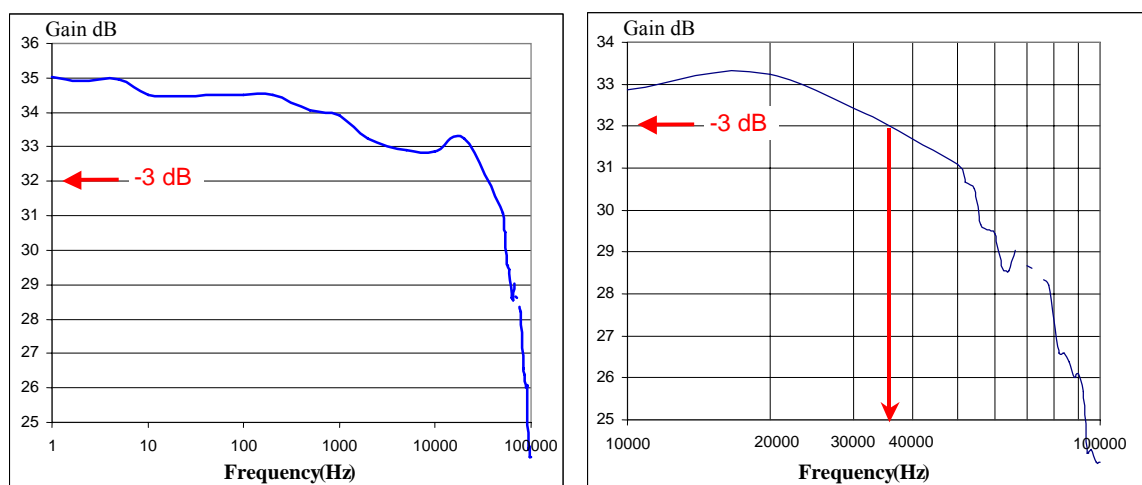
1.5 Experiment 2.1 Sensitivity and input range of the controller model 251 amplifier.

Table 8 Evaluation of static sensitivity

	ΔV	ΔT	$Slope$	S.D. of the Mean
Input Ramp	8.18	415.7	0.0197	0.0009
Output Ramp	168.6	414.8	0.4066	0.0121

Result of experiment 2.1 is not quite satisfy, because function generator is bad stability and very noisy at low frequency. Estimate average static sensitivity is 20.65 with unbiased standard uncertainty 1.13. This value is far from specification.

Experiment 2.2 Frequency response to 3 dB cutoff of the amplifier.

**Figure 42** Frequency response of the amplifier of the 251 controller

From experimented data the response curve is plot as show in figure 42. Non smooth response may caused from instability and noise from function generator.

1.6 Experiment 3.1 Unexposed I-V characteristics.

The Unexposed I-V characteristics plotted from data measure with the curve tracer HM-6042. The curve indicated that the PIN 125DPL has threshold voltage about 0.7 V the same as general silicon diode.

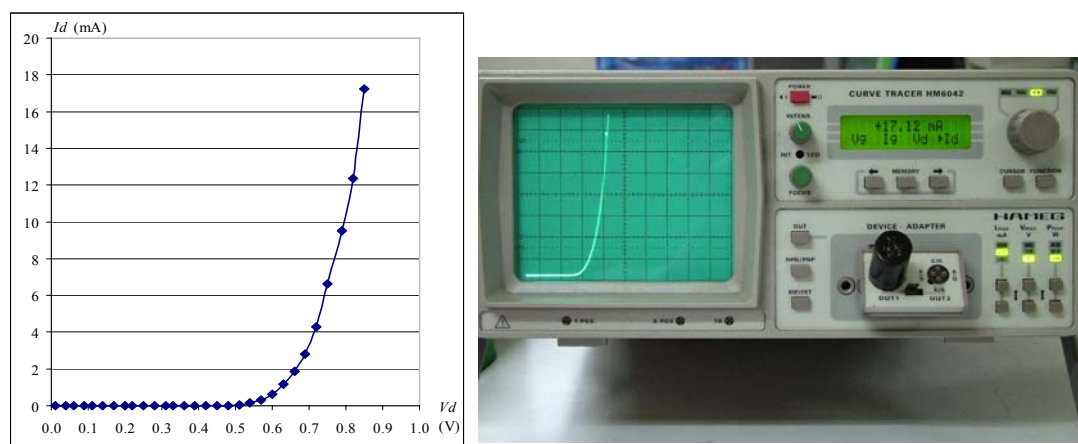


Figure 43 Unexposed I-V characteristics

1.7 Experiment 3.2 Exposed I-V characteristics.

This experiment is not yielded any result, because HM6042 designed for testing in forward region.

2. Experiment set 2 The OSA characteristics

2.1 Experiment 4.1 Etalon cavity extension & co-efficient.

To observe the repeatability of cavity extension motion, the cavity extension coefficient is measure in difference condition. The detail of experiment procedure is shown in appendix B2. Analysis result is shown in table 9.

Table 9 Analysis of the etalon cavity extension co-efficient where the ramp amplitude is change

Experiment 4.1 Extension coefficient α_V (nm/V) at difference ramp amplitude					
Rise time (s)	Amplitude (V)	α_t (nm/s)	Std. dev.	α_V (nm/V)	Std. dev.
3.840	124.0	112.2	2.162	3.476	0.067
3.856	160.8	146.0	2.795	3.502	0.062
3.868	249.5	237.6	2.159	3.684	0.039
Experiment 4.1 Extension coefficient α_V (nm/V) at difference ramp raise time					
Rise time (s)	Amplitude (V)	α_t (nm/s)	Std. Dev.	α_V (nm/V)	Std. Dev.
3.868	249.5	237.6	2.159	3.684	0.039
2.043	250.9	447.6	4.205	3.645	0.050
0.5384	250.7	1694	12	3.639	0.033

2.2 Experiment 4.2 Evaluated of finesse @ 632.8 nm.

Finesse is a parameter that indicates how fine of the interference fringes the OSA can produce. This parameter is necessary for many application and measurement with the OSA. To evaluate finesse direct measurement of FSR and FWHM is done in many conditions for a reference 632.8 nm wavelength.

Table 10 Value of FSR and FWHM at 632.8 nm

Amplitude is fix at 250 V	Rise time 5 s			Rise time 7.5 s			Rise time 9 s		
	FSR (s)	FWHM (s)	Finesse	FSR (s)	FWHM (s)	Finesse	FSR (s)	FWHM (s)	Finesse
Degree of freedom	39	39	39	39	39	39	39	39	39
Average	0.666	0.0035	192.8	0.354	0.0017	208.3	0.093	0.0004	216.1
Stadard deviation	0.021	0.0005	34.2	0.011	0.0002	21.1	0.003	0.0000	16.8
Std. Dev. Of the mean	0.003	0.0001	5.5	0.002	0.0000	3.4	0.000	0.0000	2.7
Frequency is fix at 4 Hz	Amplitude 124 V			Amplitude 160 V			Amplitude 250 V		
	FSR (s)	FWHM (s)	Finesse	FSR (s)	FWHM (s)	Finesse	FSR (s)	FWHM (s)	Finesse
Degree of freedom	19	19	19	19	19	19	19	19	19
Average	1.428	0.0073	197.2	1.173	0.0060	194.7	0.661	0.0034	199.9
Stadard deviation	0.012	0.0004	10.58	0.018	0.0004	12.58	0.022	0.0004	28.51
Std. Dev. Of the mean	0.003	0.0001	2.43	0.004	0.0001	2.89	0.005	0.0001	6.54

From table 10, the finesse at 632.8 nm is evaluated according definition using equation (25). Averaged finesse is 201.51 with standard deviation 8.94 at degree of freedom 112. Standard deviation of the mean is 0.85. So that, the finesse with unbiased standard uncertainty is 201.5 ± 0.8

3. Experiment set 3 The OSA characteristics

This set of experiment is aimed to measure wavelength from four light source, 632 nm HeNe laser model LHRP-0151, 543 nm double frequency HeNe laser model LHRP-0051, commercial laser diode (laser pointer) and Pen-Ray Mercury lamp. But some accident occurred while testing sensitivity of the detector, so its sensitivity is degenerated.

3.1 Experiment 5.1 Measure Wavelength of Laser LHRP-0151(632 nm)

The wavelength measurement result of laser head model LHRP-0151 is 634.3 nm with 17.4 nm unbiased expand uncertainty. The result does not much difference from nominal value (632 nm) but the experiment was done only two repetition that big difference result. From table 12 the uncertainty budget show the big uncertainty, so the wavelength measured did not reliable enough.

Table 11 Wavelength measurement result of laser LHRP-0151

m_i	Δt_i (s)	$\Delta m_i = i$	$i \Delta t_i$ (s)	$\Delta m_i^2 = i^2$	$\Delta t_i'$ (s)	$\Delta t_i - \Delta t_i'$
m_0	0.0000	0	0	0.000	0.0000	0.0000
m_1	0.6820	1	0.682	1.000	0.6860	-0.0040
m_2	1.3550	2	2.710	4.000	1.3720	-0.0170
m_3	2.0950	3	6.285	9.000	2.0580	0.0370
m_4	2.7120	4	10.848	16.000	2.7440	-0.0320
m_5	3.4410	5	17.205	25.000	3.4300	0.0110
Sum	-	-	37.73	55	-	-
Average	2.0570	-	-	-	-	-
Standard Deviation	-	0	-	0	-	0.026524
S. D. of the Mean	-	0	-	0	-	0.011862

Table 12 Uncertainty budget of wavelength measurement from table 11

Stanard uncertainty component	Source of Uncertainty	Type	Value of stanard uncertainty	Sensitivity coefficient	Probability distribution	Coverage factor	Stanard uncertainty	Degree of Freedom
U_{av}	Extension coeff. Rel. Uncert	A	0.003329	1	Normal	2.58	0.001290	57
$U_{\Delta t_i}$	Relative Uncertainty of Δt_i	A	0.005767	1	Normal	2.58	0.002235	5
U_n	Relative Uncertainty of refractive index of air	-	N. A.	-	-	-	-	-
U_S	Relative Uncertainty of slope	Combine	0.011862	1	Normal	2.58	0.004598	5
U_λ	Uncertainty of Wavelength (nm)	Expand	8.628	-	t	2.02	17.43	5

3.2 Experiment 5.2 Measure Wavelength of Laser LHRP-0051(543 nm)

Table 13 Wavelength measurement result of laser LHRP-0051

m_i	Δt_i (s)	$\Delta m_i = i$	$i \Delta t_i$ (s)	$\Delta m_i^2 = i^2$	$\Delta t_i'$ (s)	$\Delta t_i - \Delta t_i'$
m_0	0.0000	0	0	0.000	0.0000	0.0000
m_1	0.5530	1	0.553	1.000	0.6860	-0.1330
m_2	1.1070	2	2.214	4.000	1.3720	-0.2650
m_3	1.6600	3	4.98	9.000	2.0580	-0.3980
m_4	2.2140	4	8.856	16.000	2.7440	-0.5300
m_5	2.7670	5	13.835	25.000	3.4300	-0.6630
Sum	-	-	30.438	55	-	-
Average	1.6602	-	-	-	-	-
Standard Deviation	-	0	-	0	-	0.209501
S. D. of the Mean	-	0	-	0	-	0.093692

The wavelength measurement result of laser head model LHRP-0051 is 511.7 nm with 119.3 nm unbiased expand uncertainty. The result does some difference from nominal value (543 nm) but the experiment was done only one measurement and the transmitted peak was very low and noisy. So that, the wavelength measured was too better than that should be.

Table 14 Uncertainty budget of wavelength measurement from table 13

Stanard uncertainty component	Source of Uncertainty	Type	Value of stanard uncertainty	Sensitivity coefficient	Probability distribution	Coverage factor	Stanard uncertainty	Degree of Freedom
U_{av}	Extension coeff. Rel. Uncert.	A	0.003329	1	Normal	2.58	0.001290	57
$U_{\Delta t_i}$	Relative Uncertainty of Δt_i	A	0.056434	1	Normal	2.58	0.021874	5
U_n	Relative Uncertainty of refractive index of air	-	N. A.	-	-	-	-	-
U_S	Relative Uncertainty of slope	Combine	0.093692	1	Normal	2.58	0.036315	5
U_λ	Uncertainty of Wavelength (nm)	Expand	55.99	-	t	2.13	119.27	4

RESULTS AND DISCUSSION

RESULTS

The analyzed data from all experiments most of them yield good results as expected in the experimental hypothesis. Some experiment that does not yields or given a proper result may be from the experiment design or the available instruments that did not match the experiment procedure. The experiment results are summarized as follow.

1. Experiment set 1 Electrical Characteristics

1.1 Experiment 1.1 Frequency characteristics of the OSA controller

From table 2 and 3 show frequency stability of high voltage ramp observed at 0.25 Hz, 0.5 Hz, 1 Hz, 2.5 Hz, 5 Hz, 10 Hz, 25 Hz, 50 Hz, and amplitude of 250 V, 200 V, 150 V, and 100 V respectively. Standard deviation of the mean is lower than 0.5% of average frequency. This value comparatively small and less than that claimed in its specification. But, if compare to some brand name such as Pi Scientific, 0.5% is rather high for metrological work.

1.2 Experiment 1.2 Amplitude characteristics of the OSA controller

From table 4 the amplitude stability of high voltage ramp observed at 0.25 Hz, 0.5 Hz, 1 Hz, 2.5 Hz, 5 Hz, 10 Hz, 25 Hz, 50 Hz, and amplitude of 250 V, 200 V, 150 V, and 100 V respectively. The data analysis shows that unbiased standard uncertainty (standard deviation of the mean) is less than 0.1% of each value of average amplitude. This value is also less than that claimed in its specification but it is rather high for metrological work.

1.3 Experiment 1.3 Linearity of the ramp signal

From table 5 and 6 the percentage of nonlinearity is 0.482% with unbiased uncertainty of 0.032%. This value is too small!

1.4 Experiment 1.4 Harmonic distortion of ramp signal.

From table 7 the *THD*% is about 1.2%, this does not agree to experiment 1.3. Note that shape of harmonic peak did not look like it should be, when compare to computer simulation result. They are two possible answers. First, the simulation ramp signal is some difference compare to the real signal, such as the fall down slope. The second, the ramp generator in the controller model 251 effected some modulation that caused side band frequency as seen in figure 36.

1.5 Experiment 2.1 Sensitivity and input range of the controller model 251 amplifier.

Result of experiment 2.1 is not as expected, may be from stability and noisy at low frequency of function generator. From table 8 the average static sensitivity is 20.65 with unbiased standard uncertainty 1.13. This value is far from specification. The improvement of procedure and instruments are required.

1.6 Experiment 2.2 Frequency response to 3 dB cutoff of the amplifier.

From figure 43 the response graph 3 dB cutoff frequency of the signal amplifier, is around 35 kHz. This value far difference from specification 80 kHz. It may be from bad stability and noise low signal amplitude of the function generator. The improvement of experiment procedure and instruments are required.

1.7 Experiment 3.1 Unexposed I-V characteristics

From figure 44 the unexposed I-V characteristics plotted compare to HM-6042. The curve indicated that the PIN 125DPL has threshold voltage about 0.65 V

the same as typical silicon diode.

1.8 Experiment 3.2 Exposed I-V characteristics.

This experiment does not yield any result. The curve is the same as experiment 3.1. Note that, the diode leakage current (I_d at V_d that lower than 0.5 V) has some difference, but HM-6042 cannot measure.

2. Experiment set 2 The OSA Characteristics

2.1 Experiment 4.1 Etalon cavity extension & co-efficient.

In practical, the etalon extension coefficient is less importance than the repeatability of linear extension motion when linear ramp voltage was applied. However, etalon extension coefficient is more convenient to evaluate and its standard uncertainty can indicate repeatability of linear extension motion. From table 9 the extension coefficient is 3.605 nm/V with unbiased standard deviation 0.012 nm/V (or 0.34%) at effective degree of freedom 57. This value is in the same order of that claimed in its specification, 4 nm/V.

2.2 Experiment 4.2 Evaluation of Finesse @ 632.8 nm.

Finesse is the necessary parameter in many measurements that use OSA. The value from experiments in difference condition is 201.5 with unbiased standard uncertainty 0.8 at effective degree of freedom 112. This value is very close to 200 that claimed in its specification. But much difference if compare to the OSA certificate (367.2 at 632.8 nm). This difference may be from alignment or measurement method. The most possible influence is from HeNe laser, its frequency is not perfectly stabilized.

3. Experiment set 3 Wavelength Measurement

3.1 Experiment 5.1 Wavelength measurement of LHRP-0151 Laser

HeNe laser model LHRP-0151 with 632 nm nominal wavelength output was used in the experiment.. By shining the laser beam into the OSA head and read the output from oscilloscope screen. The measured wavelength is 634.3 nm which deviated from 632.8 nm with 17.4 nm unbiased expand uncertainty. The result was averaged from two measurements, so it does not accurate.

3.2 Experiment 5.2 Wavelength measurement of LHRP-0051 Laser

HeNe laser model LHRP-0051 with 543 nm nominal wavelength output was used in the experiment. The measured wavelength is 511.7 nm with 119.3 nm unbiased expand uncertainty. This wavelength is at the sensitivity margin of the OSA. The transmit output peak is very small and noisy. The measured data is collected from only one measurement, so the result does not reliable enough.

3.3 Experiment 5.3 Measure Wavelength of Laser diode (630 nm)

Laser pointer with 650 nm nominal wavelength output was used in the experiment. The measurement can not be done due to the instability of the output. This comes from the heat liberated form diode junction and lack off heat sink so the laser cavity length is varied.

DISCUSSION

The experiments procedure used in this research is proposed to investigate some physical characteristics of the OSA and the instruments. Method in the procedure only aimed to evaluate some parameters and depended on test instruments availability, so that, this may not be a standard procedure using in standard metrology laboratory. After trial and error many experiments and methods are abandoned. The experiment procedures in this paper are portion that yield some result.

The experiment set 1, Electrical characteristic: Most experiment results indicate that the Electrical characteristic such as those of the ramp generator and its scanning stability are qualified or better than that claimed by its specification. The average uncertainty is about 1%, except some experiment which may be caused from defect of the function generator.

Some experiments do not give an expected result for example an experiment on gain and responsivity characteristics of PIN 125DPL photodiode, required improvement of test method and instruments. The experiment should cover both continuous and pulse.

The experiment set 2, Optical characteristics: The methods and results seem reliable but more data and condition are suggested for improvement. In order to get a standard performance of the OSA the calibration of reference laser source is required. Some reference such as wavelength of others spectral source measured by others instrument that available is suggested.

Some parameters that cannot be calculate properly, such as the exact cavity length, the FSR, may be caused from limitation of instruments or the improper methodology applied. Although, the result is not good enough but if the calibrated laser source is available, the reliable value of important parameter is possible to calculate.

Experiment set 3, Wavelength measurement: Method using for wavelength measurement in this experiment is adapted and simplified from many literatures. The measurement results show wavelength uncertainty is rather high. Because of the detector damaged or sensitivity degenerate after characteristics test so, only few measurements are done and it is unable to repeat the experiment. Though, some guide such as from ISO handbook III LWS section 5.12 (esa ISO) by using some interoperation technique, may improve the measurement uncertainty.

Method of wavelength measurement used in thesis is not recommended by CIPM. This suggestion is recently found in some documents. The method that now widely used is called Comb Technique. This technique employs grating to the Faby-Perot interferometer to generate the ‘optical ruler’ which is claimed the measurement uncertainty to 10^{-12} or better. However, the OSA model 240 is a very fine instrument and widely used, but some standard document such as IEC PAS 62129 (Calibration of Optical Spectrum Analyzers) and other normative document related are needed.

CONCLUSION

The OSA model 240 and adjunct instruments that available in Photonic Metrology Laboratory at Department of Physics were purchased under The Government-World Bank Project (in year 2003) in order to develop academic strength in the field of Physics and related subject. The project was proposed to the Department to develop some subjects. Photonic Metrology and Laboratory in Photonic Metrology are new courses developed according to the aim of that project. Photonic Metrology is an interdisciplinary subject that employs another three groups of subject, Photometry, Spectroscopy and Interfero-metry. These three subjects are included many of Optical Metrology and the related such as Optical Frequency Standard, Length Standard, etc. So, Wavelength Measurement is the basic knowledge or backbone in this subject.

The literature review in former part of this thesis points out that the realization of meter according to CIPM recommendation is possible by three methods. One method that generally used and widely applied is wavelength measurement by the instrument called 'Interferometer'. Since 1983, thousands of researches working for scientific development have brought numbers of new techniques for accurate wavelength measurement. Today more recommendations and measurement conditions are added by CIPM in order to regulate and generalize the international standard of Meter Realization.

There are many types of interferometer invented since Young's Double Slit experiment in 1805. The famous one was the Michelson's double beam interferometer invented in 1887. However, the application of Faby-Perot interferometer for wavelength measurement is a high accuracy method with low operation cost when compare with other method of the same accuracy level.

The Materials and Methods in this thesis are about instruments and procedure of experiments to investigate the physical properties of the OSA and the adjunct instruments such as the controller, the detector and light source available. Also, some

measuring instruments are included. The conclusion of this good instrument is 'it is suitable for generally fine spectral measurement but may not be good enough for some metrological work such as reference wavelength that requires the uncertainty less than 10^{-9} .

However, the experiments for testing source of uncertainty of the OSA need much improvement and more data are required. In order to reach capable of international standard for wavelength calibration, standard and reference material are required, also, more investigation on standard and normative documents such as time frequency standard, the comb technique, must be done.

Though today, interferometry and application of Fabry-Perot interferometer are not popular among the Thai scientists but in the near future, I believe that, it may be an important technique and be widely used in many area such as industrial, agriculture and military.

LITERATURE CITED

- Anton H. 1994. **Elementary Linear Algebra** 7th ed. John Wiley & Son, Inc, NJ., 328-331.
- Bayer-Helms, F. 1991. Section 2.2.2 The Metre. pp. 2-34–2-44. In Madelung, O. et al. Units and Fundamental Constants. In **Physics and Chemistry Sub-volume a: Units in Physics and Chemistry**. Springer-Verlag. Berlin Heidelberg.
Available Sources:
http://public.metapress.com/download/profiles/springerlink/0284/indexes/units/t000_units_a0000.pdf, Access date: 26 Sep. 2004.
- Coherent Auburn Group. 1982. **Model 240 Spectrum Analyzer Operator Manual**. Coherent Inc., CA.
- Coherent Auburn Group. n.d. **Model 251 Controller User Guide**. Coherent Inc., CA.
- Goldwasser, S.M. 2005. **Helium-Neon Lasers**. Sam's Laser FAQ web site. Available Sources: <http://www.repairfaq.org/sam/laserhen.htm>, Sep. 30, 2005.
- Goldwasser, S.M. 2006. **Commercial HeNe Lasers**. Sam's Laser FAQ web site. Available Sources: <http://an.hitchcock.org/repairfaq/sam/laserhcl.htm>, Feb. 15, 2006.
- Goldwasser, S.M. 2006b. **Diode Lasers**. Sam's Laser FAQ web site. Available Sources: <http://an.hitchcock.org/repairfaq/sam/laserdio.htm>, Feb. 18, 2006.
- Johnson, D.A. 2005. **Handbook of Optical Through the Air Communication**, Chapter 2 Optical detector by Devid A. Johnson. Available Sources: <http://www.imagineeringezine.com/ttaoc/t-circuits.html>, Feb. 17, 2007
- Kochsiek, M. 2003. **Trends in Legal Metrology Towards a Global Measurement System**. ISO Bulletin, May 2003.

Nave C. R. 2005. **Helium-Neon Laser**. Hyper physics web site. Available Sources: <http://hyperphysics.phy-astr.gsu.edu/hbase/hframe.html>, Sep. 30, 2005.

OSI-Optoelectronics. 2006. **Photovoltaic Series** (Product Catalog). OSI Optoelectronics, Inc. Available Sources: <http://www.osioptoelectronics.com/subproducts.aspx?mainid=1&subid=4&lowid=2>, Feb 2005.

Quinn, T. J. 2003a. **Open letter concerning the growing importance of metrology and the benefits of participation in the Metre Convention**, notably the CIPM MRA. Available Sources: <http://www.bipm.fr/utis/en/pdf/importance.pdf>, May 2003.

Quinn, T.J. 2003b. Practical realization of the definition of the metre, including recommended radiations of other optical frequency standards (2001). **Metrologia** 40 (2003): 103–133.

Redgrave, F., Henson, A. and Beauvais, D. 2003. Metrology for Improved Measurements in International Regulation and Trade, **World Congress: The RegMet Project XVII**. IMEKO, Dubrovnik, Croatia.

Spectra-Physics. 1997. **Model 117A Stabilized Helium-Neon Laser Instruction Manual**. Spectra-Physics Lasers. Inc. CA.

Wyant, J.C. 2000. **Multiple Beam Interference**. Available Sources: [http://wyant.optics.arizona.edu/MultipleBeam Interference/Multiple BeamInterference.pdf](http://wyant.optics.arizona.edu/MultipleBeam%20Interference/MultipleBeamInterference.pdf), Sep. 12, 2003.

Weisstein, E.W. 1996a. **Stokes relations**. Available Sources: <http://scienceworld.wolfram.com/physics/StokesRelations.html>, June 14, 2004.

Weisstein, E.W. 1996b. **Millimeter/Submillimeter Fourier Transform Spectroscopy of Jovian Planet Atmospheres**. Thesis for the Doctor of Philosophy Degree. California Institute of Technology at Pasadena. Available Sources: <http://www.ericweisstein.com/research/thesis/node98.html>, Sep. 30, 2004.

APPENDICES

APPENDIX A

Spectral Information,
Instruments Specification and test certificate

APPENDIX A1



MODEL 240 SPECTRUM ANALYZER

MIRROR TEST REPORT

Model Number:	240-1B	Serial Number:	17G28
Part Number:	0215-072-01	Date Tested:	10-23-2001
Wavelength Range:	550nm-650nm	Wavelength Tested:	632.8nm
Peak Wavelength:	600nm	Technician:	Conny Louridas
Coating Run:	T9705/D0898	Free Spectral Rng:	7.5 GHz
Finesse Total*:	367.3		



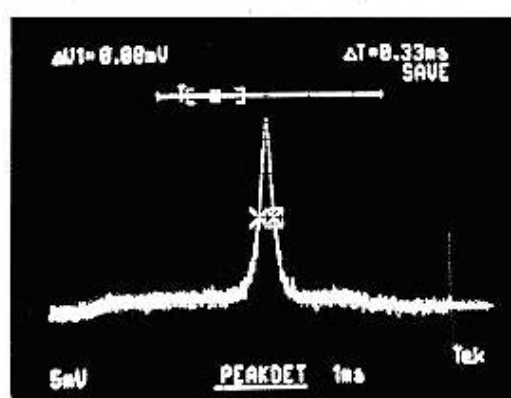
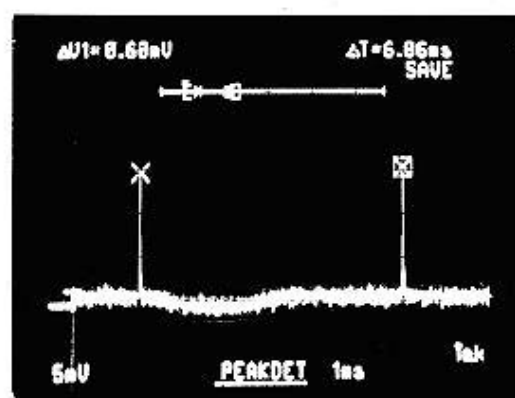
*Finesse is determined by dividing the FSR Free spectral range by the BW Bandwidth (BW @50%). Minimum guaranteed finesse for this model is 200

FSR = $\frac{6.06}{0.33/(20)_{exp}}$ = FINESSE of 367.3 Q/A



FSR picture

BW picture



E215-124-00 JAN II

Photonics Division • 2303 Lindbergh Street • Auburn, California 95602 • Ph (530) 888-5062 • FAX (530) 889-5262

Appendix Figure A1 Test certificate of the OSA model 240

Source: Coherent Auburn Group. 1982.

APPENDIX A2

SPECIFICATIONS

PHYSICAL		
Dimensions	Power Supply	30.2 x 26.0 x 9.5 cm (11.88 x 10.25 x 3.72 in.)
	Laser Head	Cylindrical 40.1 cm (15.8 in.) long 4.5 cm (1.77 in.) diameter
Weight	Power Supply	3.3 kg (7.2 lbs)
	Laser Head	1.0 kg (2.2 lbs)
Shipping Weight		6.2 kg (13.5 lbs)
ELECTRICAL		
Voltage Required		115/230 V ac $\pm 10\%$ (100 V ac available)
Power Required		40 W
Frequency		47 - 63 Hz
Fuses		500 ma SB, for 100-115 V ac 250 ma SB, for 230 V ac
ENVIRONMENTAL		
Operating Temperature		10 to 40°C (50 to 104°F)
Storage Temperature		-40 to 60°C (-40 to 140°F)
Altitude		Sea level to 3km (10,000 ft)
FREQUENCY STABILIZED MODE		
Frequency Stability	1 min	± 0.5 Mhz (± 0.3 typ)
	1 hour	± 2.0 Mhz (± 0.8 typ)
	1 day (8 hr period)	± 3.0 Mhz (± 1.2 typ)
Frequency vs. Temperature		$< \frac{1}{2}$ Mhz/°C
Temperature Range, Maintaining Lock		20 \pm 10°C
Intensity Stability		-1%
Modulation Feature (nominal value only)		10MHz/V
INTENSITY STABILIZED MODE		
Intensity Stability	1 min	$\pm 0.1\%$
	1 hour	$\pm 0.1\%$
Frequency Stability	1 min	± 3.0 Mhz
	1 hour	± 5.0 Mhz
Modulation Feature (nominal value only)		-2%/V
EITHER MODE		
Output Power @ 632.8nm		> 1.0 mW (1.4 typ)
Frequency (nominal)		473.61254 THz
Beam Characteristics	Diameter	0.5 mm
	Divergence (full cone)	1.8 mrad
Resonator Characteristics	Transverse Spatial Mode	TEM ₀₀
	Polarization	Linear, >1000:1
RMS Output Power	50/60 Hz	0.001%
Ripple (typ)	Servo Loop (-5 kHz)	0.005%
	High Voltage (~24 kHz)	0.05%

Specifications subject to change without notice

Appendix Figure A2 Specification of SP117 632.8 nm stabilized HeNe Laser

Source: Spectra-Physics (1997)

APPENDIX A3

■ Photovoltaic Series

Planar Diffused Silicon Photodiodes

The Photovoltaic Detector series is utilized for applications requiring high sensitivity and moderate response speeds, with an additional sensitivity in the visible-blue region for the blue enhanced series. The spectral response ranges from 350 to 1100 nm, making the regular photovoltaic devices ideal for visible and near IR applications. For additional sensitivity in the 350 nm to 550 nm region, the blue enhanced devices are more suitable.

These detectors have high shunt resistance and low noise, and exhibit long term stability. Unbiased operation of these detectors offers stability under wide temperature variations in DC or low speed applications. For high light levels (greater than 10mW/cm²), the Photoconductive Series detectors should be considered for better linearity.

These detectors are not designed to be reverse biased! Very slight improvement in response time may be obtained with a slight bias. Applying a reverse bias of more than a few volts (>3V) will permanently damage the detectors. If faster response times are required, the Photoconductive Series should be considered.

Refer to the Photovoltaic Mode (PV) paragraph in the "Photodiode Characteristics" section of this catalog for detailed information on electronics set up.



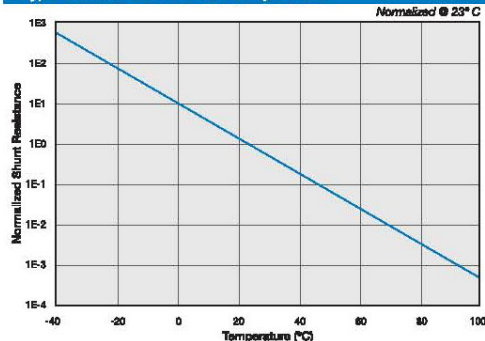
■ APPLICATIONS

- Colorimeters
- Photometers
- Spectroscopy Equipment
- Fluorescence

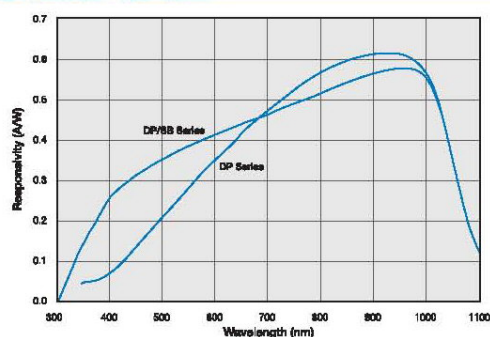
■ FEATURES

- Ultra Low Noise
- High Shunt Resistance
- Wide Dynamic Range
- Blue Enhanced

■ Typical Shunt Resistance vs. Temperature



■ Typical Spectral Responses



Appendix Figure A3 Scanned page 1 of the specification of UDT photo-voltaic series.

Source: OSI-Optoelectronics. (2006)

Photovoltaic Series

Typical Electro-Optical Specifications at $T_A=23^\circ\text{C}$

Model Number	Active Area		Peak Responsivity Wavelength	Responsivity at λ_p			Capacitance (pF)	Shunt Resistance (G Ω)		NEP (W/ $\sqrt{\text{Hz}}$)	Rise Time (ns)	Temp.* Range ($^{\circ}\text{C}$)		Package Style †			
	Area (mm 2)	Dimensions (mm)		λ_p (nm)	(A/W)			0 V	-10 mV			0V 970 nm	0 V 632 nm 50 Ω		Operating	Storage	
				typ.	min.	typ.		max.	min.			typ.	typ.				typ.
'DP' Series, Metal Package																	
CD-1705	0.88	0.93 sq	850	970	0.55	0.60	70	1.0	10	2.1 e-15	2000	-40 ~ +100	-55 ~ +125	4 / TO-18			
PIN-2DPI ‡	1.1	0.81 x 1.37	150				30				8 / TO-18						
PIN-125DPL	1.6	1.27 sq.	160				4 / TO-18										
PIN-3CDPI	3.2	1.27 x 2.54	320				0.5	5.0	3.0 e-15	50	7 / TO-18						
PIN-3CDP			500				0.4	4.0	3.4 e-15	60	2 / TO-5						
PIN-5DPI	5.1	2.54 ϕ	1200				0.35	3.5	3.6 e-15	150	5 / TO-5						
PIN-5DP	13	3.6 sq									2 / TO-5						
PIN-13DPI	16.4	4.57 ϕ									5 / TO-5						
PIN-13DP	44	6.6 sq	2000				0.2	2.0	3.9 e-15	220	3 / TO-8						
PIN-6DPI			4300				0.1	1.0	4.8 e-15	475	6 / TO-8						
PIN-6DP											3 / TO-8						
PIN-44DPI	100	11.28 ϕ	9800				0.05	0.2	6.8 e-15	1000	6 / TO-8						
PIN-44DP											10 / Lo-Prof						
PIN-10DPI											11 / BNC						
PIN-10DP	613	27.9 ϕ	60000				0.002	0.1	3.0 e-14	6600	-10 ~ +50			-20 ~ +70	12 / BNC		
PIN-25DP																	
'DP' Series, Plastic Package §																	
PIN-220DP	200	10 x 20	970	0.55	0.60	20000	0.02	0.2	1.2 e-14	2200	-10 ~ +60	-20 ~ +70	27 / Plastic				

Super Blue Enhanced 'DP/SB' Series, (All Specifications @ $\lambda=410\text{ nm}$, $V_{\text{BIAS}}=0\text{ V}$, $R_L=50\Omega$)

Model No.	Active Area/Dimensions		Responsivity (A/W)		Capacitance (pF)	R_{sh} ($M\Omega$)	NEP ($\text{W}/\sqrt{\text{Hz}}$)	Operating Current (mA)	Rise Time (μs)			Package Style †
	mm^2	mm	min.	typ.	typ.	min.	typ.	max.	typ.			
PIN-040DP/SB	0.81	1.02 ϕ			60	600	2.0 e-14	0.5	0.02			1 / TO-18
PIN-5DP/SB †	5.1	2.54 ϕ			450	150	5.2 e-14	2.0	0.2			5 / TO-5
PIN-10DP/SB	100	11.28 ϕ	0.15	0.20	8800	10	2.0 e-13	10.0	2.0			11 / BNC
PIN-10DPI/SB												10 / Metal
PIN-220DP/SB	200	10 x 20			17000	5	2.9 e-13	10.0	4.0			27 / Plastic

'5T' Series, Blue

Model No.	Active Area/Dimensions		Responsivity (A/W) 436nm		Capacitance (pF) 0V	R_{sh} ($M\Omega$)	NEP ($\text{W}/\sqrt{\text{Hz}}$)	Dark Current (pA)	Rise Time (μs)			Package Style †
	mm^2	mm	min.	typ.	max.	min.	typ.	max.	typ.			
OSD1-5T	1.0	1.0 sq			35	250	2.5 e-14	1.0	7			7 / TO-18
OSD3-5T	3.0	2.5 x 1.2			80	100	3.0 e-14	2.0	9			7 / TO-18
OSD5-5T	5.0	2.5 ϕ			130	100	3.3 e-14	2.0	9			5 / TO-5
OSD15-5T	15.0	3.8 sq			390	50	5.6 e-14	10.0	12			5 / TO-5
OSD60-5T	62.0	7.9 sq			1800	3	2.1 e-13	25.0	30			3 / TO-8
OSD100-5TA	100.0	11.3 ϕ			2500	2	2.5 e-13	30.0	45			74 / Special

‡ The 'I' suffix on the model number is indicative of the photodiode chip being isolated from the package by an additional pin connected to the case.

§ The photodiode chips in "FIL" series are isolated in a low profile plastic package. They have a large field of view as well as "in line" pins.

† For mechanical drawings please refer to pages 58 thru 69.

* Operating Temperature: -40 to +100 $^\circ\text{C}$, Storage Temperature: -55 to +125 $^\circ\text{C}$.

* Non-Condensing temperature and Storage Range, Non-Condensing Environment.

Appendix Figure A4 Scanned page 2 of the Specification of UDT photo-voltaic series that show specification of PIN 125DPL.

Source: OSI-Optoelectronics. (2006)

APPENDIX A4

Some Radiation Recommended by CIPM

Appendix Table A1 List of recommended radiations, 1983, for radiation of lasers stabilized by saturated absorption.

Absorbing molecule	Transition	Component	ν [MHz]	λ [fm]	$10^9 u_{rel}$
CH ₄	ν_3 , P(7)	F ₂ ⁽²⁾	88 376 181.608	3 392 231 397.0	0.13
¹²⁷ I ₂	17-1, P(62)	o	520 206 808.51	576 294 760.27	0.6
¹²⁷ I ₂	17-5, R(127)	I	473 612 214.8	632 991 398.1	1.0
¹²⁷ I ₂	9-2, R(47)	o	489 880 355.1	611 970 769.8	1.1
¹²⁷ I ₂	43-0, P(13)	a ₃	582 490 603.6	514 673 466.2	1.3

Note

In this list, the values of the frequency ν and of the wavelength λ should be related exactly by the relation $\lambda\nu = c_o$ with $c_o = 299\,792\,458$ m/s but the values of λ are rounded.

Radiation of lasers stabilized by saturated absorption. As a footnote: “Each of these radiations can be replaced, without degrading the accuracy, by a radiation corresponding to another component of the same transition or by another radiation, when the frequency difference is known with sufficient accuracy...” u_{rel} means: estimated overall relative uncertainty, the threefold standard deviation.

Source: Bayer-Helms (1991)

Appendix Table A2 List of recommended radiations of Spectral Lamps.

Atom	Transition	λ [pm]	u_{rel}
^{86}Kr	$2p_9 - 5d'_4$	645 807.20	$2 \cdot 10^{-8}$
	$2p_8 - 5d_4$	642 280.06	
	$1s_3 - 3p_{10}$	565 112.86	
	$1s_4 - 3p_8$	450 361.62	
^{198}Hg	$6^1P_1 - 6^1D_2$	579 226.83	$5 \cdot 10^{-8}$
	$6^1P_1 - 6^3D_2$	577 119.83	
	$6^3P_2 - 7^3S_2$	546 227.05	
	$6^3P_1 - 7^3S_1$	435 956.24	
^{114}Cd	$5^1P_1 - 5^1D_2$ * ²	644 024.80	$7 \cdot 10^{-8}$ (the red Cd line)
	$5^3P_2 - 6^3S_1$	508 723.79	
	$5^3P_1 - 6^3S_1$	480 125.21	
	$5^3P_0 - 6^3S_1$	467 945.81	

Note

1. Radiation corresponding to the transition between the levels $2p_{10}$ and $5d_5$ of the atom ^{86}Kr . The value $\lambda = 605\,780\,210\text{ fm}$, $u_{rel} = 4 \cdot 10^{-9}$ *¹, applies to the radiation emitted by a lamp operated under the conditions recommended by the CIPM.

2. Radiations of the atoms ^{86}Kr , ^{198}Hg and ^{114}Cd recommended by the CIPM in 1963.

3. *¹ The realization uncertainty of the metre definition from 1960 with the ^{86}Kr standard lamp has been quoted originally to be 10^{-8} relative only. According to further experiments and experiences it could be reduced to $4 \cdot 10^{-9}$. The meaning of quoted uncertainty values has been stated more precisely to be the threefold standard deviation here.

4. *² A misprint occurred in the classification in.

Source: Bayer-Helms (1991)

APPENDIX A5

Appendix table A3 Possible spectrum of He-Ne laser.

(1) Output Wavelength	(2) HeNe Laser Name	(3) Perceived Beam Color	(4) Lasing Transition	(5) Typical Gain (%/m)		(6) Maximum Power (mW)	
543.5 nm	Green	Green	3s2->2p10	0.52	0.59	2	(5)
594.1 nm	Yellow	Orange-Yellow	3s2->2p8	0.5	0.67	7	(10)
604.6 nm		Orange	3s2->2p7	0.6	1.0	3	
611.9 nm	Orange	Red-Orange	3s2->2p6	1.7	2.0	7	
629.4 nm		Orange-Red	3s2->2p5	1.9	2.0		
632.8 nm	Red	" "	3s2->2p4	10.0	10.0	75	(200)
635.2 nm		" "	3s2->2p3	1.0	1.25		
640.1 nm		Red	3s2->2p2	4.3	2.0	2	
730.5 nm	Border	Infra-Red	3s2->2p1	1.2	1.25	0.3	
886.5 nm		" "	2s2->2p10	1.2	1.25	0.3	
1,029.8 nm	Near-IR	Invisible	2s2->2p8	N.A.			
1,062.3 nm	" "	" "	2s2->2p7	N.A.			
1,079.8 nm	" "	" "	2s3->2p7	N.A.			
1,084.4 nm	" "	" "	2s2->2p6	N.A.			
1,140.9 nm	" "	" "	2s2->2p5	N.A.			
1,152.3 nm	" "	" "	2s2->2p4	N.A.		1.5	
1,161.4 nm	" "	" "	2s3->2p5	N.A.			
1,176.7 nm	" "	" "	2s2->2p2	N.A.			
1,198.5 nm	" "	" "	2s3->2p2	N.A.			
1,395.0 nm	" "	" "	2s2->2p?	N.A.		0.5	
1,523.1 nm	" "	" "	2s2->2p1	N.A.		1.0	
3,391.3 nm	Mid-IR	" "	3s2->3p4	N.A.	440.0	24	

Notes:

1. Output Wavelength is approximate. In addition to slight variations due to actual lasing conditions (single mode, multimode, doppler broadening, etc.), some references don't even agree on some of these values to the 4 or 5 significant digits shown.

2. HeNe Laser Name is what would be likely to be found in a catalog or spec sheet. All those that have an entry in this column are readily available commercially.

3. Perceived Beam Color is how it would appear when spread out and projected onto a white screen. Of course, depending on the revision level of your eyeballs, this may vary someone from individual to individual.

4. Lasing Transition uses the so-called "Paschen Notation" and indicates the electron shells of the neon atom energy states between which the stimulated emission takes place.

5. Typical Gain (%/m) shows the percent increase in light intensity due to stimulated emission at this wavelength inside the laser tube's bore. This is the single pass gain and will be affected by tube construction, gas fill ratio and pressure, discharge current, and other factors. The first column is from various sources. The second column is from Hecht, "The Laser Guide Book".

6. Gain at 1,523 nm may be similar to that of 543.5 nm - about 0.5%/m. Gain at 3,391 nm is by far the highest of any - possibly more than 100%/m. I know of one particular HeNe laser operating at this wavelength that used an OC with a reflectivity of only 60% with a bore less than 0.4 m long.

Source: Goldwasser (2005)

APPENDIX B

Experiments procedure

APPENDIX B1

Experiments Set 1 Procedure

Experiment 1.1 Frequency characteristics of the OSA controller.

Objective

1. Measure frequency range and resolution.
2. Observe the rise time range and stability.

Literature: See topic Material & Method section 1.1 & 1.3

From specification, Rise Time of Ramp is 10 ms to 5 s at tolerance of $\pm 10\%$.
Fall Time of Ramp is 10 ms at tolerance of $\pm 10\%$ and expects to be constant.

Experimental hypothesis (From user manual,)

1. The frequency range can approximate from rise time. It may span from 0.2 Hz to 50 Hz with uncertainty better than $\pm 10\%$.
2. Rise time span from 10 ms to 5 s with uncertainty better than $\pm 10\%$.

Instruments

1. OSA controller model 251 (UUT.)
2. DSO (TDS 220)

Procedure

1. Use the TDS 220 to measure frequency span and rise time.
2. Warm up the OSA controller model 251 and TDS 220 for 30 minute.
3. Observe maximum and minimum of the frequency span and rise time.
4. Observe the tuning point or frequency range that cause in stability
5. Observe frequency and period stability at 0.25 Hz, 0.5 Hz, 1.0 Hz, 2.5 Hz, 5 Hz, 10 Hz, 25 Hz, 50 Hz. in 1 hour, at amplitude 250 V, 200 V, 150 V, 100 V, and 50 V.
6. Measure frequency, period, and rise time. Calculate fall time and duty cycle.

7. Evaluate mean frequency and period and the uncertainties associated at 95% confidence.

Experiment 1.2 Amplitude characteristics of the OSA controller.

Objective

1. Measure Amplitude range and resolution.
2. Observe the Amplitude stability.

Literature: See topic Material & Method section 1.1 & 1.3

Experimental hypothesis (From user manual,)

1. The Amplitude range span from 0 V to 250 V with unknown tolerance.
The resolution of controllable incrimination voltage is observed.
2. The amplitude stability is not specify, but expected to be better than 1%.

Instruments

1. OSA controller model 251 (UUT.)
2. DSO (TDS 220)

Procedure

1. Observe maximum and minimum peak to peak amplitude
2. Use sampling frequency at 0.25 Hz, 0.5 Hz, 1.0 Hz, 2.5 Hz, 5 Hz, 10 Hz, 25 Hz, 50 Hz.
3. Use the TDS 220 to measure the peak to peak amplitude at zero DC offset.
4. Use sampling amplitude at (1, 2.5, 5, 10, 25, 50, 100, 250) V for each frequency. Observe the amplitude voltage range that cause instability or uncontrollable.
5. Observe minimum peak compare 0 V.
6. Evaluate mean amplitude voltage range at each step and the uncertainties associated at 95% confidence.

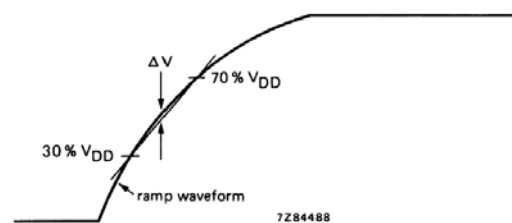
Experiment 1.3 Linearity of ramp signal.

Objective

Measure the linearity of ramp signal.

Literature

Since, there is no exact definition of linearity of the ramp signal on any standard documents. Only one found form HEF4750V data sheet (Philips Semiconductor 1995).



$$\text{Linearity} = \frac{\Delta V}{1/2 V_{DD}} \times 100\%.$$

Fig.16 Definition of the ramp linearity at full swing.
 ΔV is the maximum deviation of the ramp waveform to the straight line, which joins the 30% V_{DD} and 70% V_{DD} points.

Appendix figure B1 Measurement definition of ramp linearity

In case of extreme linearity so we change the full swing span from 10% V_{DD} to 90% V_{DD} .

Equation:
$$\text{Linearity} = \frac{\Delta V}{0.5 V_{DD}}$$

Linearity is property of signal like “error”. Its uncertainty is not defined.

Experimental hypothesis (From user manual,)

The ramp linearity is less than 1.5%.

Instruments

1. OSA controller model 251 (UUT.)
2. DSO (TDS 220)

Procedure

1. Use sampling frequency at 0.25 Hz, 0.5 Hz, 1.0 Hz, 2.5 Hz, 5 Hz, 10 Hz, 25 Hz, 50 Hz.
2. Use sampling amplitude at 5 V, 10 V, 25 V, 50 V, 100 V, 150 V, 200 V, 250V for each frequency.
3. Observe ramp voltage and time at 10% V_{DD} , and 90% V_{DD} at each frequency.
4. Evaluate average linearity (or non-linearity) at each amplitude value over the frequency range.

Experiment 1.4 DC offset characteristics.

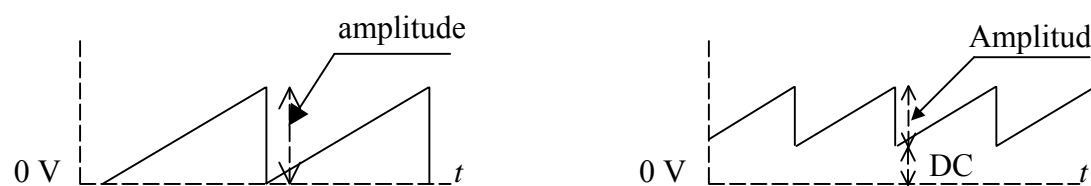
Objective

1. Measure DC offset range and resolution.
2. Observe DC offset stability.

Literature

DC offset is a DC voltage mix to ramp signal. Thus result is two cases. The first, DC voltage is added to the ramp signal. The peak voltage is increase and the peak to peak amplitude is the same. The second, DC voltage is mix in to the ramp signal. This case the peak voltage is the same but the peak to peak amplitude is previous peak voltage minus the DC offset. By this manner DC offset is not DC term of furier components.

A scanned FPI cavity some time needs to start scanning at specific length. The DC offset voltage applied to the piezo actuator elongate the cavity to this length. This mean that the extreme stability of DC offset is need.



Appendix figure B2 Zero Offset Ramp and Ramp with DC offset

Experimental hypothesis (From user manual,)

1. DC offset is 0 V to 200 V.
2. DC offset is stability is not specified, but expects to be better than 0.1%.

Instruments

1. OSA controller model 251 (UUT.)
2. DSO (TDS 220)

Procedure

1. Use the sampling test frequency at 0.25 Hz, 0.5 Hz, 1.0 Hz, 2.5 Hz, 5 Hz, 10 Hz, 25 Hz, 50 Hz.
2. Use the sampling amplitude or peak voltage at 50 V, 100 V, 250 for each frequency.
3. Select the sampling DC offset at 10 V, 25 V, 50 V, 100 V, 150 V and 200 V for each pair of amplitude-frequency.
4. Observe stability of DC offset voltage and other effect on amplitude and frequency.
5. Evaluate DC offset mean voltage at the sampling amplitude over a frequency range and the uncertainties associated at 95% confidence.

Experiment 1.5 Harmonic distortion of ramp signal**Objective**

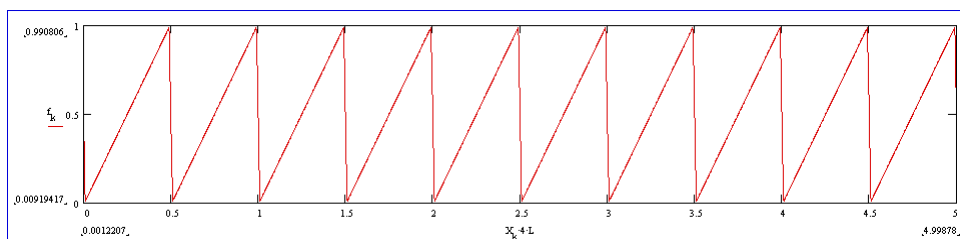
1. Measure the harmonic distortion of ramp signal.
2. Observe ramp spectrum of model 251 controller signal compare to computer FFT result of ideal ramp signal of the same frequency, amplitude and duty cycle.

Literature

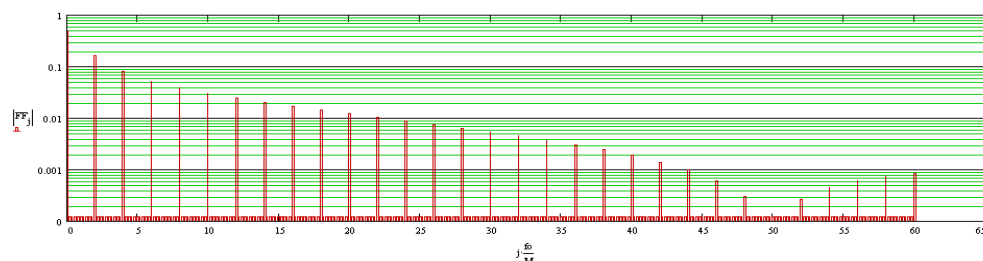
1. Harmonic distortion cause the signal shape distort from its regular shape. In case of audio frequency sinusoidal signal, the “True RMS” meter is introduced to measure voltage or current of the test signal compare to the reference signal. The

reference signal usually synthesized from very high definition signal synthesizer or arbitrary function synthesizer. If the signal is ramp wave form harmonic distortion is major cause of non-linearity. In case of small non-linearity the method in experiment 3 may be unable to show the significant figure.

2. Small harmonic distortion is difficult to distinguish by method above. If we know exactly the desired ramp waveform. Spectrum Analyzer or Fast Fourier Analyzer able to analyze harmonics of the test signal compare to a reference signal or computerize Fourier transform of geometrical wave form.



Appendix figure B3 Ramp wave form of period 0.5 s, rise time 0.49 s, duty cycle 98%.



Appendix figure B4 FFT of the same ramp, show 30 peak harmonics form 300 components. First 11 and 22 harmonics which amplitude are over 0.01 and 0.001 respectively.

3. If we consider that the algebraic sum of fourier components arise from random noise tend to zero. The DC part is 0.5, then the modulus of infinite sum on harmonics of the complex amplitude is tending to 0.5. In practice, summation on limit range of harmonics may give result more than 0.5 i.e., before phase reversal point ($f = 1/2 * T_f$).

To set comparison on the same condition. We adjust FFT analyzer to sampling 10 periods of the test ramp on the 4096 points time window. Consider the algebraic sum of the complex amplitude from the first harmonic to the first harmonic that magnitude less than 0.1 % of the test ramp.

Equation:

$$TDH_X = \frac{1}{0.5 \cdot V} \sqrt{\left(\sum_{p=1}^{q-1} FF_p \right)^2}$$

Where

V is the average amplitude of test ramp wave.

FF_p are complex amplitude of p^{th} harmonic of FFT of test ramp wave.

$q-1$ is the FFT term that $|FF_q|$ is less than $0.001V$.

$$TDH_{Ref} = \frac{1}{0.5 \cdot V_{ref}} \sqrt{\left(\sum_{p=1}^{q-1} FF_p \right)^2}$$

TDH_{Ref} is the total harmonic distortion of reference ramp wave of the same frequency, amplitude rise time and fall time.

$$TDH\% = \left(1 - \frac{TDH_X}{TDH_{ref}} \right) \times 100$$

$TDH\%$ is defined for Total Harmonics Distortion index that compare to the reference ramp wave form.

Experimental hypothesis (From user manual,)

The harmonic distortion is less than 1.00%.

Instruments

1. OSA controller model 251 (UUT.)
2. Real Time FFT analyzer (Tektonix 2642A)

Procedure

1. Use sampling frequency at 0.25 Hz, 0.5 Hz, 1.0 Hz, 2.5 Hz, 5 Hz, 10 Hz, 25 Hz, 50 Hz.

2. Use sampling amplitude at (1, 2.5, 5, 10, 25, 50, 100, 250) V for each frequency.
3. Use the 2642A to observe power and phase spectrum of the test ramp signal at each frequency and amplitude pair. Evaluate the TDH_{Ref}
4. Evaluate TDH_{Ref} from any mathematic software i.e., MathCAD.
5. Evaluate Total Harmonics Distortion index ($TDH\%$) of the test ramp wave compare to the correspondence reference ramp wave.

Experiment 2.1 Signal Amplifier Characteristics of the controller model 251

Objective

1. Measure D.C. sensitivity characteristic of ramp signal amplifier of 251 controller.
2. Measure the input range of ramp signal amplifier of 251 controller.

Literature

1. D.C. sensitivity is the ratio of output signal to input signal. This static characteristic can directly measure from output voltage which correspondence to assigned input voltage if the amplifier has D.C response.

2. Sensitivity characteristic can observe and measure by given a linear ramp signal of appropriate amplitude and frequency range. Then observe the simultaneous output such as linearity, saturation and other difference with the input signal shape.

3. Two methods above we also measure input range by observe saturation of the output signal.

4. Transfer characteristic is an I-V relation of output/input. Usually apply to sensor which may consider as current source or voltage source

Equation:

$$\text{Voltage Sensitivity } S_V = \left\langle \frac{\Delta V_O}{\Delta V_I} \right\rangle$$

ΔV_O is best linear span of output voltage range correspondence with

ΔV_I is best linear span of input voltage range.

$$\text{Transfer Sensitivity } S_T = \left\langle \frac{\Delta V_O}{\Delta I_I} \right\rangle$$

ΔI_I is best linear span of input current range.

Experimental hypothesis (From user manual,)

1. The sensitivity (or voltage gain) = 1000
2. Transfer characteristic:
 - 2.1 for current source ($R_i > 100 \text{ k}\Omega$) $V_O(\text{V}) = 50 I_I(\text{A})$
 - 2.2 for voltage source ($R_i < 100 \text{ }\Omega$) $V_O(\text{V}) = 10^3 \text{ v/v } I_I(\text{A})$

Instruments

1. OSA controller model 251 (UUT.)
2. Multimeter 8842A
3. DSO (TDS 220)
4. Arbitrary function generator AFG 5101
5. Digital multi-meter 33401A

Procedure

1. Set AFG 5101 to generate triangular signal at 5 Hz and 10 mV amplitude. Then feed to controller model 251 via the detector input channel.
2. Use the TDS 220 to observe the best linear span of output signal from the detector output channel compare to the correspondence input signal. Then calculate the average sensitivity.
3. Connect the DMM 33401A between AFG 5101 and the controller model 251. Set up the 33401A to ACmA mode (at 1 A range the resolution is 1 nA and uncertainty from specification is 1.00% of reading + 400 nA). The internal impedance of AFG 5101 is 50 Ω . This case the AFG 5101 is a voltage source with $R_i < 100 \text{ }\Omega$.
4. Use the TDS 220 to observe the best linear span of output signal from the detector output channel compare to the correspondence input signal. Then calculate the average Transfer sensitivity.

Experiment 2.2 Frequency response to 3 dB cutoff of the amplifier

Objective

1. Measure 3dB cutoff frequency of signal amplifier of 251 controller.
2. Observe the frequency response linearity of signal amplifier of 251 controller.

Literature

1. Any amplifiers always have specific frequency response. The preferred signal amplifiers must have a constant gain on broad frequency range.
2. Cutoff frequency is the frequency which the output signal is half power of the input signal or the voltage gain is $1/\sqrt{2}$.
3. There are many ways to study and observe frequency characteristics of signal amplifier. In this case a simple swept sine method is applied.

Experimental hypothesis (From user manual,)

The cutoff frequency is 80 KHz (typical).

Instruments

1. OSA controller model 251 (UUT.)
2. Multimeter 8842A
3. DSO (TDS 220)
4. Arbitrary function generator AFG 5101

Procedure

1. Set AFG 5101 to generate sine signal at 5 Hz and 10 mV amplitude. Then feed to controller model 251 via the detector input channel.
2. Use the TDS 220 to observe amplitude of output signal from the detector output channel compare to input signal. Then calculate the average voltage gain.
3. Change the input frequency from 1 Hz to 1 MHz in 1:2:5 step.

4. Redo item 3. from 50 kHz to 100 kHz by 2 kHz step and find the cutoff frequency.

Experiment 3.1 Unexposed I-V characteristic of photo diode sensor

Objective

1. Observe the Unexposed I-V characteristic of photo diode “PIN-125DPL”.
2. Measure the diode threshold voltage.

Literature

1. “PIN-125DPL” is a planar diffuse silicon photo diode designed for photovoltaic application. This detector is utilized for applications requiring high sensitivity and moderate response speeds, with an additional sensitivity in the visible-blue region for the blue enhanced series. The spectral response ranges from 350 nm to 1100 nm.

(cf. 1.1.1.3)

2. Since, this sensor detector is not designed to be reverse biased. The operation of this sensor in the OSA must be photovoltaic mode. This mode of operation the photo diode act like a solar cell. If no light expose on its junction we can find the junction voltage from I-V characteristics.

3. There are many ways to study I-V characteristics diodes. In this case, for convenient, we use a HM-6042 Curve Tracer to observe I-V diagram and measure the diode current and voltage simultaneously.

Experimental hypothesis (From user manual,)

The cutoff frequency is 80 KHz (typical).

Instruments

1. PIN-125DPL (UUT.)
2. Curve Tracer HM-6042

Procedure

1. Insert the “PIN-125DPL” PIN photo diode into test devices socket on the HM-6042. Cover the PIN-125DPL with small cap to shade it from surrounded light.



Appendix figure B5 Measurement of Diode Characteristic with HM6042

2. Push to lock the BIP/FET switch to FET/Diode mode. Set P_{max} to 0.4 W. Set I_{max} and V_{mx} to 2 mA and 2 V respectively. Then push DUT button to start the test.
3. Push the cursor button and turn the control knob to read the diode current and voltage.
4. Record the diode current and voltage. Plot I-V diagram with program EXEL.

Experiment 3.2 Exposed I-V characteristic of photo diode sensor

Objective

1. Observe the exposed I-V characteristic of photo diode “PIN-125DPL”.
2. Measure the diode threshold voltage.

Literature

1. PIN-125DPL is a planar diffuse silicon photo diode designed for photo-voltaic application. The spectral response ranges from 350 nm to 1100 nm. (cf. 1.1.3) In this application we interest its sensitivity and characteristic at 632 nm and near by wavelength.

2. From specification, PIN-125DPL active area is 1.27 mm x 1.27 mm or 1.6 mm².

3. There are many ways to study I-V characteristics diodes. In this case, for convenient, we use a HM-6042 Curve Tracer to observe I-V diagram and measure the diode current and voltage simultaneously.

Experimental hypothesis (From user manual,)

-

Instruments

1. PIN-125DPL (UUT.)
2. Curve Tracer HM-6042
3. Stabilized HeNe Laser 632.8 nm
4. Neutral density filter set
5. Optical power meter

Procedure

1. After complete experiment 3.1, remove PIN-125DPL from test devices socket and install it into a socket with extension wire.
2. Align 632.8 nm HeNe Laser and neutral density filter set. Measure the Laser beam power with pass through neutral density filter with optical power meter.
3. Varies the density of the filter set from 0, 0.1 ... to 0.5 and record the beam power.
4. Align laser beam on the PIN photo diode. Varies the density of the filter set from 0, 0.1 ... to 0.5 and record the diode current and voltage. Plot I-V diagram with program EXEL.

APPENDIX B2

Experiments Set 2 Procedure

Experiment 4.1 Etalon cavity expansion & co-efficient

Objective

1. Observe stability of linear extension of the OSA cavity when high voltage linear ramp is applied.
2. Measure the extension coefficient of the OSA cavity.

Literature

1. The OSA is application of Faby-Perot interferometer. Detailed literature confer to section 4.5
2. One of Fabry-Perot cavity mirror is attached with a hollow cylindrical piezo actuator. If this piezo actuator is applied with a liner ramp voltage, the actuator is extended linearly dependent with the applied voltage. Linear ramp voltage is linearly increasing with time then the cavity length is linearly extended with time.
3. Practical extended motion of the actuator is linear over a short distance and limited applied voltage. A transfer function of piezo element electrically equivalent to RLC circuit that response to a limit range of frequency. Furier expression of linear ramp is odd harmonic span form fundamental to infinite. When practically ramp voltage is applied to special shape piezo actuator nonlinear response is occur in some frequency and voltage range.

Experimental hypothesis

The cavity expansion & co-efficient is 4 nm/V approximately.

Instruments

1. The OSA model 240 and the controller model 251.
2. Frequency stabilized HeNe laser model SP-117
3. DSO (TDS 220)
4. Multimeter 8842A

Procedure

1. Connect 'Ramp Out' channel from OSA controller model 251 to the OSA model 240 and TDS 220 via a 3 way BNC splitter.
2. Switch on the TDS 220, wait until it's ready. Then switch on the OSA controller model 251.
3. Adjust the OSA controller model 251, set sweep expansion to x1, set amplitude to 250 V, set offset to 0 V, and set rise time to 5 s. Left it 30 minute for warm up.
4. Evaluate for α_t (nm/s), slope (V/s), and α_v (nm/V) with varying amplitude.
5. Adjust amplitude until see 6 successive interference peaks.
6. Measure time interval between the 6 peak ($n = 5$ intervals) as ΔT . Measure rise time record as T1. Measure amplitude voltage and record.
7. Observe 5 successive interference peaks. Do item 5 with $n = 4$.
8. Calculate α_t (nm/s), slope (V/s), and α_v (nm/V). Calculate average and standard deviation.
9. Adjust amplitude voltage until see 4 successive interference peaks. Do item 5 with $n = 3$. Then do item 7.
10. Adjust amplitude voltage until see 3 successive interference peaks. Do item 5 with $n = 2$. Then do item 7.
11. Evaluate for α_t (nm/s), slope (V/s), and α_v (nm/V) with varying rise time.
12. Adjust amplitude to 250 V and rise time to 5 s.
13. Do item 5 with $n = 5$ and 4. Then do item 7.
14. Adjust rise time to 7.5 s and 9 s then do item 5 with $n = 5$ and 4. Then do item 7.
15. Evaluate α_v (nm/V) and unbiased standard uncertainty.

Experiment 4.2 Evaluated the finesse @ 632.8 nm

Objective

1. Observe the FSR and FWHM from scope screen.
2. Measure the FSR and FWHM to evaluate Finesse

Literature

See section 5.7 and 5.9.

Experimental hypothesis

Finesse of the OSA is 367.3 at 632.8 nm wavelength.

Instruments

1. The OSA model 240 and the controller model 251.
2. Frequency stabilized HeNe laser model SP-117
3. DSO (TDS 220)
4. Multimeter 8842A

Procedure

1. Connect 'Ramp Out' channel from OSA controller model 251 to the OSA model 240 and TDS 220 via a 3 way BNC splitter.
2. Switch on the TDS 220, wait until it's ready. Then switch on the OSA controller model 251.
3. Adjust the OSA controller model 251, set sweep expansion to x1, set amplitude to 250 V, set offset to 0 V, and set rise time to 5 s. Left it 30 minute for warm up.
4. Measure ramp amplitude, frequency and rise time.
5. Adjust sweep expansion until see only two peak. Measure separation between the two peaks. Record the FSR.
6. Adjust sweep expansion until see only one peak. Save the wave form.
7. Recall the saved form then adjust time/div (zoom mode) and reposition, until see the peak as wide as possible. Record the FWHM.
8. Evaluate finesse and unbiased standard uncertainty.
9. Change the ramp amplitude to 150 V, 125 V and change rise time to 7.5 s and 9 s then repeat the experiments.

CIRRICULUM VITAE

NAME : Mr. Kanokpoj Areekul

BIRTH DATE : October 29, 1954

BIRTH PLACE : Bangkok, Thailand

EDUCATION	: <u>YEAR</u>	<u>INSTITUTE</u>	<u>DEGREE/DIPLOMA</u>
	1978	Kasetsart Univ.	B.Sc.(Physics)

POSITION/TITLE : Lecturer

WORK PLACE : Faculty of Science, Kasetsart University

SCHOLARSHIP/AWARD : -

